Modeling Photofunctional Transition Metal Complexes

Bolano Losada, Iria

2024

Document Version:
Publisher's PDF, also known as Version of record

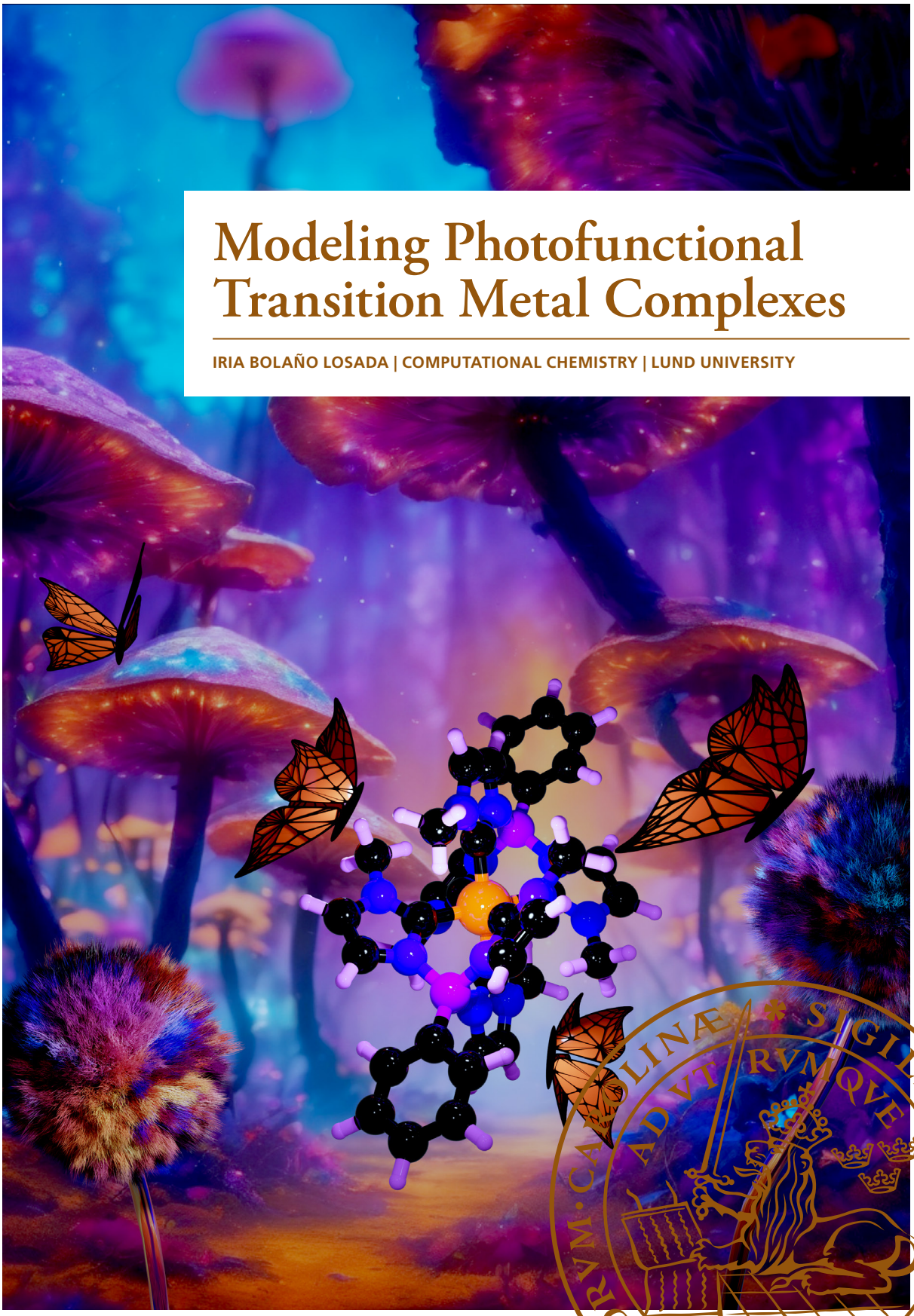

Modeling Photofunctional Transition Metal Complexes

IRIA BOLAÑO LOSADA | COMPUTATIONAL CHEMISTRY | LUND UNIVERSITY

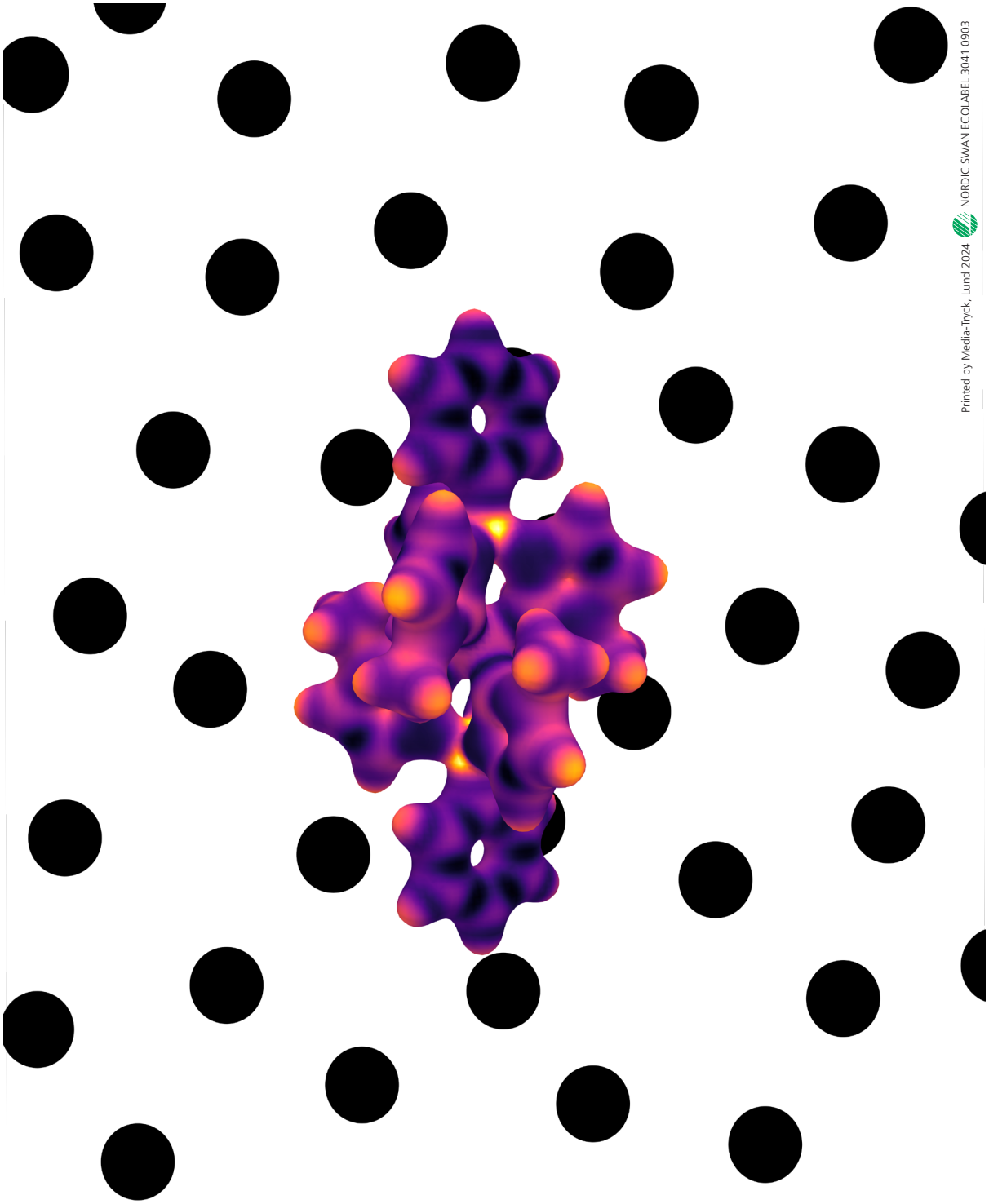

Printed by Media-Tryck, Lund 2024 NORDIC SWAN ECOLABEL 3041 0903

LUND UNIVERSITY

ISBN 978-91-8096-028-1

Computational Chemistry
Physical and Theoretical Chemistry
Department of Chemistry
Faculty of Science

Modeling Photofunctional Transition Metal Complexes

Modeling Photofunctional Transition Metal Complexes

by Iria Bolaño Losada

LUND
UNIVERSITY

Thesis for the degree of Doctor of Philosophy
Thesis advisors: Prof. Petter Persson and Prof. Ulf Ryde
Faculty opponent: Prof. Isabelle Dixon

To be presented, with the permission of the Division of Computational Chemistry of Lund University, for public criticism in lecture hall A, Center for Chemistry and Chemical Engineering, Lund, on Friday, the 12th of April 2024 at 09:00.

Organization	Document name
LUND UNIVERSITY Department of Chemistry Box 124 SE–221 00 LUND Sweden	**DOCTORAL DISSERTATION** Date of disputation 2024-04-12 Sponsoring organization
Author(s) Iria Bolaño Losada	

Title and subtitle

Modeling Photofunctional Transition Metal Complexes

Abstract

Transition metal complexes play a crucial role in solar energy conversion. These coordination compounds have promising applications in dye-sensitized solar cells and photocatalysis, with particular interest in solar fuel production. However, many of the photoactive transition metal complexes used in light-harvesting applications are still based on rare and expensive metals from the transition metal block. As an alternative to the popular Ru or Ir transition metal complexes, new research lines are emerging to solve the challenges in utilizing first-row transition metals, including Fe and Co. Density functional theory (DFT), has been broadly utilized to understand the underlying photophysics and quenching mechanisms of earth-abundant metal complexes excited states.

An optimal match of metal and ligand is essential for achieving photoactive metal complexes. The tuning effect of interchanging the metal in a d^6 hexa-carbene complex has shown the tight relationship between the metal charge and the final photoproperties. The charge induces a structural compression of the excited states favoring the occurrence of high-energy metal-centered states. The studied Co(III) complex displayed luminescence with an impressive long lifetime from a triplet metal-centered state, proving the functionality of these states. The population of triplet metal-centered states in low-spin d^6 and *quasi*-octahedral complexes promotes several near-degenerate states with distinct structural distortions. *Ab initio* molecular dynamics in a Rh(III) complex, with dual emission from ligand-centered and metal-centered states, indicate that the entropy gain by geometry distortions drives the crossover reaction. Systems without metal-centered states, such as d^0 titanocenes and scandocenes, also encounter distorted ligand-to-metal charge transfer states, which triggers radical ligand formation. Photochemical investigations on ligand-to-metal charge transfer states have been further extended to a Fe(III) carbene complex. Our results indicated that this complex shows a fast photoinduced charge disproportionation at high concentration, and the charge recombination occurs in the inverted Marcus regime. Diffusion of charge-separated species is also relevant to suppress recombination. The control of ion-pairing by solvent interactions promotes the hole migration of a donor molecule after quenching this Fe(III) complex. These active species can subsequently catalyze reactions, such as hydrogen production. A DFT protocol of (photo)redox potentials can assist the selection of optimal photosensitizer, donor, and proton reduction catalyst at a low computational cost. DFT also serves as a useful tool to assess multiple mechanistic reaction paths to generate hydrogen by proton reduction catalysts.

Key words

density functional theory, earth-abundant, molecular dynamics, quantum chemistry, photosensitizer, photophysics, photochemistry, solar fuels, solar energy conversion, transition metal complexes

Classification system and/or index terms (if any)

Supplementary bibliographical information	Language
	English
ISSN and key title	ISBN
	978-91-8096-028-1 (print) 978-91-8096-029-8 (pdf)
Recipient's notes	Number of pages: 250 / Price
	Security classification

Modeling Photofunctional Transition Metal Complexes

by Iria Bolaño Losada

LUND
UNIVERSITY

A doctoral thesis at a university in Sweden takes either the form of a single, cohesive research study (monograph) or a summary of research papers (compilation thesis), which the doctoral student has written alone or together with one or several other author(s).

In the latter case the thesis consists of two parts. An introductory text puts the research work into context and summarizes the main points of the papers. Then, the research publications themselves are reproduced, together with a description of the individual contributions of the authors. The research papers may either have been already published or are manuscripts at various stages (in press, submitted, or in draft).

Cover illustration front: Front layer created by the author using Blender, and the background generated by Gencraft.

Cover illustration back: Created by the author using Paraview and Inkscape.

Funding information: The thesis work was financially supported by the Swedish Research Council and the Knut and Alice Wallenberg foundation. It has also received support from eSSENCE and NanoLund.

Division of Computational Chemistry, Department of Chemistry

isbn: 978-91-8096-028-1 (print)
isbn: 978-91-8096-029-8 (pdf)

Printed in Sweden by Media-Tryck, Lund University, Lund 2024

Media-Tryck is a Nordic Swan Ecolabel certified provider of printed material. Read more about our environmental work at www.mediatryck.lu.se

MADE IN SWEDEN

Dedicado aos meus pais

Contents

List of publications . . . iii
Publications not included in this thesis . . . iv
Acknowledgements . . . v
Divulgación científica en galego . . . vii
Popular science in english . . . ix
Abbreviations . . . xi

Modeling Photofunctional Transition Metal Complexes 1

1 Introduction 3
1.1 Dye-sensitized solar cells . . . 4
1.2 Hydrogen as fuel . . . 5

2 Theory 7
2.1 Quantum Mechanics . . . 7
2.1.1 The Hartree–Fock method . . . 9
2.1.2 Basis set . . . 10
2.1.3 Variational principle . . . 12
2.2 Density functional theory . . . 13
2.2.1 Time-dependent density functional theory . . . 16
2.3 Molecular Mechanics . . . 17
2.4 Molecular dynamics . . . 18
2.4.1 Classical molecular dynamics . . . 18
2.4.2 *Ab initio* molecular dynamics . . . 21
2.5 Solvent effects . . . 22
2.5.1 Continuum-solvation model . . . 22
2.5.2 Quantum mechanics/molecular mechanics . . . 23
2.6 Potential energy surface exploration . . . 24

3 Excited states in transition metal complexes 27

4 Tuning the photophysics of metal complexes 33
4.1 Iron complexes as sustainable photosensitizers . . . 36
4.2 From scavengers to functional states: ^{3}MC excited states . . . 38
4.2.1 Metal oxidation state tuning . . . 39

4.3 Interplay between ^{3}LC and ^{3}MC excited states 41
4.4 Evading MC states: ^{3}LMCT excited states in d^0 complexes 44

5 Photochemistry of metal complexes **47**
5.1 Photocatalysis with earth-abundant transition metal complexes . . . 48
5.2 Electron transfer 49
5.3 Photoinduced electron transfer: charge separation and charge recombination 52
5.4 Solvent cage escape 54
5.4.1 Anomalous cage escape dynamics 55
5.4.2 Beyond the classical perspective 57
5.5 Hydrogen production by proton reduction 58
5.5.1 Finding a suitable DFT functional 60
5.6 Designing hydrogen reduction molecular catalysts 62
5.6.1 Detailed reaction mechanism 63

6 Conclusions and Outlook **67**

Scientific publications **89**
Author contributions 89
Paper I: Microsecond Photoluminescence and Photoreactivity of a Metal-Centered Excited State in a Hexacarbene–Co(III) Complex . . . . .
Paper II: Excited State Rebalancing of Hexa-Carbene d^6 Complexes – Comparative Calculations for Fe^{II}, Ru^{II}, Co^{III}, and Rh^{III} . . . . . .
Paper III: Ligand-Centered to Metal-Centered Activation of a Rh(III) Photosensitizer Revealed by Ab Initio Molecular Dynamics Simulations .
Paper IV: Modeling the Competition Between Luminescence and Photoinduced Homolysis in Titanocenes and Scandocenes . . . . . .
Paper V: Competing Dynamics of Intramolecular Deactivation and Bimolecular Charge Transfer Processes in Luminescent Fe (III) N-Heterocyclic Carbene Complexes . . . . . .
Paper VI: Understanding Anomalous Cage-Escape Dynamics in Photoredox Processes Driven by Fe(III) N-Heterocyclic Carbene Complexes
Paper VII: Photoredox Matching of Earth-Abundant Photosensitizers with Hydrogen Evolving Catalysts by First Principles Predictions . . . . .
Paper VIII: Photoinduced Hydrogen Evolution Catalyzed by New Co(II) Complexes of N5-Donor Ligands . . . . . .

List of publications

I **Microsecond Photoluminescence and Photoreactivity of a Metal-Centered Excited State in a Hexacarbene–Co(III) Complex**
S. Kaufhold, N. W. Rosemann, P. Chábera, L. Lindh, **I. B. Losada**, J. Uhlig, T. Pascher, D. Strand, K. Wärnmark, A. Yartsev and P. Persson
Journal of the American Chemical Society, 2021, 143(3), 1307-1312

II **Excited State Rebalancing of Hexa-Carbene d^6 Complexes – Comparative Calculations for Fe^{II}, Ru^{II}, Co^{III}, and Rh^{III}**
I. B. Losada and P. Persson
Manuscript

III **Ligand-Centered to Metal-Centered Activation of a Rh(III) Photosensitizer Revealed by Ab Initio Molecular Dynamics Simulations**
I. B. Losada and P. Persson
Chemical Science, 2023, 14(47), 13713-13721

IV **Modeling the Competition Between Luminescence and Photoinduced Homolysis in Titanocenes and Scandocenes**
I. B. Losada and P. Persson
Manuscript

V **Competing Dynamics of Intramolecular Deactivation and Bimolecular Charge Transfer Processes in Luminescent Fe (III) N-Heterocyclic Carbene Complexes**
N. W. Rosemann, L. Lindh, **I. B. Losada**, S. Kaufhold, O. Prakash, A. Ilic, J. Schwarz, K. Wärnmark, P. Chábera, A. Yartsev and P. Persson
Chemical Science, 2023, 14(13), 3569-3579

VI **Understanding Anomalous Cage-Escape Dynamics in Photoredox Processes Driven by Fe(III) N-Heterocyclic Carbene Complexes**
I. B. Losada, U. Ryde and P. Persson
Submitted

VII **Photoredox Matching of Earth-Abundant Photosensitizers with Hydrogen Evolving Catalysts by First Principles Predictions**
I. B. Losada and P. Persson
Journal of Chemical Physics, 2024, 160(7), 074302

VIII **Photoinduced Hydrogen Evolution Catalyzed by New Co(II) Complexes of N5-Donor Ligands**
C. Li, Y. Li, Y. Luo, K. Michaliszyn, **I. B. Losada**, Md. K. Hossain, F. Elantabli, M. Guo, L. Hizbullah, M. Haukka, P. Persson, J. Lloret-Fillol, B. Dietzek-Ivanšić, E. Nordlander
Manuscript

All papers are reproduced with permission of their respective publishers.

Publications not included in this thesis

IX **Methanol Directing the Dual Reactivity of 1,3-Dien-5-Ynes under Gold(I) Catalysis: A Computational Study**
M. Marín-Luna, **I. Bolaño**, C. S. López, O. N. Faza
Computational and Theoretical Chemistry, 2019, 1148, 33-37

X **Separation of an Aqueous Mixture of 6-Kestose/Sucrose with Zeolites: A Molecular Dynamics Simulation**
I. B. Losada, P. Grobas-Illobre, A. Misturini, J. Polaina, Y. Seminovski, G. Sastre
Microporous and Mesoporous Materials, 2021, 319, 111031-11041

XI **How Rigidity and Conjugation of Bidentate Ligands Affect the Geometry and Photophysics of Iron N-Heterocyclic Complexes – A Comparative Study**
O. Prakash, P. Chábera, N. Kaul, V. F. Hlynsson, N. W. Rosemann, **I. B. Losada**, A. Gupta, P. Huang, J. Bendix, T. Ericsson, L. Häggström, D. Strand, A. Yartsev, R. Lomoth, P. Persson, K. Wärnmark
Inorganic Chemistry, 2024

XII **Side-Group Switching between Metal-to-Ligand Charge-Transfer and Metal-Centered Excited State Properties in Iron(II) N-Heterocyclic Carbene Complexes**
L. Lindh, N. W. Rosemann, **I. B. Losada**, S. Persson, Y. Goriya, H. Fan, O. Gordivska, K. Wärnmark, J. Uhlig, P. Chábera, A. Yartsev, P. Persson
Coordination Chemistry Reviews, 2024, 506, 215709

XIII **Photophysical Integrity of the Iron(III) Scorpionate Framework in Iron(III)–NHC Complexes with Long-Lived ^{2}LMCT Excited States**
O. Prakash, L. Lindh, N. Kaul, N. W. Rosemann, **I. B. Losada**, C. Johnson, P. Chábera, A. Ilic, J. Schwarz, A. K. Gupta, J. Uhlig, T. Ericsson, L. Häggström, P. Huang, J. Bendix, D. Strand, A. Yartsev, R. Lomoth, P. Persson, and K. Wärnmark
Inorganic Chemistry, 2022, 61(44), 17515–17526

Acknowledgements

I want to start thanking my PhD supervisor Petter for always keeping the optimism even at the highest peaks of frustration. Once you said you would be happy to answer all my questions until you could not, and it still did not happen. Despite that we began working together by chance, I am very happy to have had the opportunity to work on such fascinating research work and collaborations. Also, I want to thank my second supervisor Ulf for always supporting me during the PhD, inviting me to the group's journal club, and correcting my manuscripts at an unbelievable speed. I would also like to thank my previous supervisor Hermida, who is the main reason I came to Lund, and who has taught me the most challenging computational techniques. I also want to acknowledge Germán who although only supervising me for a short time in Valencia, I still remember it as a very rewarding experience.

I am very thankful for working with the best professionals in spectroscopy, Arkady, Christina, Jens, Neus, Nils, Pavel, and Zehan. I was also very lucky to have had two "sisters" in the group, Linnea and Yen. You both have made my journey much easier and more enjoyable. I want to also thank our collaborators Ebbe and Carmina, with whom I learned so much about catalysis. Also, thanks to all collaborators in Wärnmark's and Elliott's groups for providing the most spectacular molecule designs.

There is almost nothing in Lund that I will miss more than my group of friends, I have never met so peculiar people before, with so much drama, chaos, and fun. I am very proud to say I was the only member of this group who has never been kicked out of a place. I will always remember our gatherings, awkward discussions, and internal jokes.

This is an acknowledgment/apology list:
Alex or the "Romanian Alejandro", for being always the spark of the most random conversations. Eric, sorry for taking a baby beaker from your lab (might be returned). Erik, for all the funny conversations about the Danish way of pronouncing things. Ernst, I apologize for having kidnapped your Molcas cup. Jason, for bringing the most exquisite British humor to the group. Jen, for surviving a night out in the forest with me. Hao, for never complaining despite annoying you so much. Ismail for all your 3 h lessons starting with "Look, let me tell you something …". Jing, for teaching me the tastiest Chinese food. Joel for amazing us with all your excuses for not hanging out. Justine, for all the amazing trips in nature and teaching me just a bit of discipline. Marcos, for your patience every time I say "Uma esmolinha" and also for starting our addiction to chai latte. Mona, for always bringing fun and joy to our gatherings. Najla, for sharing your excess of happiness with all of us. Nikol, for providing the extra drama to everything we do together. Pappu, for your valuable friendship and for

changing my currency to rupees. Kristoffer, for sharing your knowledge on random data in random topics. Samuel, for providing the most wanted sofa in TeoKem and giving me more than 70 SEK in empty cans. Sara, for being my first friend in Lund. Simon, for being an excellent and obedient team worker. Stefan, for all the conversation and the Moomin tea, my favorite. Victor, for sharing your valuable knowledge in theory with me. Vilhelm, I confess to stealing time to time lemon candies from your desk. Vidar for starting the Teokem versus PhysChem competition. Zakiyeh, for all the funny conversations happening in our office.

General thanks to everyone in the TeoKem division, as well as all my friends in the PhysChem and ChemPhys divisions.

Last but not least, I would like to thank my family and friends for their unconditional support. I want to give a special mention to my parents who supported me through my ups and downs and always found the positive side and humor. In addition, I would also like to thank my brother for always providing me with valuable guidance.

Divulgación científica en galego

A enerxía solar é a fonte de enerxía máis abundante dispoñible no noso planeta, e esta é facilmente accesible. Non obstante, só o 14 % da enerxía xerada no mundo orixinouse de fontes de enerxía renovables durante o ano 2021, mentres que máis do 80 % da enerxía produciuse a partir de fontes de combustibles fósiles, destacando o gas natural, o petróleo ou o carbón.[1] Coa crecente demanda de enerxía, as emisións de CO_2 fóronse incrementando anualmente, de tal maneira que chegaronse a estimar en máis de 32.000 millóns de toneladas en 2021. As crecentes preocupacións económicas e ambientais intensificaron a urxencia de atopar solucións máis accesibles e ecolóxicas.

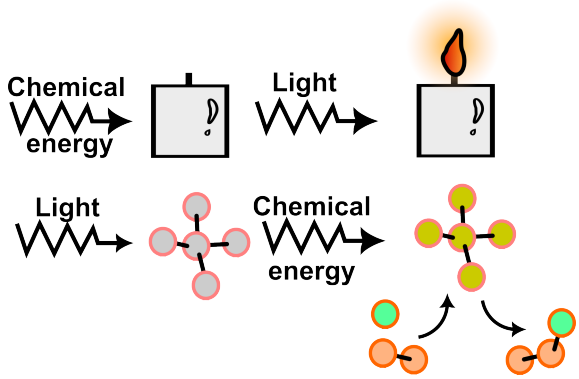

Figura 1: Exemplos de transformación de enerxía.

Algunhas das liñas de investigación máis recentes céntranse na utilización de moléculas para captar enerxía solar. Estas moléculas coñécense comunmente como fotosensibilizadores. A luz, que é enerxía en forma de fotón, pódese transformar noutro tipo de enerxía, incluindo enerxía eléctrica, química ou térmica. Do mesmo xeito que unha vela pode converter a enerxía química en luz mediante reaccións de combustión, os fotosensibilizadores poden desencadear reaccións químicas ao absorber un fotón (Figura 1). Recentemente, as reaccións químicas inducidas pola luz chamaron moito a atención, especialmente a produción de hidróxeno molecular. O hidróxeno postulouse como un dos principais candidatos entre os combustibles solares para substituír os combustibles tradicionais baseados en carbono. Estes combustibles solares ofrecen unha solución sostible, mais aínda non práctica para a demanda actual de enerxía.[2] A produción de hidróxeno economicamente sostible é un obxectivo primordial, especialmente nas rexións con certos recursos limitados de combustibles fósiles como Europa.[3] A auga é a materia prima con máis interese para a xeneración de hidróxeno, aínda que require dunha fonte externa de enerxía para romper os seus enlaces. Non obstante, os fotosensibilizadores tamén se poden integrar en dispositivos como células solares para producir enerxía renovable e alimentar células electroquímicas para

finalmente fragmentar as moléculas de auga.

Nesta tese, exploramos construcións químicas baseadas nun metal incrustado nunha estrutura de orixe orgánica (formada con átomos de carbono, nitróxeno ou osíxeno). Estes compostos, normalmente chamados complexos metálicos, teñen múltiples aplicacións na captación e emisión de luz. Ademais da súa funcionalidade en células solares ou catálise, poden ofrecer outros usos non convencionais como sensores, ordenadores ou memorias moleculares. Estes últimos exemplos baséase no cambio das propiedades químicas ou físicas da molécula (emisión-absorción ou transferencia de electróns) a disparadores externos. As operacións lóxicas, semellantes ás instrucións lóxicas informáticas (SE, OU e E), pódense deseñar segundo a resposta aos estímulos.

Os nosos proxectos abordan problemas fundamentais nos procesos de captación de luz e nas reaccións químicas fotoinducidas, pero aínda de gran relevancia para a súa posterior aplicación en dispositivos ou producións químicas a gran escala. Un dos principais obxectivos desta tese é estudar a transición do uso de metais escasos a materias primas abundantes na terra en procesos impulsados pola luz. A substitución de compoñentes introduce novos obstáculos, aínda que poida parecer sinxelo. Usando os avances computacionais e os fundamentos da química cuántica, pretendemos comprender e predecir as propiedades físicas e químicas dos complexos de metais de transición utilizados con fins de captación de luz. Unha vantaxe das simulacións moleculares é reducir a complexidade dos sistemas reais a problemas máis illados, o que permite un exame enfocado de cuestións máis particulares. Non obstante, un modelo simplificado pode omitir certos niveis de detalles. Polo tanto, un esforzo combinado entre computación e experimentos é esencial para a comprensión en profundidade dos procesos físicos e químicos abordados nesta tese.

A descrición de sistemas químicos mediante a resolución da ecuación de Schrödinger é o caso máis ideal. Non obstante, a complexidade das expresións matemáticas son un desafío para case todos os sistemas químicos, polo que son necesarias varias aproximacións. Existen múltiples métodos deseñados para aproximar a solución exacta da ecuación de Schrödinger, entre eles a teoría funcional da densidade (DFT). En contraste con moitos outros métodos, DFT pretende describir o sistema baseándose na súa densidade, que é unha observable experimental, mentres que a función de onda é unha ferramenta matemática. A vantaxe de usar DFT é a súa eficiencia no manexo de sistemas con múltiples electróns con custos computacionais modestos. Outras estratexias computacionais como as simulacións de dinámica molecular pretenden describir como evoluciona un sistema ao paso do tempo. Nesta tese, aproveitamos as vantaxes de DFT e das simulacións de dinámica molecular para describir a riqueza dos complexos de metais de transición.

Popular science in english

Solar energy is the most abundant source of energy available on our planet, and it is also freely accessible.[4] However, only 14 % of the world's generated energy originated from renewable energy sources during the year 2021, while over 80 % of the energy was produced from fossil fuel sources, including natural gas, oil, or coal.[1] With increasing energy demands, the CO_2 emissions have been escalating yearly and are estimated to exceed 32.000 million tonnes in 2021. The growing economic and environmental concerns have intensified the urgency to discover more affordable and eco-friendly solutions.

Some of the most recent research lines focus on utilizing molecules to capture solar energy. These molecules are commonly known as photosensitizers. Light, which is energy in the form of photons, can be transformed into other types of energy, including electrical, chemical, or thermal energy. Just as a candle can convert chemical energy into light by combustion reactions, photosensitizers can trigger chemical reactions by absorbing a photon (Figure 1). Light-induced chemical reactions have recently attracted a lot of attention, particularly regarding the generation of molecular hydrogen. Hydrogen is postulated as one of the top candidates among solar fuels for replacing traditional carbon-based fuels. These solar fuels offer a sustainable, although still not practical, solution to the current energy demand.[2] Financially sustainable hydrogen production is a primary goal, particularly among regions with limited fossil fuel resources like Europe.[3] Water is the most promising raw material to generate hydrogen, albeit an energy supply is required for the bond rupture. However, photosensitizers can also be integrated into devices like solar cells to produce renewable energy, and power electrochemical cells for water-splitting.

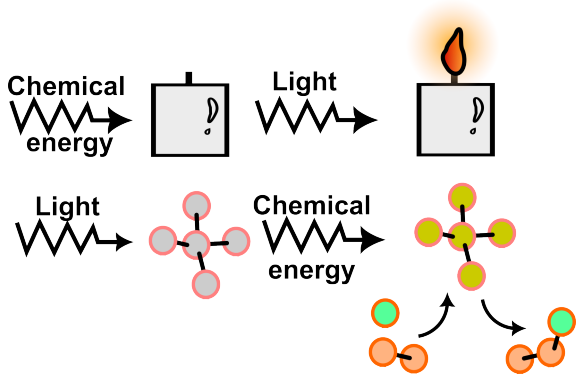

Figure 1: Energy transformation from chemical energy to light and *vice versa*.

In this thesis, we have explored unique chemical constructions based on one metal

embedded in an organic scaffold (with carbon, nitrogen, or oxygen blocks). These compounds, typically called metal complexes, have multiple applications in light-harvesting and light-emission. In addition to their functionality in solar cells or catalysis, they can offer other unconventional uses in sensors or molecular computers and memories. The latter is based on the response of the chemical or physical properties of the molecule e.g. emission-absorption or electron transfer to external triggers. Logic operations, similar to computer logic statements (IF, OR, and AND), can be created according to the response to the stimuli.

We have addressed fundamental problems in light-harvesting processes and photoinduced chemical reactions of high relevance for further application in devices or large-scale chemical productions. One of the major concerns in this thesis is the transition from light-driven processes using scarce metals to earth-abundant raw materials. The replacement of components introduces new obstacles to address, although the shift in perspective may seem straightforward. By using computational advances and the foundations of quantum chemistry, we aim at elucidating and predicting physical and chemical properties of transition metal complexes used for light-harvesting purposes. One advantage of molecular simulations is reducing the complexity of real systems to more isolated problems, which allows a focused examination of particular questions. However, a simplified model might omit certain levels of details. Therefore, a combined effort between computation and experiments is essential to the in-depth understanding of the physical and chemical processes addressed in this thesis.

The description of chemical systems by solving the Schrödinger equation is the ideal case scenario. However, such complex mathematical expressions are a challenge for nearly all chemical systems, so many approximations are required. There are multiple methods designed to approximate the exact solution of the Schrödinger equation, among them the density functional theory (DFT). In contrast to many other methods, DFT aims to describe the system based on its density, which is an experimental observable, whereas the wavefunction is a mathematical constant. The advantage of using DFT is its efficiency in handling complex multielectron systems with modest computational demands. Other computational strategies like molecular dynamics simulations aim to describe how the system evolves with time. In this thesis, we have exploited the advantages of DFT and molecular dynamics to describe the richness of the chemistry of transition metal complexes.

Abbreviations

AIMD Ab Initio Molecular Dynamics

AO Atomic Orbital

BO Born–Oppenheimer

BOMD Born–Oppenheimer Molecular Dynamics

CC Coupled Cluster

CI Configuration Interaction

DFT Density Functional Theory

DSSC Dye-Sensitized Solar Cell

GGA Generalized Gradient Approximation

GTO Gaussian-Type Orbital

HF Hartree–Fock

HOMO Highest Occupied Molecular Orbital

HS High-Spin

KS Kohn–Sham

LC Ligand-Centered

LDA Local Density Approximation

LCAO Linear Combination of Atomic Orbitals

LMCT Ligand-to-Metal Charge Transfer

LS Low-Spin

LSDA Local Spin Density Approximation

LUMO Lowest Unoccupied Molecular Orbital

MC Metal-Centered

MD Molecular Dynamics

MEP Minimum Energy Path

MLCT Metal-to-Ligand Charge Transfer

MM Molecular Mechanics

MO Molecular Orbital

MP Møller–Plesset

NEB Nudged Elastic Band

NHC N-Heterocyclic Carbene

PBC Periodic Boundary Conditions

PES Potential Energy Surface

PRC Proton Reduction Catalyst

QM Quantum Mechanics

STO Slater-Type Orbital

TD-DFT Time-Dependent Density Functional Theory

TON Turnover Number

Modeling Photofunctional Transition Metal Complexes

Chapter 1

Introduction

Metal complexes are molecular systems characterized by a central metal in coordination with ligands. The ligands in question can adopt multiple geometries and compositions ranging from inorganic to organic components.[5] These complexes can be observed as ionic solids or simple molecular systems. When the central metal belongs to the transition metal block, these complexes are typically denoted transition metal complexes. The most recent ligand designs for molecular transition metal complexes rely on sophisticated organic frameworks, often narrowing the borderline between organic and inorganic chemistry.[6] The combination of metal and ligand brings up unique chemical features distinct from the original chemical units.

Transition metal complexes offer numerous tuning opportunities by controlling the interplay between the electronic and geometry properties of the ligand and the metal valence shell.[6, 7] Therefore, these molecules offer a broad selection of applications depending on the molecular design. An adequate metal and ligand combination can either provide reactivity properties or high stability. Various examples of functional transition metal complexes extend from Prussian blue $[Fe(CN)_6]^{4-}$, widely used as pigment due to its vibrant blue color, or the heme cofactor in myoglobin, which gives the red color to human blood and transports oxygen to the cells.[8, 9]

One of the most desired properties of transition metal complexes is their ability to behave as light harvesters, i.e. molecules that can absorb a photon from the solar light. An optimal photosensitizer should meet four main criteria; (i) proper stability and photostability, (ii) absorption spectra in the visible spectra range, (iii) long-lived excited states, and (iv) significant excited state energy.[10] Other factors lately prioritized are the search for environmentally friendly materials, with low-cost components and low toxicity.[11, 12] Nowadays, many efforts are dedicated for replacing scarce

transition metals with other more available options, including Fe, Ti, Mn, and Cr, in descending order with respect to their availability in the Earth's crust.[13] Metal complexes with these harvesting capabilities can be utilized for applications in photochemistry, or light-harvesting devices.[7, 14–16] Here, dye-sensitized solar cells and photocatalyzed hydrogen will be discussed as two practical examples.

1.1 Dye-sensitized solar cells

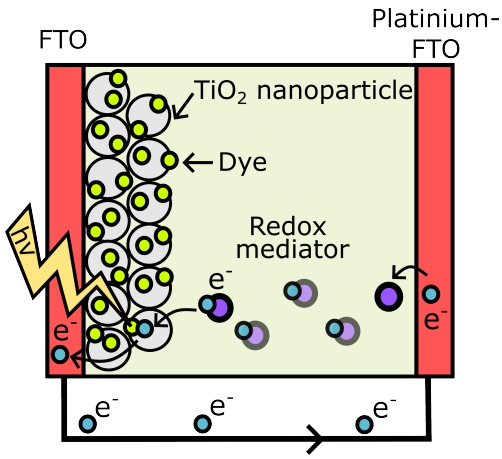

Figure 1.1: Schematic representation of a dye-sensitized solar cells. Fluorine-doped tin oxide layer (FTO) is represented in red.

Dye-sensitized solar cells (DSSC) are emerging among light-harvesting devices as a cheap alternative to silicon solar cells,[17–19] albeit their conversion efficiencies are still low compared to other solar cells.[20] A DSSC comprises three key elements: a dye, a semiconductor, and a redox mediator. A schematic representation of a DSSC is introduced in Figure 1.1.

The fundamental workflow of a DSSC device starts with the light-harvesting by the dye molecules (e.g. transition metal complexes or organic molecules). These molecules, anchored to the surface of (typically) TiO_2 nanoparticles, provide a more extended surface than regular surface layers.[21, 22] TiO_2 serves as an anchoring site for the photosensitizer but also as an electron conductor material. Thus, the excited electron of the dye is injected into the nanoparticle surface. This process will depend on whether the excited state lifetime of the dye is longer than the injection times.[23] An adequate energy level matching between the dye and the conductive band is also relevant for a favorable electron transfer, which will compete with the undesirable charge recombination i.e. electron back-transfer reaction.[19] The successfully injected electron is subsequently transported through the n-type semiconductor layer, generating

an empty hole in the dye. The medium between the cathode and anode of the DSSC contains the redox mediators, for instance I^-/I_3^- couple, which transport electrons from the anode to the oxidized dye through diffusion. The redox mediator's role in the overall DSSC performance is critical since its diffusion rate can hinder or favor the charge recombination process.[24] The final performance of the DSSCs will depend on multiple factors e.g. the interplay between the nature of the n-semiconductor, the type of dye, or the redox mediator.

1.2 Hydrogen as fuel

Solar fuels are one of the most attractive solutions to the extensive use of fossil combustibles.[25, 26] This change of perspective is motivated by the urgency to reduce greenhouse emissions and their negative environmental impact. Hydrogen is an ideal energy source since its instant reaction with oxygen only produces inert water. The reaction of hydrogen and oxygen releases high amounts of energy previously stored in the chemical bonds.[27, 28] Therefore, hydrogen is proposed as a potential energy container, more convenient than the limited storage capabilities of batteries. Furthermore, hydrogen has the advantage to be utilized as reactant in multiple chemical reactions for the chemical industry, for instance, the large-escale production of ammonia.[29] Unfortunately, the current bottleneck of hydrogen generation resides in its still inefficient production and physical storage.

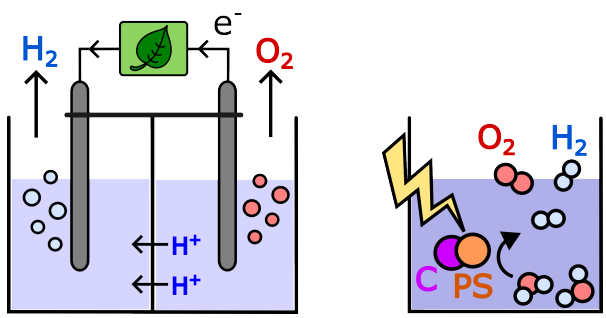

Figure 1.2: (left) Electrochemical water-splitting cell. (right) Homogeneous catalysis of hydrogen.

Reducing water molecules to hydrogen in electrochemical cells is possible (left hand side of Figure 1.2).[28, 30] The redox reaction is described by the two half-reactions below:

$$Anode : 2\,H_2O \longrightarrow O_2 + 4\,H^+ + 4\,e^-$$

$$Cathode : 4\,H^+ + 4\,e^- \longrightarrow 2\,H_2$$

In the anode, two water molecules provide four electrons and four protons to the overall reaction while generating oxygen. On the other hand, two molecules of hydrogen are formed in the cathode from the protons and electrons migrated from the anode. However, the high driving forces of 1.23 V vs NHE at 25 °C and 1 atm drastically limit the efficient hydrogen production.[28, 30]

One alternative to splitting water in electrochemical cells is to power the process with green energy generated with, for instance, solar cells. Another shortcut to the problem inspired by nature is the direct use of sunlight to drive reactions.[15, 26, 31] Therefore, photosensitizers can be utilized to harvest light, in analogy to photosystem II in photosynthesis. The chemical reaction can be driven by combining a photosensitizer and a catalyst, and if the components are molecular elements, this is known as homogeneous photocatalysis (see right hand side of Figure 1.2).[32–34] Many other types of photocatalysis, such as heterogeneous (use of semiconductors) and hybrid catalysis (combination of semiconductors with molecular catalyst) are also in the spotlight in the hydrogen production research field.[33, 35] However, only homogeneous catalysis to drive proton reduction reactions is addressed in this thesis. The advantage of homogeneous catalysis is its specificity and easier control of the molecular mechanisms.[33] The drawback is the lower stability and the inconvenient final product mixing.

Chapter 2

Theory

2.1 Quantum Mechanics

Molecular systems can be mathematically described by a wavefunction, Ψ, which comprises all the information of the system of interest. Operators are mathematical tools utilized to extract certain properties from the wavefunction. The Hamiltonian operator, $\hat{\mathrm{H}}$, is the most well-known operator, relating to the total energy of the molecular system. The relationship between operator, wavefunction and total energy is described by the time-dependent Schrödinger equation, expressed as:

$$\hat{H}\Psi(t) = i\hbar\frac{\delta}{\delta t}\Psi(t) \tag{2.1}$$

where i is the imaginary unit and $\hbar$ is Planck's constant divided by 2π. This equation describes the evolution of the system over time. When only a stationary state is of interest, i.e. for a time-independent case, equation 2.1 can be simplified to:

$$\hat{H}\Psi = E\Psi \tag{2.2}$$

where E is the energy of the system described by the wavefunction Ψ, which are the eigenvalue and eigenfunction of the Hamiltonian operator, respectively. The Hamiltonian is given by five terms:

$$\hat{H} = \underbrace{-\frac{1}{2}\sum_{i=1}^{N}\nabla_i^2}_{\text{electron kinetic energy}} \underbrace{-\frac{1}{2}\sum_{A=1}^{M}\frac{1}{M_A}\nabla_A^2}_{\text{nuclei kinetic energy}} \underbrace{-\sum_{i=1}^{N}\sum_{A=1}^{M}\frac{Z_A}{r_{iA}}}_{\text{nuclei-electron attraction}} + \underbrace{\sum_{i=1}^{N}\sum_{j>i}^{N}\frac{1}{r_{ij}}}_{\text{electron-electron repulsion}} + \underbrace{\sum_{A=1}^{M}\sum_{B>A}^{M}\frac{Z_A Z_B}{R_{AB}}}_{\text{nuclei-nuclei repulsion}} \quad (2.3)$$

where ∇_i^2 and ∇_A^2 are the Laplacian operators for electron i and nucleus A, M_A is the mass of nucleus A, Z_A and Z_B atomic numbers at nuclei A and B, r_{iA}, is the distance between electron i and nucleus A distance, r_{ij}, is the distance between electrons i and j and R_{AB} is the distance between nuclei A and B. The five terms account for (i) kinetic energy of the electrons, (ii) kinetic energy of the nuclei, (iii) attraction forces between nuclei and electrons, (iv) repulsion forces between electrons, and (v) repulsion forces between the nuclei and electrons, respectively.

Based on the Born–Oppenheimer (BO) approximation, the Hamiltonian can be split into an electronic Hamiltonian and a nuclear Hamiltonian. The basis of this approximation is the significant difference in masses between the nuclei and the electrons because nuclei are more than 1000 times heavier than the electron. Such a prominent difference in masses is also consistent with a large difference in velocities according to Newton's second law. Therefore, the nuclei can be considered as fixed in the space. One of the implications of this approximation is the reduction of the number of terms in equation 2.3 to three terms equation, because the nuclei kinetic energy is equal to zero (no displacement of the nuclei) and the nuclei-nuclei repulsion is reduced to a constant (fixed distances). Thus, the electronic Hamiltonian depends only on the nuclei positions, and not their momenta. Although the BO approximation is a quite robust approximation and widely used, there are some cases for which the nuclei and electron movements are strongly coupled. A typical situation where the approximation can break is in the vicinity of conical intersections between excited states.

The bottleneck for the exact solution of equation 2.3 is the electron-electron interaction term (iv). Therefore, analytical solutions of equation 2.3 can only be achieved for one-electron chemical systems such as the hydrogen atom, helium cation, or the dihydrogen molecule cation. The vast majority of interesting chemical systems are many-electron systems, so a series of additional approximations need to be considered to treat more complex molecular systems. The detailed description of the Schrödinger equation and all further approximations have been extensively addressed in multiple quantum chemical books.[36–39]

2.1.1 The Hartree–Fock method

A common simplification of the Schrödinger equation is to consider the wavefunction as a product of one-electron wavefunction:

$$\Psi(x_1, x_2, .., x_N) = \chi_1(x_1)\chi_2(x_2)\cdots\chi_N(x_N) \tag{2.4}$$

Here, $\chi(x_N)$ is the one-electron wavefunction for an electron, at position x. However, this approximation encounters two immediate challenges; the electrons are not indistinguishable and the wavefunction should be antisymmetric with respect to the interchange of electrons (a property intrinsic to any fermion particle). Fock introduced the mathematical properties of a determinant into the Hartree wavefunction concept (Hartree–Fock method, HF)[40, 41] to fulfill the fermion conditions (i) the determinant is proportional to the linear combination of all possible electron interchanges, and (ii) row interchange in a determinant results in a change of the sign, equivalent to an antisymmetry operation of exchanging two electrons. This is called the Slater determinant:

$$\Psi(x_1, x_2, .., x_N) = \frac{1}{\sqrt{N!}} \begin{bmatrix} \chi_1(x_1) & \chi_2(x_1) & \cdots & \chi_N(x_1) \\ \chi_1(x_2) & \chi_2(x_2) & \cdots & \chi_N(x_2) \\ \vdots & \vdots & \ddots & \vdots \\ \chi_1(x_N) & \chi_2(x_N) & \cdots & \chi_N(x_N) \end{bmatrix} \tag{2.5}$$

In equation 2.5, the prefactor is a normalization term (N corresponds to the number of electrons) and χ_N is the one-electron orbital in position x. To fulfill Pauli's exclusion principle i.e. that only two electrons of different spin can be hosted in a single molecular orbital (MO), the Slater determinant is multiplied by a spin-orbital function. The one-electron orbital can therefore be expressed as a two-component orbital, viz. the product of a spatial and a spin functions. Nevertheless, at this stage, there is still no function with a known expression that fully describes one molecular orbital. The next section will address the search for a mathematical expression for a molecular orbital.

The construction of the Slater determinant relies on the case of double-occupied orbitals i.e. even number of electrons. This description is commonly known as restricted HF. Nevertheless, many chemical systems, such as radicals, or many transition metals, do not fulfill a closed-shell picture. The HF method can be modified for open-shell systems by slightly readapting the Slater determinant. There are two primary choices to account for unpaired electrons. The first is the unrestricted HF (UHF) method. In this approach, each spin part belongs to its own spatial function rather than associating one spatial part to two spin functions. Separating alpha electrons from beta electrons results in variations in the mean potential so that the MO energies might

differ slightly between spins. The second approach is the restricted open-shell HF (ROHF) method. It still uses the restricted HF formalism to maintain the spatial part associated with two spin parts for the doubly occupied orbitals, while the singly-occupied orbitals are treated separately. Despite that the ROHF formulation is simpler than UHF, the code implementation is complex and the UHF method is often preferred. However, the drawback of using UHF is that the Slater determinant is no longer an eigenfunction of the spin operator. As a consequence, the multiplicity can diverge from the expected value and there is a risk of contamination from states of other multiplicity.

2.1.2 Basis set

A convenient approximation to the unknown molecular orbitals is to rewrite χ_i as a linear combination of M atomic orbitals localized on the nuclei, with a known mathematical expression ϕ_j (called basis functions); the total contribution to the molecular orbital is described by a coefficient c_j according to equation 2.6.

$$\chi_i = \sum_{j=1}^{M} c_j \phi_j \tag{2.6}$$

The expansion of the MOs atomic orbital contributions is known as the linear combination of atomic orbitals (LCAO). Despite approximating the wavefunction by a linear combination of basis functions, the exact solution to the HF energy can be (hypothetically) achieved by using an infinite number of basis functions. This is commonly known as the basis-set limit. However, as the basis set gets closer to completeness, problems of linear dependency also arise.

Many types of functions can be used to expand the MO, such as exponential functions, Gaussian functions, or plane waves. Exponential functions with the general formula $\propto e^{-\alpha r}$ accurately described the electronic structure near and far from the nuclei. Essentially, the eigenvectors from the analytical solution of the hydrogen atom are exponential functions. Despite the suitability of these functions popularly known as Slater-type orbitals (STO),[42] their complicated integration at the computational level has motivated the application of other alternatives. Gaussian-type orbitals (GTO),[43] on the other hand, provide effective computational solutions (easier integration of $e^{-\alpha r^2}$ type functions) although they describe the electronic structure near and far from the nuclei worse than STOs. A popular compromise between atomic description and computational efficiency is to expand an STO as a linear combination of GTOs (see schematic representation in Figure 2.1). A combination of two to six GTO functions with different exponential values is often used to properly de-

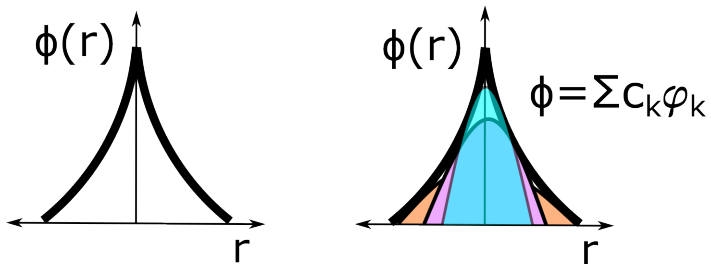

Figure 2.1: (left) Draft of a Slater-type orbital function, and a (right) Slater-type orbital function fitted with three Gaussian-type orbital functions (represented in blue, purple and orange).

scribe one STO function: small exponents describe the wavefunction in the vicinity of the nuclei whereas large exponents better adjust the tail region of STO functions.

There are several strategies to find an accurate basis set at a moderate computational cost. A relevant choice within the available basis sets is for instance the choice of the number of GTO functions (primitive functions) to fit a final STO function (contracted functions) as well as the total number of contracted functions per atom. While a single-zeta (SZ) basis set uses one contracted function per atomic orbital, a double-zeta (DZ) basis set assigns two contracted functions per atom. If the same strategy is extended to three, four, etc contracted functions, then the basis sets are called triple-zeta, quadruple-zeta, ... etc. Since valence electrons are most involved in chemical events, one can simplify a DZ approach by only duplicating the basis functions of the valence orbitals. This approach is commonly known as a split-valence basis set.

Further improvement in the bonding description can be obtained by including polarization functions in the basis set. These are functions of a higher angular momentum than the electron they should describe e.g. utilizing d-orbitals to s-electrons. In cases where a good description far from the nuclei is fundamental, such as in anions, extending the basis set with functions that contain small exponents (diffuse functions) can improve the performance of the basis set. Some examples of basis sets are introduced in the box below.

Basis set

Many types of basis sets depend on how the basis set parameters are defined or how the functions are contracted. Pople basis sets (3-21G, 6-31G, 6-311G),[44] Karlsruhe basis sets (def2-SVP, def2-TVP or def2-QZV),[45] or Dunning's correlation consistent basis sets (cc-pVDZ, cc-pVTZ or cc-pVQZ)[46] are a few examples of popular choices to describe molecular systems.

2.1.3 Variational principle

Now, it is known a mathematical expression for the wavefunction of a target chemical system. However, the optimal values of the basis set expansion coefficients (c_{ij} in equation 2.6), are not known. The variational principle states that for a normalized wavefunction, Ψ_{trial}, the energy calculated as expressed in equation 2.7, E_{trial}, is always larger than or equal to the true eigenvalue, E_0, of the Hamiltonian.

$$\langle \Psi_{trial} | \hat{H} | \Psi_{trial} \rangle = E_{trial} \geq E_0 \tag{2.7}$$

Thus, optimum coefficients c_i in equation 2.6 can be determined to minimize the corresponding E_{trial} of the Ψ_{trial} function, which can be constructed by the Hückel method, for instance. By diagonalizing equation 2.7, a new set of parameters (eigenvectors) and the energy (eigenvalue) are determined. Since each electron is moving in an average field of all the other atoms, the optimal solution is solved by iteratively, minimizing this function until reaching a convergence threshold (known as the self-consistent field, SCF). Based on the variational principle, the electronic Hamiltonian introduced in equation 2.7 is now approximated in HF theory by considering the independent electron assumption. Both one-electron operators (electron kinetic and electron-nuclei attraction) and electron-electron repulsion are reformulated as a sum of individual electron combinations. So the variation of the energy is described by the one-electron Fock operator:

$$F_i = h_i + \sum_{i}^{N_{elec}} (J_i - K_i) \tag{2.8}$$

where h_i describes the one-electron attraction to the nuclei and the kinetic energy for electron i, N_{elec} is the total number of electrons, J is the Coulombic operator (repulsion term), and K is the exchange operator. This K contribution to the Fock operator, which is the energy cost of exchanging two electrons, it neutralizes the self-interaction of the electrons introduced by the J term. The one-electron operator is:

$$h_i = -\frac{1}{2}\nabla_i^2 - \sum_{A}^{N_{nuclei}} \frac{Z_A}{|R_A - r_i|} \tag{2.9}$$

where N_{nuclei} is the total number of nuclei, Z_A is the atomic number of nucleus A, and R_A and r_i are the positions of nucleus A and electron i, respectively. The MO energies are given by the expression,

$$\varepsilon_i = h_i + \sum_{j}^{N_{elec}} (J_{ij} - K_{ij}) \tag{2.10}$$

and the total energy,

$$E = \sum_{i=1}^{N_{elec}} \varepsilon_i - \frac{1}{2} \sum_{ij}^{N_{elec}} (J_{ij} - K_{ij}) + V_{nn} \tag{2.11}$$

where V_{nn} is the nuclear repulsion, J_{ij} and K_{ij} the repulsion and exchange energies between two electrons.

If the MO is expanded in terms of atomic orbitals (expressed in the basis functions), according to the LCAO, the integration of the HF equations is given the Roothaan–Hall equation[47]:

$$FC = SC\varepsilon \tag{2.12}$$

Equation 2.12 is formulated in matrix format, where F is the matrix containing all the Fock operators, C is the matrix comprising the basis set expansion coefficients (c_{ij} in equation 2.6), S is the matrix with the basis set overlaps, and ε the matrix containing the MO energies, in equation 2.10. By iteratively diagonalizing this equation, the final energy is derived.

Many approximations are needed to determine the energy of the system in the HF formalism. Considering the repulsion interactions between electrons as an average response, this is known as mean-field approximation. As a consequence, the error of the final HF energy with respect to the real energy (within the BO approximation) is known as the correlation energy. Depending on the source of the error, it can be subdivided into static correlation and dynamic correlation. The former energy arises as a consequence of neglecting the multideterminant characteristics of the system i.e. neglecting other possible electron configurations. The dynamic correlation instead accounts for the approximation that each electron move in the mean potential of all the other electrons so that repulsion between electrons is often overemphasized.

All post-HF methods aim to estimate the correlation energy. Among them, the most popular methods are Møller–Plesset (MP) perturbation theory, coupled cluster (CC), and configuration interaction (CI) method. These methods are characterized by a high computational cost, scaling from O(N^4) for HF, where N is the number of basis functions, to O(N^5) for MP2 and CISDT, O(N^6) for CCSD and even O(N^7) for MP4 and CCSD(T).

2.2 Density functional theory

Since the wavefunction contains information regarding the energy of the system, the electron density, which is Ψ^2, should also relate to the energy. According to the

Hohenberg–Kohn theorem,[48] the ground state energy can be derived from the electronic density, meaning that it is a functional of the ground state electronic density, $E[\rho]$. The electron density has the advantage of reducing the number of variables from $3N$ spatial and N spin variables in wavefunction methods to only 3 variables (representing the three spatial dimensions), regardless of the number of electrons. However, the exact expression of the energy functional remains unknown.

It has been suggested that the energy functional can be expressed as the sum of three terms the kinetic energy, T, the attraction between nuclei and electrons, V_{ne}, and the electron-electron repulsion. The latter term includes both the Coulomb, J, and exchange components, K (equation 2.13).

$$E[\rho] = T[\rho] + V_{ne}[\rho] + J[\rho] + K[\rho] \tag{2.13}$$

Here, the V_{ne} and J can be solved by integrating over the electron density, similarly as for the Hamiltonian operator (equation 2.3). A clear disadvantage of using the density is that the formulation of the kinetic energy cannot be derived, since the positions of the particles are unknown based solely on the density. The correlation term is also unknown, but both can be approximated by assuming a uniform electron gas. This if the density changes are small, as proposed in the Thomas–Fermi–Dirac method.[49] Despite some improvements, the quality of the results are still inaccurate, with the kinetic energy estimation contributing the most to the overall energy deviation.

$$E^{KS}[\rho] = T[\rho] + V_{ne}[\rho] + J[\rho] + E_{xc}[\rho] \tag{2.14}$$

The Kohn–Sham (KS) theory,[50] similar to the HF formalism, incorporates the one-electron orbitals (χ_i, KS orbitals) to partially provide a solution to the kinetic energy. However, due to the assumption of non-interacting electrons, another part of the kinetic energy is missing. This correlation kinetic energy is instead incorporated into the exchange-correlation term (E_{xc}). Once defined as a function of the density, the energy can be derived from the diagonalization of the KS-equations (equation 2.14). The initial density is a guess density that is often built from a superposition of atomic densities, for instance. The wavefunction that minimizes the energy is derived by utilizing the variational method to solve the KS equations iteratively. The effective potential which depends on the density is also iteratively updated with the new density. The density (ρ_{KS}) is then approximated according to 2.15.

$$\rho_{KS} = \sum_{i=1}^{N} \int |\chi_i|^2 \tag{2.15}$$

The introduction of parameters in the functional formulation becomes necessary due to the elusive nature of the exchange-correlation term. These parameters, similarly to those in semi-empirical methods, are fitted to experimental data or the results of other wavefunction methods. Depending on how the expression of the exchange-correlation term is approximated, different DFT methods arise. Among the most common approximations are the local density approximation (LDA) or local spin density approximation (LSDA) and the generalized gradient approximation (GGA). While LDA aims to recover the exchange-correlation energy based on the density under the assumption of a uniform electron gas, GGA considers the irregularities of the electron density by incorporating the first derivative of the density. Introducing the first derivative of the density increases the cost, but provides more accurate results. The GGA approach can be enhanced even more by including the Laplacian as a variable i.e. the second derivative of the density, or equivalently the orbital kinetic energy density. These methods are known as meta-GGA.

DFT additionally has to cope with the self-interaction error i.e. the non-physical interaction of an electron with its own density. Only a few DFT functionals in use today correct for the self-interaction error, meaning that most functionals tend to overdelocalise the electron density. In contrast, in the HF method, the self-interaction is completely canceled by the exchange term. Therefore, another series of functionals include an exchange-correlation term based on the HF exchange to reduce the self-interaction error. These functionals are known as hybrid functionals. This is the case of the popular B3LYP functional whose exchange-correlation term consists of LSDA exchange (E_x) and correlation (E_c) energies with additional correction terms.[51, 52] The exchange-correction term has HF and B88 contributions while the exchange is further corrected with LYP. Three parameters ($a = 0.20$, $b = 0.72$, and $c = 0.81$) are included in the expression, by a fit to experimental data:

$$E_{xc}^{B3LYP} = (1-a)E_x^{LSDA} + aE_x^{HF} + b\Delta E_x^{B88} + (1-c)E_c^{LSDA} + cE_c^{LYP} \quad (2.16)$$

Range-separated functionals aim to provide an even more detailed approach to recover the self-interaction error. In these cases, the electron-electron Coulombic term of the exchange energy is divided into short- and long-range parts, each term described by different exchange functionals. This type of functionals also includes a parameter that regulates the interchange between short- and long-range terms. This type of approach often provides a good description of excitation energies involving charge-transfer states.

Despite all the consequences of the handling of orbitals, KS-DFT performance still provides a competitive alternative to other wavefunction methods at a low computational cost (typically an accuracy similar to that of MP2 at a cost similar to that of

HF), as has been illustrated by the success of this method in multiple applications. A couple of functionals are listed in the box below.

Some examples of functionals

- **GGA:** BP86[51, 53], BLYP[51, 52], PBE[54]
- **Meta-GGA:** M06L[55], TPSS[56]
- **Hybrid-GGA:** B3LYP[57], B3LYP*[58], PBE0[59]
- **Hybrid-meta-GGA:** TPSSh[60], M06[61]
- **Hybrid range-separated:** ωB97X[62], CAM-B3LYP[63]

2.2.1 Time-dependent density functional theory

Up to here, DFT is only intended to calculate ground-state properties. However, there are properties of great interest that require a time-dependent description within the DFT formalism such as the optical properties of molecular photosensitizers. This can be obtained by time-dependent density functional theory (TD-DFT).[36] This involves the solution of the time-dependent Schrödinger equation (equation 2.1). If the light responsible for inducing an electron transition is regarded as a perturbation in the electric field, the Hamiltonian can be expressed as the sum of the time-independent Hamiltonian, $\hat{H}_0(r)$, and an external potential, $V_{ext}(r,t)$ (equation 2.17). This external potential represents the time-dependent external electric field.

$$\hat{H}(r,t) = \hat{H}_0(r) + V_{ext}(r,t) \tag{2.17}$$

In analogy to DFT, the time-dependent electron density can be calculated from a wavefunction described as a Slater determinant based on Kohn–Sham orbitals. Introducing the Kohn–Sham orbitals also implies that the non-interacting electrons approximation is applied. Therefore, TD-DFT also considers exchange-correlation terms in the effective potential. In contrast, with DFT, the exchange-correlation term depends on the electron density at the initial time t_0 as well as during the time frame $t - t_0$. To reduce the necessity of solving the exchange-correlation term in a self-consistent manner, it can be approximated by employing the adiabatic approximation i.e assuming that the change of the density is slow on that time frame so that the exchange-correlation can be approximated to the time-independent form at an instantaneous time. The adiabatic approximation limits TD-DFT to only single-electron excitations.

In this thesis, TD-DFT has been used to approximate excited-state energies, as well as the relaxed structure of excited states. The numerical Hessian matrix (the derivative of the forces) was also computed at the TD-DFT level to extract frequencies intrinsic to the excited states, as a tool to evaluate the non-radiative decays of the excited states to the ground state.

2.3 Molecular Mechanics

We have explored how quantum mechanics (QM) can be applied to study a system composed of nuclei and electrons, allowing us to uncover intrinsic properties, including the total energy. However, with the fast scaling of the computational cost with the number of electrons for wavefunction methods and DFT, these options become inaccessible for systems with more than some hundreds of atoms. This is the particular case for macromolecular systems such as proteins or lipid aggregates, but also for smaller chemical systems studied in solution or other media. One solution to this multi-electron problem involves simplifying the atomic picture into a more straightforward model in which the mechanical and electronic properties of each atom are treated together. So atoms with nuclei and electrons are transformed into a classical model governed by classical physics laws. This treatment is known as molecular mechanics (MM).

The energy of the whole molecular system is described as a sum of individual energies. These energy terms can be subdivided into energy contributions from bonded atoms and non-bonded atoms. While bonded contributions comprise all the bond lengths, angles, and torsion angles, the non-bonded contributions include electrostatic interactions and Van der Waals interactions. The final energy is derived from the potential of the system, whose expression can vary depending on the choice of force field. A list of terms used in the AMBER force field (the force field utilized in this thesis) is given in Table 2.1.[64, 65]

All bonds and angles are described based by a harmonic oscillator (Hook's law) model according to equations 2.18-2.19, each described by a spring constant (k) and an equilibrium distance (l_0) or equilibrium angle (θ_0). One disadvantage in modeling atom bonding is that this model describes fairly well the potential close to the equilibrium values but deteriorates as the bond stretches and it does not allow bonds to break or form. Equation 2.20 defines the energy as a function of torsion angles by a periodic function, which can be thus reformulated as a Fourier series, with torsion angle ω, periodicity n, and phase γ and force constant V_n.

The Van der Waals interactions are modeled by the Lennard-Jones pairwise potential

Table 2.1: Force-field energy terms: bond energy (E_{bonds}), angle energy (E_{angles}), dihedral energy (E_{dih}), intermolecular Van der Waals energy (E_{VdW}) and electrostatic energy (E_{elec}).

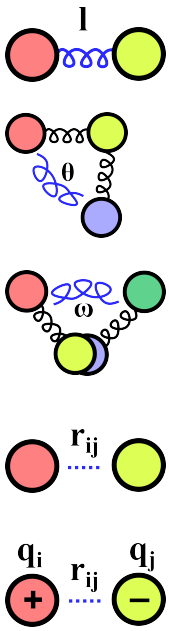

$$E_{bonds} = \sum_{bonds} \frac{1}{2} k_b (l - l_0)^2 \tag{2.18}$$

$$E_{angles} = \sum_{angles} \frac{1}{2} k_a (\theta - \theta_0)^2 \tag{2.19}$$

$$E_{dih} = \sum_{torsions} \sum_{n=1}^{6} \frac{1}{2} V_n (1 + cos(n\omega - \gamma_n)) \tag{2.20}$$

$$E_{VdW} = \sum_{i<j} 4\epsilon_{ij} \left[\left(\frac{\sigma_{ij}}{r_{ij}}\right)^{12} - \left(\frac{\sigma_{ij}}{r_{ij}}\right)^{6} \right] \tag{2.21}$$

$$E_{elec} = \sum_{i<j} \left(\frac{q_i q_j}{4\pi\epsilon_0 r_{ij}}\right) \tag{2.22}$$

(two-body interaction) as defined in equation 2.21, where ϵ_{ij} is the depth of the potential, r_{ij} is the distance between particles and σ_{ij} is the distance where the interaction becomes zero. While the r^{-12} term accounts for the electronic repulsion term that dominates at short distances (the function decay is chosen for computational convenience), the r^{-6} represents the attractive forces at somewhat longer distances (as the London dispersion forces). Due to the characteristics of the Lennard-Jones potential, the interaction energy beyond a certain distance (3σ) becomes negligible. Therefore, a distance cutoff for computing the interaction energy is commonly applied to significantly reduce the computational costs. On the other hand, the electrostatic interactions between two particles with charge, q_i and q_j, at a distance, r, are described by Coulomb's law as expressed in equation 2.22.

2.4 Molecular dynamics

2.4.1 Classical molecular dynamics

From a classical point of view, Newton's equations describe the dynamic characteristics of the system over time. Newton's second law, equation 2.23, relates the force F on

each atom i with the corresponding mass m and acceleration a, which at the same time correlates with the velocity v and the position R.

$$F_i = m_i a_i = m_i \frac{dv_i}{dt} = m_i \frac{d^2 R_i}{dt^2} \tag{2.23}$$

The force depends on the specific interactions between atoms. These interactions are described by the interatomic potential (U), often known as force field. The force is related to U as expressed in equation 2.24.

$$F_i = -\frac{dU(R)}{dR_i} \tag{2.24}$$

Unfortunately, such second-order differential equations, although possible to solve, are particularly complicated to be directly computed for a system of N atoms. Instead, the trajectories can be handled by expressing the velocities and positions as a sum of terms by applying a Taylor series to the differential problem. In the specific case of the Verlet algorithm, expanding R and v in a time step Δt:

$$R(t + \Delta t) = R(t) + v(t)\Delta t + \frac{1}{2} a(t)\Delta t^2 + ... \tag{2.25}$$

$$R(t - \Delta t) = R(t) - v(t)\Delta t + \frac{1}{2} a(t)\Delta t^2 + ... \tag{2.26}$$

$$v(t + \Delta t) = v(t) + a(t)\Delta t + ... \tag{2.27}$$

Assuming that the potential remains constant within the time interval Δt, equation 2.25 and 2.26 can be truncated to the first three terms, and equation 2.27 to the first two terms. By adding both equation 2.25 and 2.26, the atom positions at time $t + \Delta t$ are:

$$R(t + \Delta t) = 2R(t) - R(t - \Delta t) + a(t)\Delta t^2 \tag{2.28}$$

The new set of positions depends only on the past and present positions and the acceleration. The fact that the velocities are not needed to define the trajectories, brings a problem for temperature control since this is kept constant by scaling the velocities. Other alternative models try to address some of the Verlet's drawbacks such as the leap-frog algorithm or the velocity Verlet algorithm.

To avoid nonphysical results, the time step has to be chosen carefully so that the velocities, acceleration, and forces are constant in the time interval. A conservative choice of the time step is to keep Δt significantly smaller than the fastest atom vibration frequency. In the context of most molecular systems discussed in this thesis, hydrogen vibration frequencies, which occur in the range of 10^{-14} s, represent the faster vibrations. Therefore, a typical step size for such molecular systems is 0.5 fs. Reducing the

time step leads to more accurate trajectories, albeit at the expense of increased computational demands. Since hydrogen frequencies are usually the limiting time step, it is a common practice to impose constraints on bonds involving hydrogen atoms during the simulations with the SHAKE algorithm.[66] The time steps with this approximation can be increased to 2 fs. A brief description of a MD workflow is illustrated in Box 1.

Box 1: Molecular dynamics simulations

- To evaluate and track the molecular or atomic motion, the initial positions and velocities of each atom are needed. The set of initial velocities is usually unknown, therefore it is common to start with a set of random velocities following a Maxwell–Boltzmann distribution.
- With the initial information of positions and velocities, the forces can be calculated and subsequently used to find a new set of positions and velocities for the next time, as stated by the integration algorithm.
- This protocol is repeated until the desired simulation time is reached.

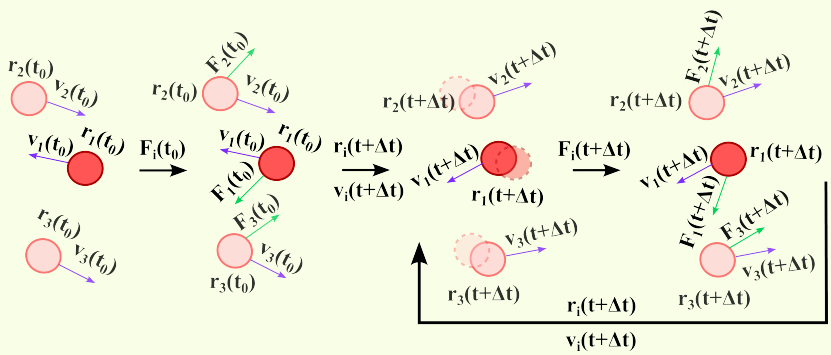

Enlargering the model to a more realistic picture of a macromolecular system is often done by using periodic boundary conditions (PBC). This model introduces periodicity into the system by repeating the simulation box all around, while only the central box is simulated (Figure 2.2). A cutoff for the long-range interaction needs to be considered so that non-physical self-interactions are avoided. An advantage with periodic systems is that electrostatic interactions (the most long-ranged intermolecular interactions) can be exactly estimated by Ewald summation,[67] avoiding any cutoff for such interaction.

The collection of microstates, which corresponds to every single time step of the simulations, belong to a common macrostate, known as an ensemble. There are several ensembles under different macroscopic conditions, constant number of particles (N),

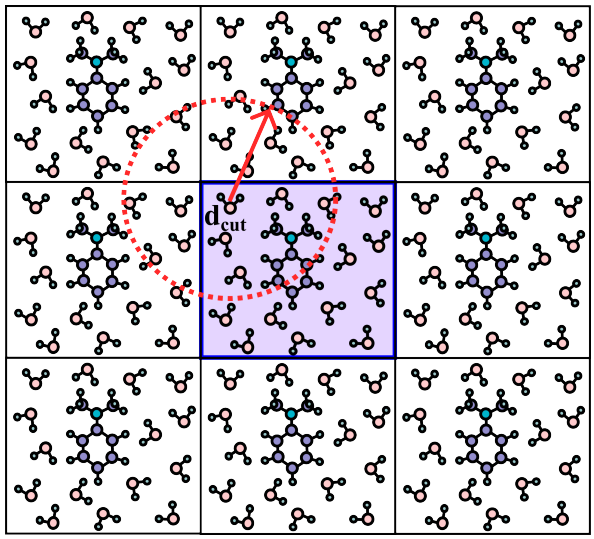

Figure 2.2: Periodic boundary conditions

constant volume (V), constant temperature (T), and constant pressure (P). The most common ensembles, and employed also in this thesis, are the microcanonical (NVE), the canonical (NVT) and isobaric-isothermal (NPT) ensembles.

The temperature of the system is governed by the average kinetic energy, which is at the same time related to the velocity of the particles. If the velocities can be controlled by a scaling factor, the temperature can be regulated and the system approaches a NVT ensemble. A thermostat has been used in the simulations to add or remove energy in the system e.g. the Langevin thersmostat.[68] In analogy to a thermostat, the pressure can also be controlled to achieve an NPT ensemble by using a barostat (e.g. Beredsen barostat), which regulates the volume of the system by scaling the positions of the particles.[69]

2.4.2 Ab initio molecular dynamics

The evolution of a system over time is governed by the time-dependent Schrödinger equation (equation 2.1). The complexity of the problem can be reduced drastically by approximating the motion of the nuclei classically, ruled by Newton's second equation (nuclear motion dynamics as described in the previous subsection), while the electrons are described by quantum mechanics. Hence, the forces and velocities of each atom are derived from the electronic structure calculated by wavefunction methods or DFT.[36, 70, 71] This method is known as *ab initio* molecular dynamics (AIMD). There are two main flavours of this approach; Born–Oppenheimer molecular dynam-

ics (BOMD) and Car–Parrinello molecular dynamics.[72, 73]

In the BOMD, a solution of the time-independent Schrödinger equation to full convergence of the wavefunction is needed at each time step during the simulation frame. On the other hand, in the Car–Parrinello scheme, the wavefunction is propagated along with the nuclear motion, without converging the wavefunction. To properly correlate the electron cloud with the nuclei displacements, the coefficients of the wavefunction or the density matrix elements are treated as variables associated with fictive masses, and the dynamics are addressed by extended Lagrange functions. The equations of motion for the nuclei and electrons assuming that the potential energy surface is described by DFT-KS formalism as:

$$M\frac{d^2R_A}{dt^2}(t) = \frac{dE}{dR_A} \tag{2.29}$$

$$\mu_i\frac{d^2\psi_i}{dt^2}(t) = -\frac{dE}{d\psi_i^*} + \sum_j \lambda_{ij}\psi_j(x) \tag{2.30}$$

where M_A and μ_i are the mass of the nuclei and fictive mass respectively, R_A the nuclear position of atom A, E is the DFT energy, ψ_i are the orbitals, and λ_{ij} is the Lagrange multiplier matrix. Due to the approximated evolution of the nuclear positions and the fast electron dynamics, the time steps are typically chosen shorter than in BOMD. A proper fictive mass variable ensures energy-conservation and the adiabaticity of the system by controlling the kinetic energy exchange between nuclei and wavefunction or density parameters.

2.5 Solvent effects

2.5.1 Continuum-solvation model

Continuum-solvation models are popular for providing a practical solution to macrosolvated systems at an affordable cost.[74, 75] The idea is to represent the solvent implicitly by a continuum potential with the features of the solvent. The most important property is the dielectric constant of the solvent, ϵ. A cavity is made in the solvent to accommodate the system of interest (a transition metal complex or small organic molecules in this thesis). This cavity can be defined by a sphere or any other shape e.g. defined by the Van der Waals surface of the molecule. The contribution of the electrostatic interactions to the solvation free energy is derived from Poisson equations in the surface cavity. Due to the complexity of computing the charge density, a common approximation derives from describing the charge density as a truncated multipolar expansion (charge, dipole moment, ..., etc) minimizing the numerical cost.

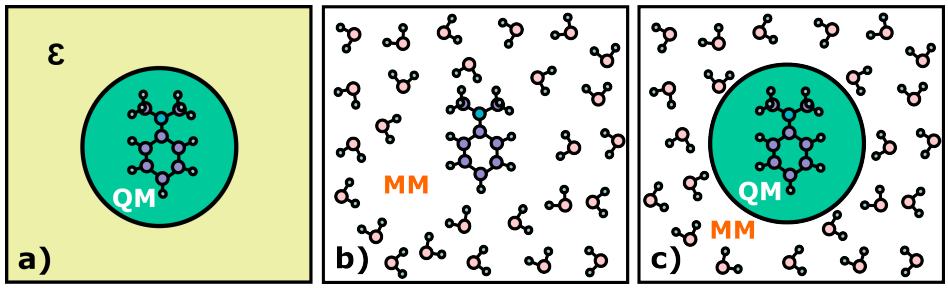

Figure 2.3: Three different approaches to model the solvent in this thesis. (a) Continuum model, (b) MM model, (c) QM/MM model.

In addition to the electrostatics interactions of the system described by the dielectric constant, other interactions between solute and solvent are also of relevance. These includes, for instance, the dispersion, induction, the exchange-repulsion intermolecular interactions, or the cost of forming the cavity. When the solute is treated quantum mechanically, its wavefunction induces polarization in the solvent potential, and conversely, the solvent polarizes the solute's wavefunction. This iterative process resolves the polarization according to the self-consistent reaction field (SCRF) method. The polarizable continuum model (PCM) tries to include the polarization effects as well as dipole moment induction between solvent and solute.[76] This model provides an overall good representation of the solvent at a low computational cost. However, discrete interactions and information on the solvent structure and dynamics are missing.

2.5.2 Quantum mechanics/molecular mechanics

Most chemical systems exist in a solution, and continuum-solvent models do not always adequately capture solvent effects. In this thesis, we have additionally included the solvent explicitly by a full atomistic MM description to recover information regarding the solvent structure around the solute. This provides a fast solution to such a multimolecular system. However, in certain cases, a detailed description of the electronic structure of the solute is necessary. This is the particular case of describing the electron distribution of a radical cation dimer in solution. In such scenarios, the system can be subdivided into a QM part, comprised of the solute, and an MM part, containing the surrounding system (solvent) as illustrated in Figure 2.3. This scenario is commonly referred to as a QM/MM method.[77, 78]

The QM/MM scheme provides detailed information on the solvent structure and discrete, directional interactions of the solvent surrounding the system of interest. The total energy of the system is expressed as the sum of individual energies, which includes the QM energy, MM energy, and QM/MM interface energy. The description of the

QM/MM interface can be complicated to address, and many sophisticated models try to describe the interaction between regions such as electrostatic interactions, dispersion, and exchange-repulsion among others. In this thesis, we have employed the electrostatic-embedding QM/MM approach available in AMBER to incorporate the electrostatic interactions of the MM region into the polarization of the QM part. In this approach, the QM region is polarized by the MM region, while no back-polarization of the MM region is considered.

2.6 Potential energy surface exploration

The potential energy surface (PES) is the energy as a function of all coordinates in the system. In this, many stationary points may exist (i.e. points where all forces vanish). Some of them are of particular interest, such as global and/or local minima as well as saddle points. The multidimensional richness of the PES complicates a straightforward search for these stationary points. Several algorithms are designed to investigate the PES aided by the gradients and the Hessian.[36] The steepest-descendent algorithm as well as the conjugate gradient method are the most general strategies to approximate the search to a minimum based on the gradients. Other algorithms such as the Newton–Raphson methods are furthermore directed by the Hessian (exact or approximate).

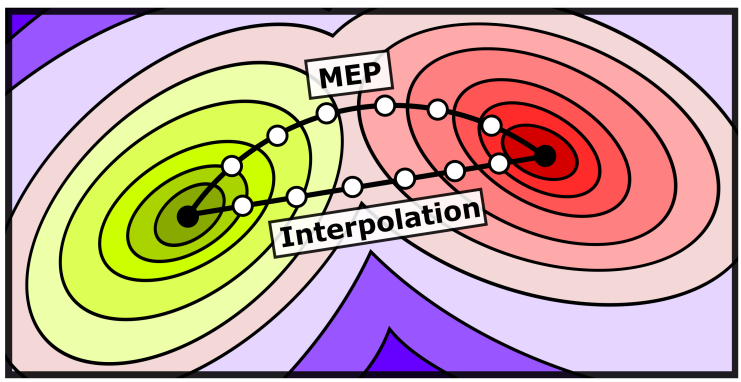

Figure 2.4: Scheme of a potential energy surface. The black curves represent both interpolated path and minimum energy path (MEP).

Often the reaction paths or any connecting path between minima are in the spotlight to explain the intramolecular or intermolecular reactivity or state crossover reactions. The simplest approximation to the minimum energy path (MEP) connecting two minima is to interpolate the initial and final structures, and subsequently calculate its electronic energy (scheme in Figure 2.4). If the reaction coordinate is well defined, the initial path can be minimized with respect to an internal coordinate to get closer to

the real minimum energy path. When the internal coordinate is not readily apparent, alternative procedures can be employed, for instance, the nudged elastic band (NEB) method.[79] The NEB method consists of minimizing several nodes or images of an initial guess path (often an interpolated path) along the PES. To avoid each node being minimized back to the minima states and to keep them evenly distributed, a spring constant is associated between images and the forces parallel to the reaction path are neglected. This is a useful strategy to simply explore MEPs regardless of a defined internal coordinate.

To calculate the free-energy path along a pre-defined reaction coordinate, the umbrella sampling method can be used by establishing a potential with a harmonic constraint so that only a certain part of the potential near the equilibrium position is explored.[80] To sample the path along the internal coordinate, several positions are explored to generate the potential of mean force, with the help of weighted histogram analysis.[81]

Chapter 3

Excited states in transition metal complexes

The excited states of transition metal complexes are characterized by a large variety of potential energy surface and electronic properties.[7, 82] The nature of each electronic transition will depend on the hole-electron availability of each complex, and many distinct type of transitions can be observed in the same molecule.[83] Some of the most typical electronic transitions in mononuclear metal complexes are described in Box 2. UV-vis absorption spectroscopy is a broadly utilized technique to evaluate the excited states profile in multiple chemical systems. The fundamental basis of this technique is the favorable transition dipole moment change (μ_t) induced by the interaction of the molecule with light. Equation 3.1 exemplifies in Dirac notation the terms contributing to the final transition dipole moment, this defined by the initial and final electronic state, ϕ_i and ϕ_f, initial and final spin states, S_i and S_f, and initial and final vibrational states, Θ_i and Θ_f. This expression suggests that any successful electronic transition in a molecule should fulfill three conditions; (i) the electronic transition should involve a change of symmetry (symmetry a.k.a. Laporte selection rules), (ii) the electronic transition should maintain the overall multiplicity of the molecule (spin selection rules), and (iii) the vibrational transition should overlap adequately.

$$\mu_t \approx \underbrace{\langle \phi_i | \hat{\mu} | \phi_f \rangle}_{\text{Symmetry}} \underbrace{\langle S_i | S_f \rangle}_{\text{Spin}} \underbrace{\langle \Theta_i | \Theta_f \rangle}_{\text{Frank-Condon}} \tag{3.1}$$

Box 2: Excited states

- **Metal-to-ligand charge transfer (MLCT) excited states:** it consists of an electronic transition from an occupied metal orbital to a ligand orbital, e.g. from a d orbital to a π^* orbital.
- **Ligand-to-metal charge transfer (LMCT) excited states:** it is the reverse electronic transition compared to MLCT excites states. e.g. from a π orbital to a d orbital.
- **Ligand-to-ligand charge transfer (LLCT) excited states:** it consists of an electronic transition between two orbital from different ligands in the complex.
- **Ligand-centered (LC) excited states:** it is characterized by electron transition between two different orbitals on the same ligand.
- **Metal-centered (MC) excited states:** it comprises states which involve electronic transitions between metal orbitals.

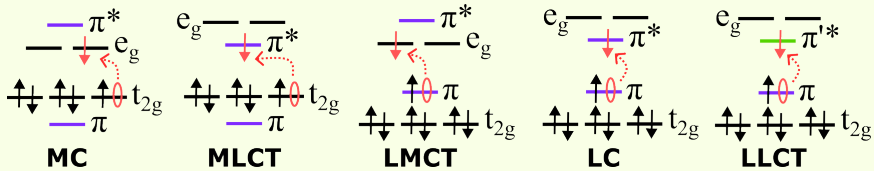

Electronic transitions in a model octahedral metal complex.

Electronic transitions that violate one of these conditions can still occur, however, the overall intensity of the absorption bands becomes significantly weaker. This phenomenon occurs due to vibronic coupling i.e. the symmetry breaks because of the coupling between electronic transition and the molecular vibrations.[7] An allowed electronic transition will depend on the symmetry group of the molecule.[84] For instance, the $\pi \rightarrow \pi*$ transitions are symmetry allowed in metal complexes with octahedral symmetry (O_h), and often yield very intense absorption bands in the spectrum. In contrast, $d \rightarrow d$ transitions are largely weak as there is no change of parity ($g \rightarrow g$). The same electronic transition in a tetrahedral complex (T_d), which has no center of inversion, is Laporte allowed. Therefore, the nature of each absorption band in the spectrum can be evaluated according to the band intensities and the selection rules. A schematic representation of the absorption bands intensity typical in O_h complexes is provided in Figure 3.1. There are many other strategies for elucidating the nature of the excited states. For instance, evaluating the solvathochromic effects, i.e. red- or blue-shifting of the absorption bands under different solvent conditions. Charge transfer states are often more solvent-sensitive than other excited states such as

MC states.[85] However, discerning between charge transfer states (e.g. MLCT and LMCT states) can become challenging. Other assessment tools consist of correlating the optical data with electrochemical measurements. This is based on the similarities of exciting an electron with a simultaneous chemical electron removal and addition e.g. an MLCT transition could be treated in analogy to a combined metal oxidation and ligand reduction reaction.[86]

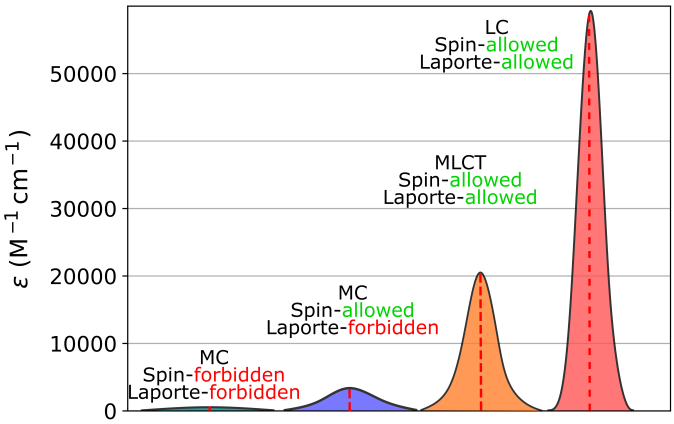

Figure 3.1: Schematic representation of the intensity of absorption bands characterized by different electronic transitions in a hypothetical octahedral complex.

Despite the excited state richness of transition metal complexes, the most relevant photophysics and photochemistry often occur in the lowest-energy excited state. This is motivated by the efficient electronic coupling between states at higher energies, where the state density is significantly higher and the decay *via* internal conversion or intersystem crossing favored.[7] Kasha's rule states that emission events occur from the lowest-lying excited states of a specific multiplicity (except in certain chemical systems such as azulene).[87] The most typical photophysical events are represented in a Jablonski diagram in Figure 3.2, including absorption, fluorescence, and phosphorescence (according to the multiplicity of the emissive state and the ground state). The coordination style, multiplicity, and population of the metal *d*-valence shell are some of the aspects that define the ground state and excited states features; the state energy, electronic structure, and geometry. Transition metal complexes can attain many different coordination geometries, including octahedral (coordination number 6), tetrahedral (coordination number 4), or square-planar (coordination number 4) conformations, among others. In this thesis, we have primarily focused on the first two, the octahedral and the tetrahedral coordination compounds. Ligand-field theory describes the *d*-orbital shell degeneracy break in transition metal ions due to the perturbation of the free metal symmetry after its coordination with the ligands (schematically represented in Figure 3.3).[88] The ordering and energy gap of the five

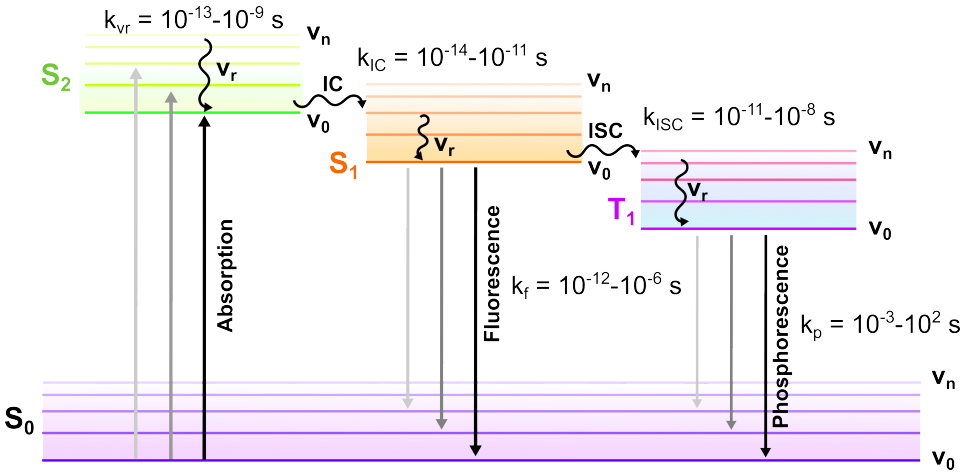

Figure 3.2: Jablonski diagram describing photophysical processes between singlet ground state (S_0) and singlet and triplet excited states ($S_{1/2}$ and T_1). v_r is vibration relaxation, IC the internal conversion, ISC the intersystem crossing. Typical rate ranges for selected processes are also included.[82]

d-orbital (Δ) will depend on the complex symmetry e.g. three degenerate orbitals of t_{2g} symmetry and two degenerate e_g orbitals split in the O_h symmetry, but three t_2 and two e orbitals in T_d symmetry. It is worth noting that the omission of the g subindex defining the orbitals symmetry in a tetrahedral environment is motivated by the absence of inversion symmetry.

Degeneracy of the d-orbitals also results in the occurrence of alternative electronic configurations. For a d^6 complex in O_h symmetry, the electrons can be paired in the lower energy t_{2g} orbitals (low-spin, LS) obeying the Pauli exclusion principle and the Aufbau principle, or first singly occupying the t_{2g} and e_g orbitals (high-spin, HS). Which of these electronic configurations, HS or LS, has the lower energy will depend on whether the energy cost of pairing the electrons in the same orbital (defined by the Racah parameter, B) is higher or lower than the energy gap Δ_o (or Δ_t for T_d) of the crystal field. The tuning of these energy parameters influences the final photophysics of the molecule.[89] The interplay between HS and LS states as well as the factors that affect the energy gap have been broadly investigated in these types of coordination compounds.[90–92]

In addition to the strength of the ligand-field splitting, the occupancy of the d-orbitals is tightly related to the nature of the low-lying excited states of the transition metal complexes. For instance, the nature of the lower-energy excited states of LS d^6 complexes are typically MLCT states in competition with MC states, due to the availability of empty e_g orbitals. On the other hand, the LS d^5 complexes can furthermore present LMCT states at low energies, this promoted by the occurrence of a hole in the t_{2g} level. In other cases, such as LS d^0 complexes, both MLCT and MC states are

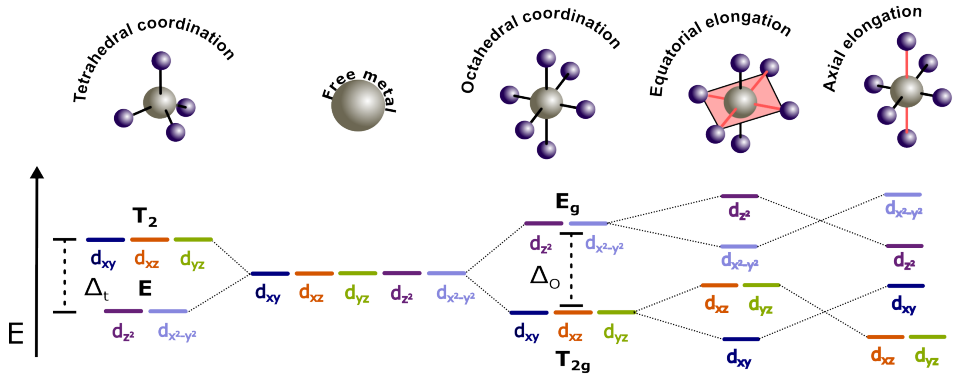

Figure 3.3: (left) Ligand-field splitting of octahedral and tetrahedral complexes. Axial and equatorial stretching Jahn–Teller distortions in octahedral complexes are also illustrated.

absent. These are just a few examples illustrating the tuning effect of the electronic configuration in the excited state diversity of transition metal complexes.[83]

The degeneracy of the d-orbitals can be further exploited upon the population of one of the σ-orbitals, e_g (O_h) or t_2 (T_d), promoting structural distortions in the molecule. This is caused by repulsion between the unpaired electron and the ligand orbitals. The exhibited distortions in the geometry trigger an energy shift between orbitals that were previously degenerate (see Figure 3.3). This effect is known as the Jahn–Teller effect.[88] The population of any of the degenerate orbitals results in the occurrence of different states. The vibronic coupling originated from the interaction between the antisymmetric stretching modes and the e_g orbitals, as well as the bending modes and the t_{2g} orbitals. Thus, three distorted states emerge: two stretching-type distortions and one bending-type distortion for O_h symmetry.[93–95] In T_d symmetry, one stretching-type distortion and two bending-type distortions can be expected.[95–97] Focusing on the popular O_h symmetry, the two stretching distortions are governed by the population of either a d_{z^2} or a $d_{x^2-y^2}$ orbitals. Due to the distinctive monodirectional nature of the d_{z^2} orbital, the geometry is axially elongated along the d_{z^2} lobe direction. In contrast, the bidirectional character of the $d_{x^2-y^2}$ yields four bond elongations in an equatorial fashion distortion (see the orbital representations in Figure 3.3).

Despite that this structural effect has been primarily observed in the ground state of several complexes with O_h d^9 or LS d^7 configurations,[94, 98] active Jahn–Teller distortions can be also observed in complexes with fully empty σ d-orbitals.[99] As a practical case, the excitation of the ground state of a LS d^6 complex in O_h symmetry can feature the electron population of one e_g orbital (MC state), and therefore sev-

eral Jahn–Teller states can be expected in the excited states of these transition metal complexes.[100–102]

Chapter 4

Tuning the photophysics of metal complexes

Research of transition metal complexes with light-harvesting applications has been primarily focused on developing HS d^6 complexes based on Ru(II) and Ir(III) transition metals in coordination with polypyridine ligands.[7, 16] Among all investigated transition metal complexes, $[Ru(II)(bpy)_3]^{2+}$ might have become the most popular and widely used photosensitizer, target of multiple studies.[103–105] The reasons are (i) good stability and photostability, (ii) easy synthesis or commercial availability, and (iii) long-lived and highly energetic excited states.

The $[Ru(II)(bpy)_3]^{2+}$ (bpy = 2,2'-bipyridine) complex strongly absorbs light in the visible range of the spectra (maximum absorption at 452 nm with an extinction coefficient of ϵ = 1.5 x 10^4 $M^{-1}cm^{-1}$ in acetonitrile) which maximizes the capture of energy.[106, 107] The photon absorption in this Ru complex (similar to many other Ru(II) derivatives) triggers an electron transition from the fully occupied t_{2g} orbital to an empty e_g orbital, resulting in a singlet ^{1}MLCT state.[104, 108] Assuming the Frank–Condon approximation, which states that the absorption of the photon is much faster than the overall geometry relaxation, the electron transition is vertical on the PES (fix nuclei). This implies that, as observed in the Jablonski diagram introduced in Figure 3.2, the excitation can potentially populate high-energy vibrations, and subsequently relax to the lowest-energy vibration.[7] Studies on the early dynamics of $[Ru(II)(bpy)_3]^{2+}$ have shown that the populations of the lower-lying ^{3}MLCT, including intersystem crossing, occurs in less than a picosecond.[109]

One advantage of utilizing transition metal complexes over other light harvesters based on only organic elements is the population of higher spin states.[108, 110, 111] The

central metal in the complex induces the so-called heavy-atom effect or the weakening of the bonds,[112] which boosts the spin-orbit coupling efficiency and therefore intersystem crossing dynamics. The primary advantage of higher multiplicity states (compared to the ground state) is that the electron transition from the excited state to the ground state is spin-forbidden i.e. hindering non-radioactive decay and presumably enhancing the excited state lifetimes.[82] Hence, the population of the $[Ru(II)(bpy)_3]^{2+}$ ^{3}MLCT excited state *via* the ^{1}MLCT is fast, and the charge transfer state lives long enough to be utilized in many photophysical and photochemical applications.[104, 108, 113, 114]

Box 3: $[Ru(II)(bpy)_3]^{2+}$ versus $[Fe(II)(bpy)_3]^{2+}$

The $[Ru(II)(bpy)_3]^{2+}$ complex is a popular example showcasing the relevance of the ligand-field splitting strength in the intrinsic photophysics of transition metal complexes. This d^6 Ru-polypyridine complex exhibits phosphorescence and lifetimes of $\sim$ 1 μs from a ^{3}MLCT state.[113] However, the same octahedral coordination and ligand in the isoelectronic Fe(II) counterpart yield a complex with no long-lived ^{3}MLCT state. The weaker ligand-field is caused by the less efficient valence-d orbital overlap with the ligand orbitals i.e. a 3d orbital of the first-row in the transition-metal block is less voluminous compared to a 4d orbital in the second-row.[115] This effects is popularly known as the "primogenic" effect. As a consequence, the MC states of both triplet and quintet multiplicities are displaced to lower energies in the PES, favoring a fast excited states deactivation cascade back to the ground state.[116–118] The ground state recovery from the ^{5}MC occurs in $\sim$ 600 ps.[119]

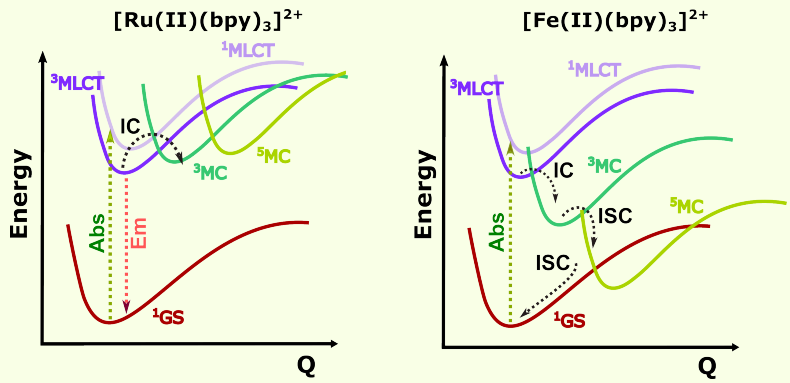

However, particular attention is given nowadays to the replacement of noble metals by earth-abundant transition metals, turning the light conversion into a completely environmentally friendly process. Recent research in earth-abundant transition metal complexes with light-harvesting applications have explored the capabilities of transi-

tion metals of the first row such as Cr, Mn, Fe, or Co.[11, 12, 120, 121] However, a bottleneck of utilizing earth-abundant transition metals is the fast excited state deactivation, typically through MC states, as occurs in the $[Fe(II)(bpy)_3]^{2+}$ complex (see Box 3).[110, 111, 122] Therefore, designing metal and ligand combinations that provide optimal physical properties for a functional photosensitizer are in the spotlight.[123–126]

Iron has emerged as the most promising alternative for ruthenium complexes, motivated by its large abundance in the Earth's crust.[127–129] Iron complexes typically have an HS ground state, or occasionally HS states comparable in energy to the LS ground state. These HS states can achieve long-lived lifetimes, and therefore the spin-crossover reaction to the LS ground state has been widely studied experimentally and computationally.[90, 91, 130] However, the modest driving energy gained by the population of a ligand-field state through photon absorption is often insufficient to trigger reactions. In addition, charge transfer states are often desirable in DSSC devices since they enhance the efficiency of the electron injection into the semiconductor layer.[23] Therefore, molecular design of d^6 Fe complexes generally aims for maximizing the ligand-field splitting between e_g and t_{2g} orbitals. In the box below, a few approaches are listed.

Designing photofunctional complexes

Among the most popular strategies to accommodate efficient and stable long-lived charge transfer states[10, 123, 128, 129, 131]:

- **Including strong σ donating interactions**, which accentuate the destabilization of the e_g orbital.
- **Including $\pi*$-backdonation interactions** increases the stabilization of the t_{2g} level.
- **Designing highly octahedral ligand architectures** maximizes the Δ_o energy gap between e_g and t_{2g} orbitals.
- **Tuning the metal oxidation state**, by shifting the d-orbitals with respect to the ligand orbitals.
- **Increasing the ligand rigidity** reduces the excited state distortions.

Sweden has for decades owned and exploited the largest iron reserves in Europe. Their particular interest in iron has been also extended to molecular design. In 2018, Chábera *et al.* reported the first functional iron-based photosensitizer. The tris-bidentate $[Fe(II)(btz)_3]^{2+}$ (btz = 3,3'-dimethyl-1,1'-bis(p-tolyl)-4,4'-bis(1,2,3-triazol-

5-ylidene)) complex, which has a d^6 configuration, featured a 528 ps excited state lifetime aided by the N-heterocyclic carbene (NHC) ligands (see Box 4).[131, 132] The strong ligand-field imposed by the NHC σ-donation enhances a LS ground state and a low energy ^{3}MLCT excited state, in contrast to many Fe(II) complexes, which adopt HS configurations and several lower-lying MC states.[91, 131, 133, 134] The extended lifetimes of the hexa-carbene $[Fe(III)(btz)_3]^{3+}$, compared to its tetra-carbene parent $[Fe(II)(bip)_2]^{2+}$ (bip = 2,6-bis[imidazol-2-ylidene]pyridine), provides clear evidence of the NHCs impact on the ligand-field strength.[135] See chemical structures in Figure 4.1. Surprisingly, the oxidized analogue $[Fe(III)(btz)_3]^{3+}$, showcased a long-lived ^{2}LMCT excited states (100 ps), but particularly exhibiting the first observed luminescence from a Fe complex.[136] The success of $[Fe(III)(btz)_3]^{3+}$ has prompted a lot of research towards new ligand designs for d^5 iron complexes.[133]

Box 4: N-heterocyclic carbenes

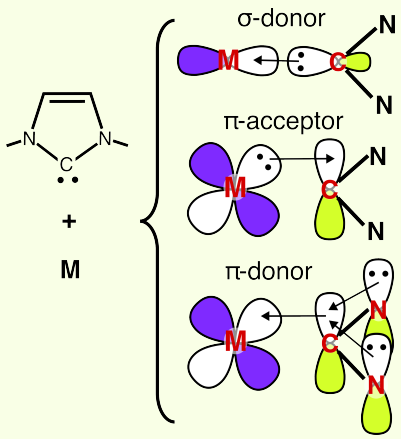

The coordination of a transition metal complex with NHC ligand involves three interactions showing stronger to weaker contributions to the final bonding. σ-donation from the lone pairs of the carbene to an empty σ-orbital of the metal, in octahedral complexes associated with e_g orbitals, is the strongest interaction. π-bonding with occupied metal orbitals can occur aided by π-accepting bonding through the carbene empty p-orbital, or π-donating binding *via* electron-rich neighbouring Ns.

4.1 Iron complexes as sustainable photosensitizers

Further improvement of the ^{2}LMCT excited state lifetimes was accomplished by the $[Fe(III)(phtmeimb)_2]^+$ (phtmeimb = phenyl[tris(3-methylimidazol-1-ylidene)]borate) complex, which not only achieves 2 ns lifetime but also luminescence.[137] On one hand, the NHC provides strong σ-donation while the scorpionate architecture ensures a rigid octahedral geometry (Figure 4.1). On the other hand, the negative charge arising from the boron atoms included in the phtmeimb ligand offers additional σ-donation strength to increase the ligand-field, as well as stabilizing the higher oxida-

tion state of the metal.

The excitation of the $[Fe(III)(phtmeimb)_2]^+$ complex (at 502 nm) and its subsequent luminescence (at 655 nm) occurs from the same ^{2}LMCT state, which is supported by the minor Stokes' shift of 0.58 eV. It also indicates a minor geometry distortions between ground and excited state.[138] Therefore, the direct excitation to the same emissive state has the advantage of minimizing the energy loss through internal conversion or intersystem crossing. Temperature-dependent spectroscopy measurement (included in paper V) of the ^{2}LMCT state revealed the non-radiative decay to the ground state as the main deactivating pathway. The ground state recovery is potentially favored by the spin-allowed nature of the transition since both the ground and the excited state are doublets. The intersystem crossing to ^{4}MC states was discarded as the main deactivation channel, in contrast to the active role of ^{3}MC states in d^6 Fe(II) complexes. Due to the occurrence of an empty hole among the t_{2g} states $[(t_{2g})^5]$, a manifold of near degenerate states emerges. Vertical excitations calculated by TD-DFT revealed that the most intense electron transition from the ground state occurs to the second excited state of ^{2}LMCT nature. Therefore, the luminescence from the lowest-energy ^{2}LMCT could also unfold in any of the three near degenerate ground states, depending on the transition dipole moment.

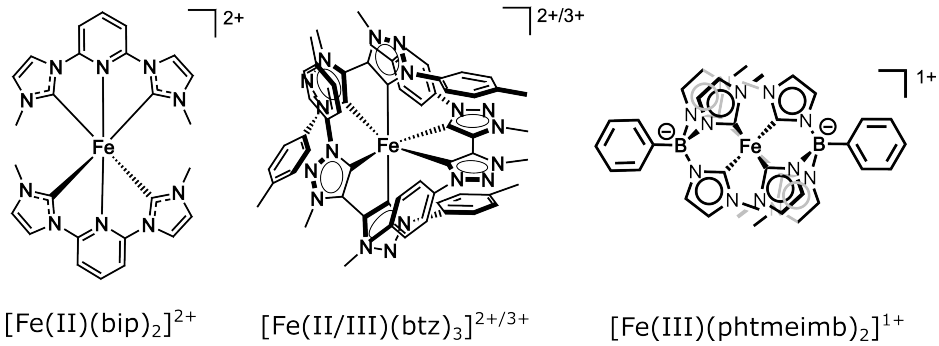

Figure 4.1: A series of iron complexes. (left) $[Fe(II)(bip)_2]^{2+}$, (middle) $[Fe(II/III)(btz)_3]^{2+/3+}$, (right) $[Fe(III)(phtmeimb)_2]^{+}$.

Another case with a long-lived ^{2}LMCT excited state was observed for the $[Fe(III)(imp)_2]^+$ (imp = bis(2,6-bis(3-methylimidazol-2-ylidene-1-yl)phenylene)) complex, with a ^{2}LMCT state with 240 ps of lifetime.[139, 140] Similarly, emission from a ^{2}LMCT has been observed in a Fe (III) heteroleptic complex, although with a shorter lifetime (80 ps).[141] Up to date, more photofunctional Fe(III) complexes have been reported than for the Fe(II) analog. The different electronic structure and excited state profile of d^5 complexes compared to d^6 complexes could potentially explain the success of Fe d^5 complexes.[131, 133] While the transition between ^{4}MC states and ^{2}LMCT states in d^5 systems is spin-forbidden, the same transition involving the ^{3}MLCT and ^{3}MC states

in d^6 complexes is spin-allowed. Therefore, the slower intersystem crossing dynamics between ^{2}LMCT and ^{4}MC states could favor longer excited state lifetimes. However, the doublet-to-doublet non-radiative decay to the ground state can be at the same time favored and particularly affected by the energy difference amount according to the energy gap law (see box below).

The energy gap law

An exponential relationship between the energy gap, i.e. energy difference corresponding to the emission energy, and the non-radiative decay rates is known as the energy-gap law (equation 4.1). It has been observed in organic dyes and transition metal complexes that increasing the vertical energy separation decreases the non-radiative decay rates. This effect is supported by the better vibrational overlap as the states align. Therefore, it is often expected that vibrations of high energy should behave as the acceptor modes. These are mainly comprised C–H vibrations (typical in organic molecules and metals ligands). However, other vibrations of the type C–C, C–O, and N–H have also been observed to contribute to the non-radiative decay. The energy gap law has been confirmed in complexes with LMCT and MLCT excited states.[142–144]

$$k_{nr} \propto e^{E_{gap}} \tag{4.1}$$

4.2 From scavengers to functional states: ^{3}MC excited states

The undesirable effect of MC states has been discussed on multiple occasions in this thesis for the occurrence of long-lived charge transfer states in first-row transition metal complexes. However, the general role of MC states as scavengers has been drastically revised after the report of a long-lived and weakly emissive ^{3}MC from a d^6 cobalt complex. In paper **I**, spectroscopy investigations of the $[Co(III)(phtmeimb)_2]^+$ complex revealed absorption bands significantly displaced towards the UV region. One band is found at 250 nm (ε = 18000 $M^{-1}cm^{-1}$) and a second band at 310 nm (ε = 400 $M^{-1}cm^{-1}$). Both absorption features were associated with regular absorption intensities of charge transfer states, while a weak absorption tail in the far visible was attributed to d-d transitions. The direct excitation of any of these electronic bands results in weak emission at 690 nm, associated with a triplet state according to energy transfer studies with $^3O_2$. Since energy transfer to form $^1O_2$ is allowed when the quenched excited state is a triplet, which discard a quintet excited state. Time-resolved spectroscopy measurements quantified excited state lifetime on the order of 1 μs.

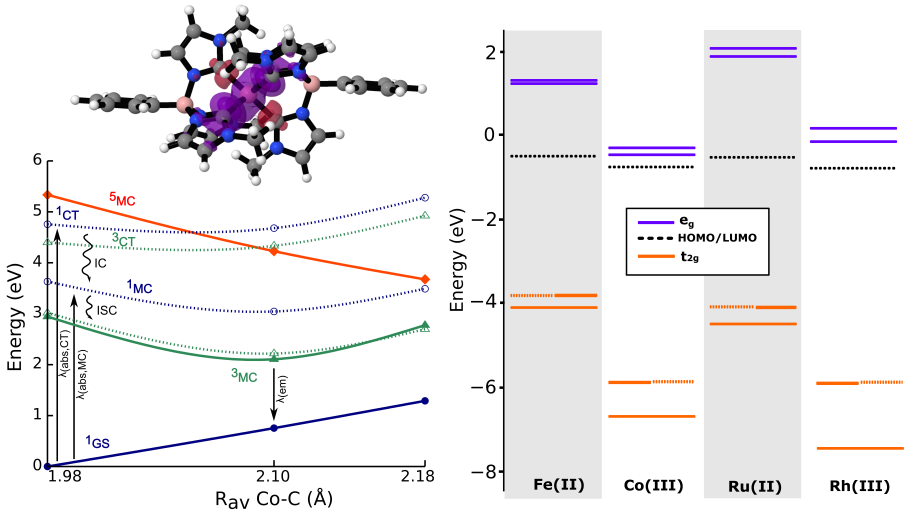

Figure 4.2: (left) Singlet and triplet potential energy surface of the $[Co(III)(phtmeimb)_2]^+$ complex with respect to the average metal-ligand bonds (R_{av}) and spin density of the ^{3}MC state (right) HOMO-LUMO frontier for the $[M(phtmeimb)_2]^{(n-2)+}$ (M(n) = Fe(II), Co(III), Ru(II) and Rh(III)) transition metal complex series.

DFT and TD-DFT calculations (B3LYP*/6-311G(d,f)/PCM(acetonitrile)) of the singlet and triplet PES of $[Co(III)(phtmeimb)_2]^+$ complex (left panel in Figure 4.2) disclose an intense singlet-singlet vertical excitation to a charge transfer state at $\sim$ 260 nm. d-d electron transitions associated with ^{1}MC states were observed at significantly lower energies ($\sim$ 400 nm). As the spectroscopy measurements suggest intersystem crossing and population of a triplet excited state after excitation, the geometry optimization of the triplet PES revealed that the lowest-energy excited state has a ^{3}MC nature. These findings agree with the calculated weak emission signal. This is further supported by the similar photophysical properties of a prototype Co(III) complex reported in the late 70s, $[Co(III)(CN)_6]^{3+}$, whose absorption spectra lie in the UV region and the emission was attributed to phosphorescence from a ^{3}MC excited state.[145] Despite the fascinating atypical physical properties of these cobalt complexes,[121, 146, 147] the absence of any light absorption in the visible spectrum of this complex proves to be its most significant weakness for light-harvesting applications.

4.2.1 Metal oxidation state tuning

Although these $[Co(III)(phtmeimb)_2]^+$ complex in paper **I** is structurally similar to the corresponding Fe(III) complex and isoelectronic to many other Fe(II) complexes, the photophysics of the MC state in this cobalt complex is unique. With the aim to

disentangle the features that define the excited states properties of this complex, we have conducted comparative DFT studies in paper **II** for the transition metal series: Fe(II), Co(III), Ru(II), and Rh(III) complexes. On one hand, we analyzed the effect of increasing the metal oxidation state by comparing the two isoelectronic pairs Fe(II) and Co(III) or Ru(II) and Rh(III). On the other hand, the ligand-field strength effects from first-row metals to second-row metals were also outlined.

Electronic structure analysis of the Fe(II), Co(III), Ru(II), and Rh(III) complexes show distinct highest occupied molecular orbital (HOMO) and lowest occupied molecular orbital (LUMO) energy gaps, see the right panel in Figure 4.2. The overall effect of replacing e.g. Fe(II) by Co(III) is an energies shift of the d-orbital set by $\sim$ 2 eV. On the other hand, the energy of the ligand π-levels remains steady, which agrees with the observed HOMO-LUMO trend. High oxidation states promote the accumulation of positive charge in the central metal, stabilizing the electrons of the valence shell of the metal. This *d*-orbital shift drastically affects the optical properties of these complexes. For instance, the UV-vis absorption spectra for Fe(II) and Ru(II) are observed at the 350-450 nm range, while for Co(III) and Rh(III) they are blue-shifted to $\sim$ 230 nm. TD-DFT absorption spectra were analyzed, and the nature of each electron transition is illustrated in Figure 4.3 for Fe(II) and Co(III). The oxidation state tuning also influences the PES of the four complexes. While two charge transfer states were identified among the low-energy excited state manifold of the Fe(II) complex and Ru(II), none were observed for Co(III) and Rh(III) complexes.

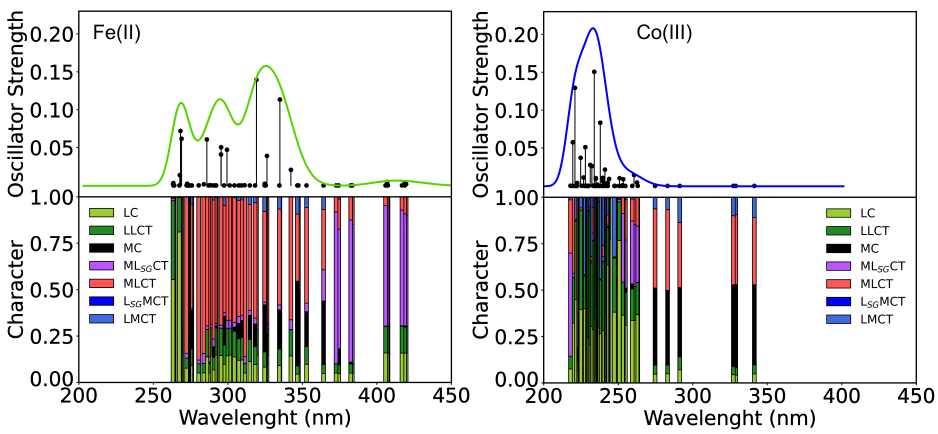

Figure 4.3: Calculated UV-vis absorption spectra for (left) Fe(II), (right) Co(III) complexes, and vertical electronic transitions analysis. ML$_{SG}$CT denotes a MLCT involving the ligand side groups.

A near degeneracy of the ^{3}MC excited state with the singlet ground state in the Fe(II) complex contrasts with the significant vertical energy gap ($\sim$ 1.4 eV) observed in the Co(III) isoelectronic complex. Surprisingly, the electronic properties tuning also combines with structural modifications. The metal-ligand bonds of the ^{3}MC relaxed

geometry are predicted to be more expanded in the Fe(II) version if compared with the analogous Co(III) state (two bonds stretched by 0.2 Å). The geometry compression of the ^{3}MC excited states in the Co(III) complex, and lower energy losses of the excited state, is associated with stronger electrostatic interactions with the ligand. Therefore, the combination of charge and strong σ-donation associated with the NHC-ligand provides the characteristic MC of this long-lived Co complex. In contrast, the feasible ^{3}MLCT-^{3}MC transition (estimated activation barrier of $\sim$ 0.01 eV) and the similar ^{3}MC-^{1}MC state balance indicate a favorable excited state non-radiative decay.

One feature in charge transfer states e.g. LMCT and MLCT states, is the minimal energy loss after excitation. This is motivated by the subtle distortion along the internal coordinate, only slightly influenced by the weak Jahn–Teller effect.[110] In contrast, a ^{3}MC state shows significant structural distortions in the internal coordinates promoted by the $^*\sigma$-bonding of the e_g orbital set. As briefly introduced in Chapter 3, different possible electron excitations to any of the e_g orbitals promote the occurrence of multiple near degenerate states. These states are characterized by axial or equatorial geometry distortions. For complexes like $[Co(III)(phtmeimb)_2]^+$, which lacks a perfect octahedral symmetry, more than two distinct distorted states can be expected. We have identified two distinct ^{3}MC states with similar adiabatic energies in this Co(III) complex. Both ^{3}MC states were observed to adopt axial-type elongations (metal-ligand bonds achieving 2.26 Å). However, the third axial state was not localized, owing to steric effects imposed by the planar phenyl groups (see chemical structure in Figure 4.1). Therefore, the side group in the phtmeimb ligand imposes steric constraints to the accessible triplet PES, offering further tuning opportunities in these complexes.[10] The constrained PES can potentially reduce non-radiative decay channels and the vibrational coupling with the ground state.

Paper **II** also includes redox potential calculations to assess the driving forces tuning for the studied metal series. The general effect is that Co(IV/III) and Rh(IV/III) redox potentials are more positively shifted by 0.5 V compared to the Fe(III/II) and Ru(III/II) redox potentials. The redox potential trend correlates with the d-orbital shift. Furthermore, the calculations illustrate that both the iron and the cobalt complexes adopt the natural oxidation state of III, as experimentally observed in paper **I** and other studies.[137] Therefore, we further predicted that both ruthenium and rhodium complexes adopt the same oxidation state of III.

4.3 Interplay between ^{3}LC and ^{3}MC excited states

Functional ^{3}MC states have previously also been observed for a series of Rh(III) complexes.[148] The transition metal complex $[Rh(III)(phen)_2(NH_3)_2]^{3+}$ (phen =

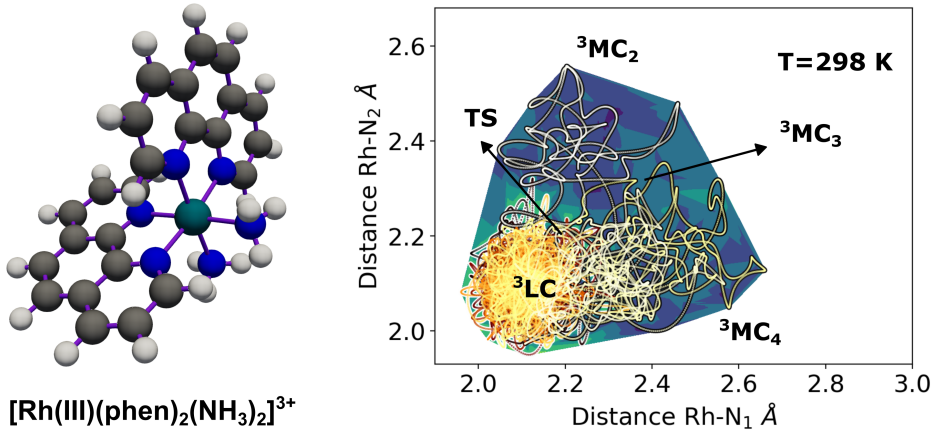

Figure 4.4: (left) Chemical structure of $[Rh(III)(phen)_2(NH_3)_2]^{3+}$ (right) Trajectory contour plot showing the accessible area in term of Rh-N bond distances of a set of the LC, and MC states, as well as the crossover transition state (TS) at the temperature of 298K.

1,10-phenanthroline) is a particular case, together with the $[Rh(III)(phen)_3]^{3+}$ parent complex, which exhibits dual emission from two states, ^{3}LC and ^{3}MC.[149, 150] Indelli *et al* investigated a series of three complexes with tuned ligand-field strengths to investigate the effect of the energy balance between ^{3}LC and ^{3}MC states in the luminescence properties of the complex.[151] While the $[Rh(III)(phen)_2(CN)_2]^+$ complex showed a sharp intense emission spectrum, the $[Rh(III)(phen)_2(NH_3)Cl]^{2+}$ spectrum was very broad and weak. The distinct luminescence data reflects the different origins of the emission and how the stabilization or destabilization of the ^{3}MC state can hinder or favor its population and emission.

With the aim to further investigate intramolecular energy transfer processes beyond the classical one-electron transfer ^{3}MLCT $\rightarrow$ ^{3}MC crossover reaction in the popular $[Ru(II)(bpy)_3]^{+2}$ complex,[134, 152, 153] we focused our attention on the description of a two-electron process involving a ^{3}LC $\rightarrow$ ^{3}MC transition in the peculiar $[Rh(III)(phen)_2(NH_3)_2]^{3+}$ complex (chemical structure in Figure 4.4). The equilibrium and interstate dynamics from the primarily populated ^{3}LC state after relaxation were addressed by *ab initio* molecular dynamic simulations in paper **III**.

While the early study of the local dynamics of the ^{3}LC state reveals a highly localized electronic structure, the ^{3}MC state was untangled with a manifold of various MC states with distinct structural distortions. Temperature-dependent investigations were performed to clarify the dynamic conversions between the variuos ^{3}MC states. The two low-energy ^{3}MC states, with similar Jahn–Teller equatorial-type distortions, establish a crossover equilibrium *via* an intermediate ^{3}MC state of higher energy and axial distortion. AIMD outcomes outlined the multitude of states and the multi-

dimensionality of the potential energy landscape beyond a local and fundamental analysis of the fully relaxed states.

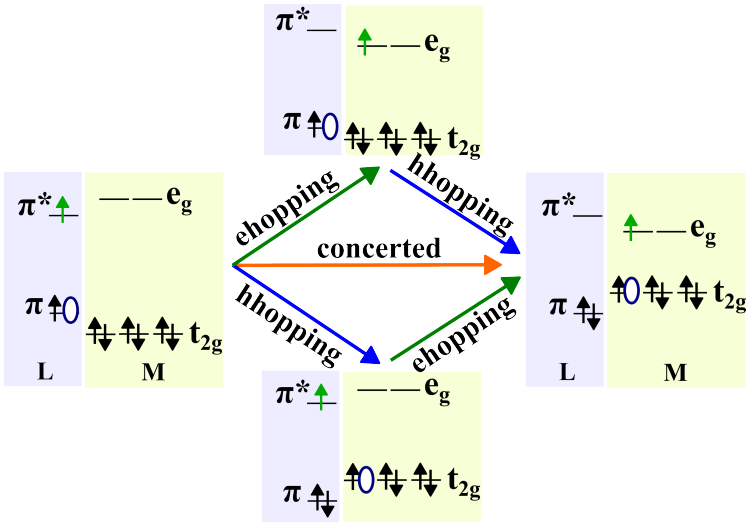

Figure 4.5: Two-electron transfer mechanisms in a ^{3}LC $\rightarrow$ ^{3}MC crossover reaction. Green arrows represent electron hopping (ehopping) and blue arrows hole hopping (hhopping).

The AIMD crossover ^{3}LC $\rightarrow$ ^{3}MC reaction dynamics results reinforce the interplay between the often neglected higher-energy excited states with the lower-energy states in the interstate conversion in a step-wise ^{3}LC deactivation mode (Figure 4.4, right panel). Furthermore, the crossover reaction entropy (ΔS_r) was quantified in terms of the accessible volume of each of the excited states (V_{MC} and V_{LC}) in the triplet potential energy surface according to equation 4.2, where k_b is the Boltzmann constant. The entropy was calculated to be 42 J/K.mol, which indicates that the particular metal-ligand distortions of the MC states contribute significantly to the entropy.

$$\Delta S_r = k_b \ln\left(\frac{V_{\mathrm{MC}}}{V_{\mathrm{LC}}}\right) \tag{4.2}$$

The two-electron ^{3}LC $\rightarrow$ ^{3}MC crossover reaction can proceed *via* three alternative mechanisms: one concerted and two step-wise pathways (Figure 4.5). The concerted mechanism consists of the simultaneous transfer of electrons from the ligand to the metal. In contrast, the step-wise mechanism progresses by first an electron hopping from the ligand and subsequent a hole hopping, or *vice versa*. An analysis of the electronic structure in the vicinity of the energy transfer transition reveals a concerted mechanism for the two-electron reactions. More details in paper **III**.

4.4 Evading MC states: ^{3}LMCT excited states in d^0 complexes

In previous discussions, two distinct perspectives regarding metal-centered excited states were outlined: as scavengers or as functional states. An alternative excited states profile is the complete absence of MC states, a typical scenario for metal complexes with an empty d-shell i.e. adopting a ground state d^0 electronic configuration. This electronic configuration is observed frequently among transition metal complexes belonging to the III and IV groups of the transition block of the periodic table.[83, 120] Popular examples of d^0 complexes are titanocenes with oxidation number IV and scandocenes with oxidation number III.[154–159] Despite that MC states are absent in the excited state landscapes in these systems, the empty d-shell can behave as an electron acceptor, in LMCT excited states, in a way similar to what was described previously for Fe(III) d^5 complexes. In contrast to Fe(III) complexes, titanocenes and scandocenes adopt singlet ground states, and after electron excitation, ^{3}LMCT excited states are often populated. Therefore, the electron transitions from the ^{3}LMCT state to the ground state is spin-forbidden, motivating the fact that scandocenes can reach μs of lifetime while $[Fe(III)(phtmeimb)_2]^+$ and $[Fe(III)(btz)_3]^{2+}$ complexes have instead lifetimes in the ns time range.[136, 137, 159]

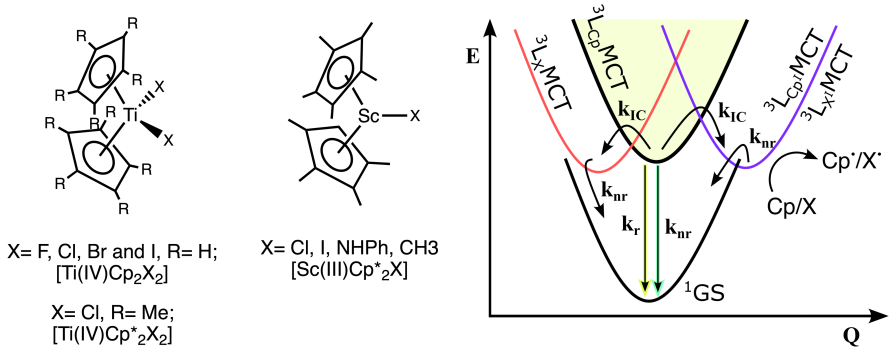

Figure 4.6: (left) Chemical structure of a series of titanocenes and scandocenes. (right) Schematic representation of the excited states of titanocenes.

The most notorious disadvantage of utilizing titanocenes for light harvesting is their low stability and photostability.[160–162] Some titanocenes, for instance $[Ti(IV)Cp_2X_2]$ (Cp = cyclopentadienyl) (X = F, Cl, and Br), feature long-lived lifetimes from a ^{3}LMCT state in solid state, albeit suffering an efficiently excited state deactivation in solution at room temperature.[163] In contrast, the isoelectronic scandocenes are luminescent in both solid and solvent states (see structures in Figure 4.6).[163] Previous investigations on halogenated $[Ti(IV)Cp_2X_2]$ (X = F, Cl, Br, and I) titanocenes observed the favorable photoinduced bond homolysis, either by Ti-Cp or Ti-X rup-

ture.[161, 164] Among the titanocenes series, [Ti(IV)Cp_2F_2] and [Ti(IV)Cp_2Cl_2] feature the most long-lived excited states in solid state (730 μs), while [Ti(IV)Cp_2I_2] was non-emissive and short-lived.[163] Despite the similar electronic structure of titanocenes and scandocenes, it is unclear why the titanocenes are so unstable in solution.

With the aim to reveal the multiple deactivation pathways of the luminescence of titanocenes, DFT and TD-DFT calculations were conducted and collected in paper **IV**. The PES exploration for the [Ti(IV)Cp_2X_2] (X = F, Cl, Br, and I) series revealed the occurrence of four distinct states on the lowest-energy triplet surface (see scheme in Figure 4.6). Among them, two states adopt structural distortions associated with ligand bending, significantly more distorted involving the halogen ligands. For instance, the Cl-Ti-Cl folded state of [Ti(IV)Cp_2Cl_2] is compressed by $\sim$ 30 degrees with respect to the ground state geometry. On the other hand, the two remaining ^{3}LMCT states feature an intense metal-ligand stretch, these distortions promoted by the strong σ^* bonding interaction. This is further supported by the analysis of the electronic structure, in which the alpha singly occupied molecular orbital ($^\alpha$SOMO) of the partial Cp dechelation contains significant contributions from the metal d-e orbitals (more than 50 %). This state is therefore associated with the homolysis bond cleavage.

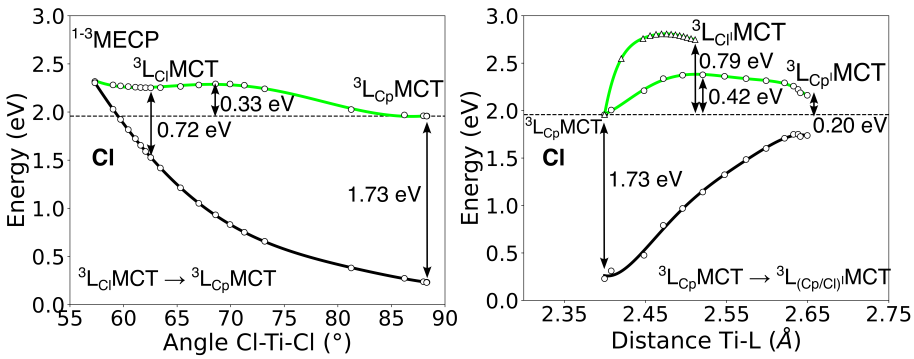

Figure 4.7: Minimum energy paths (left) between the emissive state ($^3L_{Cp}$MCT) and the folded state ($^3L_{Cl}$MCT) with respect to ligand-Ti-ligand angles, (right) between $^3L_{Cp}$MCT and bond cleavage ($^3L_{Cp^I}$MCT and $^3L_{Cl^I}$MCT) states with respect to the average metal-ligand bonds (Ti-L) in [Ti(IV)Cp_2Cl_2] complex.

Calculations of emission energy from the four ^{3}LMCT revealed that the emissive state corresponds to the weakly Cp-bended excited state. We have found a good agreement between DFT calculations at the TPSSh/def2-TZVP level and experiments, achieving mean absolute errors of $\sim$ 0.01 eV. Exploring the minimum energy path connecting the low-lying ^{3}LMCT excited states shows the feasible population of the halogen-folded ^{3}LMCT in the dichlorine and dibromide titanocenes. Accessing the folded

state from the emissive state only requires 0.1-0.3 eV, which competes with the side homolysis bond cleavage ($\sim$ 0.4 eV) (see Figure 4.7). This distorted state can facilitate the ground state recovery according to the minimal energy differences with the ground state surface (0.5-0.7 eV). The absence of these highly distorted states in the scandocene parents supports the possible scavenging nature of these ^{3}LMCT excited states. Therefore, the overall state balance associated with folding and stretching distortions favors luminescence, non-radiative decay, or ligand radical formation. Furthermore, these results also show that even LMCT excited states can have undesirable effects on the optical properties of transition metal complexes.

Chapter 5

Photochemistry of metal complexes

The photophysical properties of transition metal complexes are also relevant for their final photochemical properties and applications.[16] The energy inserted into the molecule by the absorption of a photon may increase the driving forces toward chemical transformations.[7, 82] One of the advantages of driving reactions in the excited states is the characteristic shallower PES compared to the ground state landscape. Reactions with high activation barriers in the ground state can become almost barrierless in the excited state. For instance, in photoinduced isomerization reactions in 2-butene.[138] However, photochemistry not only applies to intramolecular transformations but also to intermolecular reactions.

An advantage of utilizing transition metal complexes over organic photosensitizers for redox reactions is the presence of two redox sites, the metal and the ligand.[7] Since both reduction and oxidation potentials lie in a similar energy window, the metal complex can behave as both a reductive and oxidative agent, depending on the redox partner. Bimolecular photoinduced electron transfer occurs when electrons are transferred between donor and acceptor molecules, and this is triggered by light. The additional energy harvested by the photosensizer increases its redox power, turning it into a better electron donor and electron acceptor. For a test case such as $[Ru(II)(bpy)_3]^{2+}$, the population of the lowest energy and long-lived ^{3}MLCT excited state promotes an empty hole in the t_{2g} shell, and an unpaired electron in a high-energy π^* orbital. Hence, the presence of a donor molecule triggers an electron transfer to the empty hole of the photosensitizer. In contrast, the presence of an acceptor molecule triggers the transfer of the excited electron from the PS to an empty energy level of the acceptor molecule (scheme shown in Figure 5.1). In analogy to MLCT states, LMCT excited states are also useful for driving reactions.[165] The occurrence of a hole in a ligand π-orbital promotes strong driving forces towards photoxidation, as has been

recently investigated in Fe(III) complexes.[166] These electron transfer reactions often yield highly energetic products like radicals or free ions that can afterward initiate a wide selection of reactions.[127, 167]

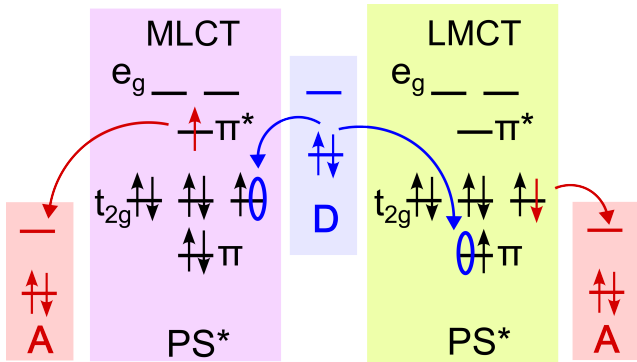

Figure 5.1: Scheme of the photoxidation and photoreduction of an excited photosensitizer (PS*) with respect to an electron acceptor (A) and an electron donor (D). Metal-to-ligand charge transfer (MLCT) excitation in the left side, and ligand-to-metal charge transfer (LMCT) excitation in the right side.

5.1 Photocatalysis with earth-abundant transition metal complexes

The recent discovery of long-lived photoactive charge transfer states in several earth-abundant transition metal complexes has recently prompted the systematic study of their photocatalytic opportunities.[11, 121, 123, 166] However, MC states in Fe complexes also showcased their potential to be used in photocatalysis. For example, the $[Fe(II)(tren(py)_3)]^{2+}$ (tren(py)$_3$ = tris(2-pyridyl-methylimino-ethyl)amine) complex can initiate bimolecular electron transfer with various electron acceptors.[122, 168] However, the low photoredox potentials, attributed to ligand-field states, restrict the width of their applications. The activity of short-lived MLCT excited states in $[Fe(II)(bpy)_3]^{2+}$ complex for driving chemical reactions such as enantioselective alkylation reactions have been previously addressed.[169] However, the short excited state lifetimes limit their applications, because they may decay before they encounter their reactive partner.[138] Photocatalytic transformations can be achieved through both electron and energy transfer. A Cr(III) complex, which features an impressive lifetime of $\sim$ 900 μs and spin-flip luminescence from a ^{2}MC state, can trigger photoinduced energy transfer to $^3O_2$, generating the active $^1O_2$ species able to trigger selective α-aminonitrile functionalization of C–H bonds.[170] Photocatalysis driven by electron transfer reactions has been observed from the ^{3}MLCT excited state of a Mo(0) complex, whose highly negative oxidation potential can initiate rearrangement

Table 5.1: Chemical and physical properties of photocatalysts, including lifetimes (τ), oxidation potentials (E_{ox}), reduction potentials (E_{red}), photooxidation potentials (E^*_{ox}), photoreduction potential (E^*_{red}) and excited state energy gap (E_{0-0}). Redox potentials given relative to ferrocene, Fc(+1/0).

Complex	τ (ns)	E_{ox} (V)	E_{red} (V)	E^*_{ox} (V)	E^*_{red} (V)	E_{0-0} (eV)
$[Fe(III)(phtmeimb)_2]^{+}$ †[a]	2.0	0.25	-1.16	-1.88	0.97	2.13
$[Fe(II)(btz)_3]^{3+}$ †[a]	0.1	–	-0.58	–	1.60	2.18
$[Fe(II)(tren(py)_3)]^{2+}$ †[b]	55	0.77	-1.58	-0.25	-0.56	1.02
$[Co(III)(dgpz)_2]^{3+}$ †[c]	5.07	1.35	-0.97	-1.49	1.87	2.84
$[Mo(0)(CN^{Me}Ar_3NC)_3]$ ‡[c]	74	-0.40	-2.5	-2.6	-0.3	2.2

† In acetonitrile. ‡ In THF. [a] A ^{2}LMCT state. [b] A ^{5}MC state. [c] A ^{3}MLCT state.

of acyl cyclopropane.[171] These are just a few examples of the large number of studies addressing sustainable light-induced catalysis.[11, 166]

Many investigations concerning charge transfer states of Fe complexes have been published after the discovery of the 9 ps excited state in the $[Fe(II)(bip)_2]^{2+}$ complex.[135, 172] The long-lived $[Fe(III)(phtmeimb)_2]^{+}$ complex has been shown to drive catalytic reactions further than the first quenching stage with one electron donor or acceptor.[173] Aydogan *et al.* demonstrated the capabilities of $[Fe(III)(phtmeimb)_2]^{+}$ to trigger dehalogenation reactions[174] and further quenching studies for dehalogenation/cyclization reactions and proton reduction reactions as reported by Schwarz *et al.*[175, 176] Other active Fe complex that has been observed to be catalytically promising is the $[Fe(II)(btz)_3]^{3+}$complex, which can undergo atom transfer radical addition reactions *via* two-photon absorption by each photosensitizer redox couple.[177] Cobalt-based photosensitizers were also proven to undergo chemical transformations, including trifluoromethylation reactions with $[Co(III)(dgpz)_2]^{3+}$ and a parent complex.[178] A list of photophysical and photochemical features of some complexes is shown in Table 5.1, illustrating the promising future of sustainable photochemistry.

5.2 Electron transfer

The most fundamental step involved in many of the photocatalytic reactions discussed previously is the electron transfer reaction, comprising one electron donor, D, and one electron acceptor, A. The electron transfer from an initially neutral system, results in the formation of two charged species, $D^{\bullet+}$ and $A^{\bullet-}$.[7, 179] These products are commonly designated as charge-separated species, and the process is referred to as a charge separation. To elucidate the rates of such a process, various models have been proposed to describe the electron transfer kinetics and thermodynamics.[7] Marcus theory is a pioneering model to describe the electron transfer processes, and the foundation for other more sophisticated models.[180] The electron transfer reaction for a

hypothetical electron transfer can be written as:

$$\mathrm{D} + \mathrm{A} \longrightarrow \mathrm{D}^{\bullet+} + \mathrm{A}^{\bullet-}$$

Marcus theory tries to approximate the multidimensional $3N - 6$ potential energy surface of a bimolecular electron transfer in a simplified two-dimensional picture. Such an approximation is based on the definition of a harmonic potential describing the reactants and a second harmonic potential for the products, which replaces all the degrees of freedom of the system by a single reaction coordinate. A standard expression for the rate constant of the electron transfer including quantum effects can be derived:

$$k_{ET} = \frac{2\pi}{\hbar} \frac{H_{DA}^2}{\sqrt{4\pi\lambda k_b T}} \exp\Big(\underbrace{- \frac{(\Delta G^\circ + \lambda)^2}{4\lambda k_b T}}_{\Delta G^\ddagger / k_b T} \Big) \tag{5.1}$$

Here, $\hbar$ is the reduced Planck constant, k_b is the Boltzmann constant and T is the temperature. Equation 5.1 resembles significantly the Arrhenius equation, with a pre-exponential and an exponential term, emphasizing that electron transfer is an activated process. It is then logical that activation free energy ($\Delta G^\ddagger$) occurs that relates to the driving force of the process, ΔG° (energy difference between reactant and product). However, the activation energy is also affected by a second energy term, the reorganization energy (λ), which reflects the energy cost of changing the charge state. This arises from the two contributions, the inner-sphere and outer-sphere reorganization energies, of which the outer-sphere part often dominates the final λ. The pre-exponential factor involves the electronic coupling between the A and D wavefunctions (H_{DA}), which decreases exponentially with the distance, following the decay of the wavefunction. In general terms, the pre-exponential factor relates to the probability of jumping between the neutral and the charge-separated free energy potentials.

There are three distinct regimes within Marcus theory; (i) normal, (ii) barrierless, and (iii) inverted Marcus regimes (representated in Figure 5.2). These three scenarios arise from the relative balance between λ and ΔG°. Marcus theory predicts that by increasing the driving forces, the electron transfer rate increases up to the barrierless regime (reaches the maximum rate), where λ and ΔG° are of similar magnitude. On the other hand, as ΔG° increases over λ, the rates are predicted to gradually decelerate. The validity of Marcus theory for electron transfer reactions has been experimentally tested, albeit with some shortcomings.

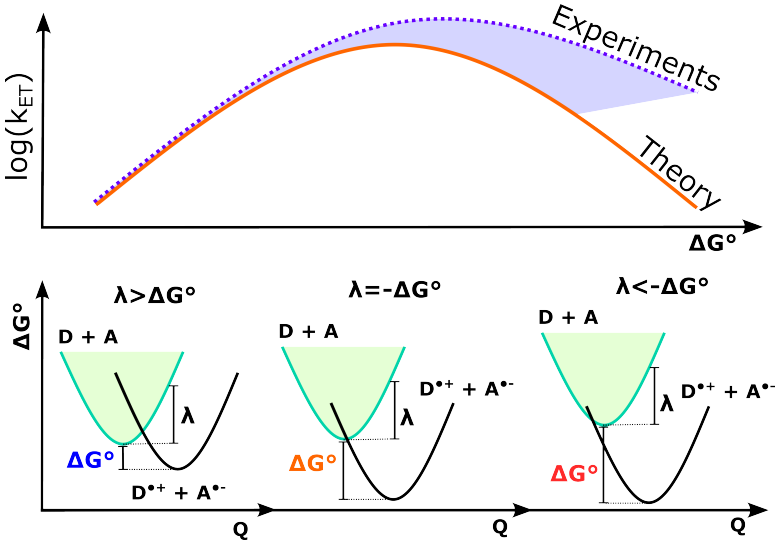

Figure 5.2: (top) Schematic representation of the electron transfer rate logaritmic vale with respect to the driving forces according to Marcus theory (orange) or experiments (purple). (bottom) schematic representation of the three distinct Marcus regimes.

Rehm–Weller evaluated the quenching rates for a series of bimolecular chemical systems of increasing driving forces, finding that the rates were constantly increasing until reaching a plateau.[181] Despite this disparity between theory and experiments, it was evidenced later on that the quenching rates are not always equivalent to electron transfer rate. The reason is that quenching rates involve electron transfer rates as well as diffusion rates. To avoid the diffusion limit, which causes the plateau observed in the Rehm–Weller experiment, intramolecular electron transfer working under electron-donating or -accepting solvents can be considered.[182] A noteworthy observation is that the rate evolution in the inverted Marcus regime differs from the anticipated decay pattern (schematically depicted in top Figure 5.2),[183] caused by the larger vibrational coupling of the nested potentials in the inverted regime.

For photoinduced electron transfer, other factors determine the feasibility of the transfer. The lifetimes of the excited state of the photosensitizer are required to be long enough so that the quenching occurs before the excited state is deactivated.[138] These facts support that the photophysics of the photosensitizer is of high relevance to achieving effective photochemical performance.

5.3 Photoinduced electron transfer: charge separation and charge recombination

Once the photoinduced charge-separated species are formed, two alternative paths open up. On one hand, the charge-separated species can diffuse apart for which a broader discussion will be given in subsection 5.4. On the other hand, the recovery to the ground state may occur by electron back-transfer.[7] The latter is commonly called charge recombination (see left panel in Figure 5.3).

The charge recombination kinetics can also be modeled by Marcus theory with respect to the ground state. The right panel of Figure 5.3 illustrates the normal and inverted Marcus regimes for charge recombination in photoinduced electron transfer. In contrast to charge separation, the increase of the driving force promotes a deceleration of the electron back-transfer reaction. As photochemistry is closely tied to the charge transfer lifetimes, an optimal scenario involves fast charge separation and slow charge recombination, which hinders the deactivation of the photoproducts.

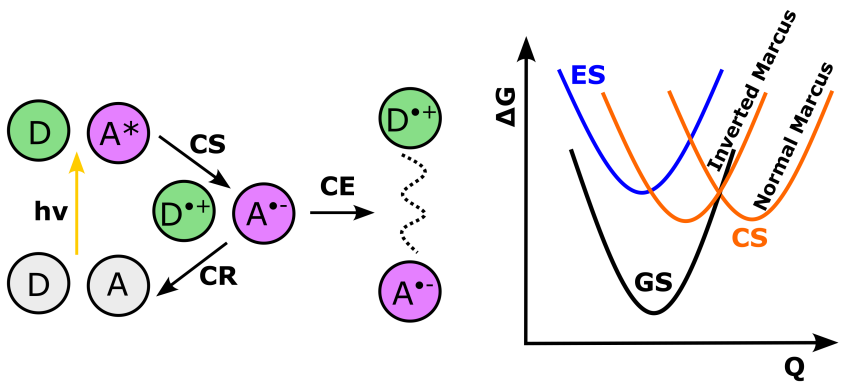

Figure 5.3: (left) Model case of a bimolecular photoinduced electron transfer between a donor (D) and acceptor (A) molecule. Charge separation (CS), charge recombination (CR), and cage escape (CE) processes are also depicted. (right) Graphical representation of the inverted and the normal Marcus charge recombination.

The relevance of an adequate balance between charge separation and charge recombination rates for achieving final photoproducts was evidenced experimentally for the $[Fe(III)(phtmeimb)_2]^+$ complex.[173] The bimolecular quenching of the ^{2}LMCT excited state in this complex was tested against two different electron donors, dimethylaniline (DMA) and trimethylamine (TEA). The charge separation was observed to be more efficient for DMA (0.8 ps) than for TEA (20 ps), whereas the charge recombination was observed to be very fast regardless of the donor molecule (5 ps). Consequently, a significant amount of photoproduct was observed only for DMA, whose charge separation was faster than the competing charge recombination rate.

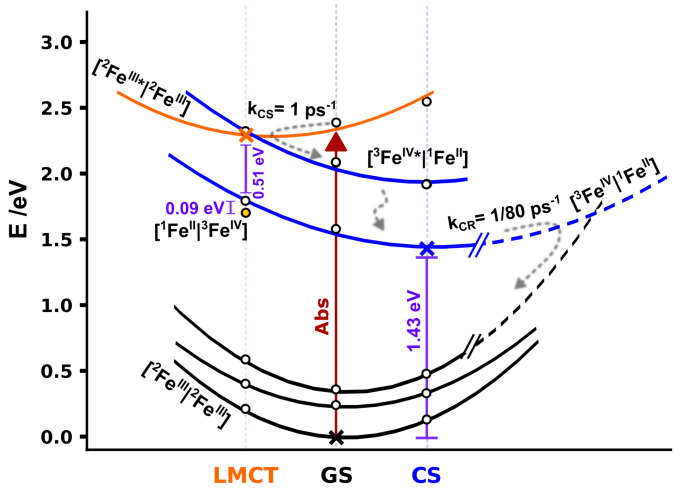

Figure 5.4: Energy profile of the photoinduced charge disproportionation involving two [Fe(III)(phtmeimb)$_2$]$^+$ complexes. Ligand-to-metal charge transfer (LMCT), ground state (GS) and charge-separated state (CS) states are represented.

At high photosensitizer concentrations, a second photosensitizer molecule can take the role of electron donor or acceptor, quenching a neighboring excited molecule.[184] This particular type of electron transfer is called photoinduced charge disproportionation.[185] Temperature-dependent studies of this system by transient absorption spectroscopy revealed a barrierless charge separation while the charge recombination has a significant activation barrier (paper **V**). Such differences indicate that charge recombination occurs in the inverted Marcus regime. This suggestion was further explored by DFT and TD-DFT calculations in paper **V**. Figure 5.4 shows the potential energy surface of the ground state, the local excited state, and the charge disproportionation state. The excited states were obtained by TD-DFT optimization on the doublet energy surface, while the charge-separated state was calculated from the oxidative and reductive pairs.

The energy of the charge disproportionation state on the excited state nuclear positions showed a non-zero energy barrier (0.51 eV) as expected from the spectroscopy findings in paper **V**. Nevertheless, the open-shell nature of the charge-separated Fe(IV) state entails several states that are nearly degenerate with the ground state. The proximity between the Fe(IV) excited states and the charge separation state in terms of energy is evidenced by potential electron transfer channels involving these excited states (see crossing point between orange and blue lines in Figure 5.4). DFT and TD-DFT calculations also predict that the charge recombination occurs in the inverted Marcus regime (adiabatic energy of 1.43 eV), as is indicated by the nested potential energy

surfaces in Figure 5.4. Despite the current limited knowledge about photoinduced charge disproportionation processes, a combination of experimental and computational research can provide us with more promising photochemical processes.

5.4 Solvent cage escape

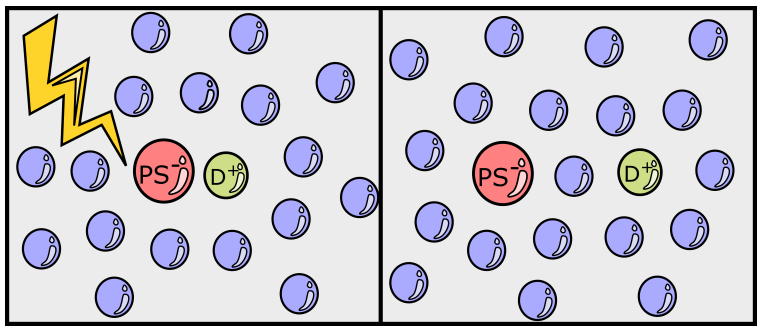

Figure 5.5: Scheme of solvent cage escape of photoinduced charge-separated species.

A key factor that can ensure long-lived photoproducts is the full solvation of each charge-separated species i.e. the photoproducts diffuse away from each other in the solvent media. This dynamical process is typically designated solvent cage escape (Figure 5.5). Clearly, the cage escape channel will compete with the charge recombination. Therefore, a slow charge recombination will favor the cage escape. Many factors can affect the solvation cage surrounding the photoproducts, including the intrinsic permittivity of the solvent, its viscosity, the density or width of the solvation shell.[186] Other factors are the establishment of solute-solvent intermolecular interactions, extending from strong electrostatics interactions to weaker Van der Waals interactions.[187]

Most of the models to describe the driving forces for the formation of the charge separation state are based on the assumption that the molecules have a spherical shape, and therefore the only mechanical parameter to be defined is the distance.[180] However, it has been demonstrated that the orientation of the reactants has a decisive effect on the driving forces. This orientation matter is based on the fact that a proper orientation can maximize the electronic coupling, regardless of the distance, and therefore the rate of the charge separation.

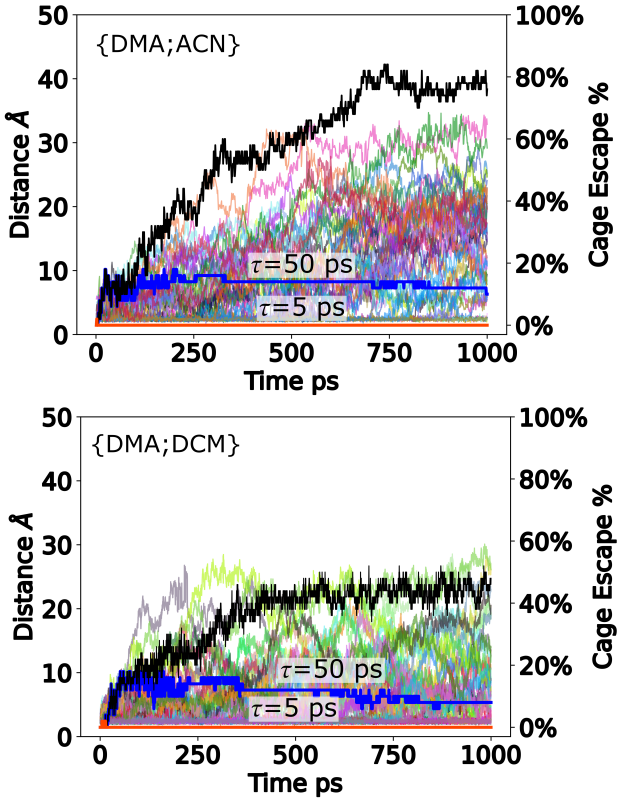

Figure 5.6: Calculated solvent cage escape yields in two solvent boxes of (top) {DMA;ACN} mixture and (bottom) {DMA;DCM} mixtures.

5.4.1 Anomalous cage escape dynamics

A study of the excited state quenching of $[Fe(III)(phtmeimb)_2]^+$ with DMA and TEA donor molecules in acetonitrile observed none or low cage escape yields. Only DMA showed successful cage escape under high concentration of the quencher.[173] A follow-up study of the same bimolecular system further investigated the cage escape response to different solvent media and a large variety of electron donor molecules.[174] One of the intriguing findings was that the cage escape yield increased from 3 % in acetonitrile to more than 60 % in dichloromethane. It is worth noting the large polarity difference between these solvents: The dielectric constant of acetonitrile and dichloromethane are 37.5 and 8.9 Debye, respectively.[13] Understanding this drastic difference is relevant for the design of appropriate conditions for efficient photochemical applications.

Up to this point, we have assumed the classical picture of two neutral reactants that

yield an ion pair, a radical-cation, and a radical-anion. However, our case involves a photoinduced electron transfer between a positively charged photosensitizer and a neutral electron donor, generating a neutral Fe(II) complex and a radical-cation e.g. $DMA^{\bullet+}$. Therefore, the strength of the electrostatic interactions between the charge-separated species are different, as well as the solvent response to the change of charge. The light-induced electron transfer equations for a classical and an alternative picture, including the acceptor (A), donor (D), and counterion (C), are:

$$Classical : A^{*} + D \longrightarrow A^{\bullet-} + D^{\bullet+}$$

$$This\ system : (A^{+})^{*} + C^{-} + D \longrightarrow A + C^{-} + D^{\bullet+}$$

MD simulations in paper **VI** showed that the solvent structure around the reduced photosensitizers did not change much upon photoinduced electron transfer. On the other hand, the localized charge in the smaller organic DMA molecule triggers a larger response in the solvation cage. The solvent molecules rotate to align their dipole moment to the new positive charge of $DMA^{\bullet+}$. Therefore, this solvent reorganization may accelerate charge recombination while hindering diffusion. However, a similar solvent reorganization and solvent shell characteristics for the two different solvents, acetonitrile and dichloromethane, indicate that the solvent structure is not responsible for the differences in the cage escape yields.

Classical MD simulations used to model the cage escape dynamics of $DMA^{\bullet+}$ in both solvents, revealed a more efficient diffusion of $DMA^{\bullet+}$ in the more polar solvent acetonitrile (Figure 5.6). The cage escape reaches 80 % in acetonitrile and 45 % in dichloromethane, assuming no charge recombination. Albeit these findings are supported by the classical knowledge of better ion stability in polar environments, the cage escape by diffusion does not explain the experimental evidence. Furthermore, assuming charge recombination rates of 5 ps, the calculated cage escape yields become almost zero in both solvents. The results indicate that cage escape yields of 60 % in dichloromethane are achieved only by slowing down the recombination rates 100 times. The alternative photoinduced electron transfer picture, with a non-neutral reactant, indicates the presence of a counterion in the solution which should be considered.

The photophysics of the electron transfer, which is similar to the relevance of ion-pairing, a counterion-donor pairing (in this particular system) might have an effect. Analysis of MD trajectories of the three-body systems reveals distinct $DMA^{\bullet+}$-PF_6^- ion-pairing depending on the solvent choice. We observed that tighter ion pairs formed in dichloromethane than in acetonitrile, both before and after electron trans-

fer. Therefore, the charge neutralization of $DMA^{\bullet+}$ by the counterion might be relevant to hinder the charge-recombination pathway in dichloromethane.

5.4.2 Beyond the classical perspective

According to quantum chemical calculations in paper **VI**, the ion-pairing affects the reduction potential of DMA. We observed that the calculated redox potentials for the ion pairs shift by more than 0.2 eV towards more positive potentials with respect to the redox potentials of the free radical-cation. This effect is more pronounced in dichloromethane. This alteration of the overall driving force caused by the ion-pair suggests a favorable oxidation of the DMA molecules close to the counterion. These molecules are localized around the metal center of the photosensitizer (attracted by the charge). Therefore, the counterion can direct the oxidation reaction as well as hinder the electron back-transfer reaction.

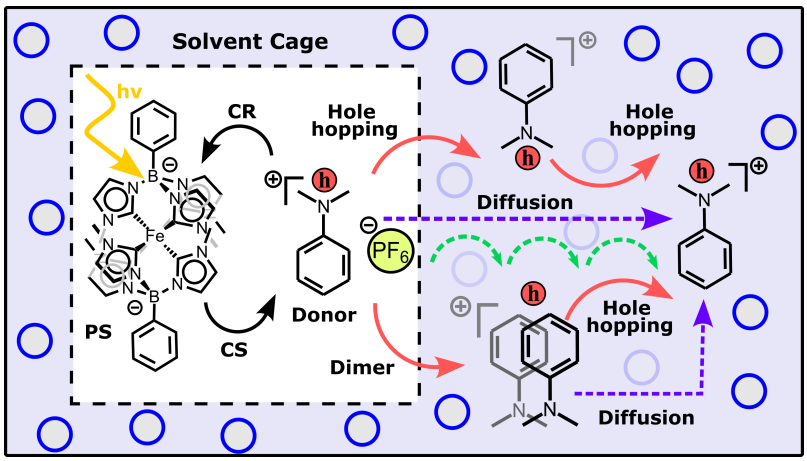

Figure 5.7: Solvent cage escape competing mechanisms. Charge recombination (CR), charge separation (CS), hole hopping and diffusion processes are depicted.

The high donor concentration utilized in the experimental setup (more than 300 mM) can facilitate the encounter of two or more donor molecules. It has been observed that aromatic amines, similar to DMA, can form radical-cation dimers with particular spectroscopic features in the near-IR absorption spectra.[188] Quantum chemical calculations of dimer and trimer composed by one $DMA^{\bullet+}$ and one or two neutral DMA reveal delocalized electronic structure over the aggregated structure. Spin-density analysis shows the hole to be evenly delocalized between the dimer units, while in the trimer the hole is mainly accommodated in the inner DMA unit. The formation of dimer or trimer radical-cations also affects the redox potentials, shifting the reduction potentials to more negative values. Therefore, the dimer formation may

compete with the diffusion mechanism.

QM/MM calculations, including a dimer and a counterion in the QM part, revealed two scenarios depending on the coupling efficiency between the three units, (i) a strong formation of the $DMA^{\bullet+}$-PF_6^- ion-pair, and (ii) the formation of a radical-cation dimer and the counterion diffusion. Under such a large concentration of donor molecules around the oxidized donor molecule, neighboring DMA molecules can behave as electron donor intermediates. The diffusion of the counterion, by interacting with a neutral DMA, can favor a hole hopping event (see mechanisms in Figure 5.7). This event has been observed in QM/MM calculations by including an additional neighboring DMA molecule in the QM region. Therefore, the counterion diffusion and electrostatic interactions, which are controlled by the solvent, could drive an alternative cage escape mechanism ruled by the hole hopping dynamics.

5.5 Hydrogen production by proton reduction

In photochemistry, similarly to any ground state reaction, two main aspects drive a reaction; the kinetics of the reaction and the thermodynamics. We have seen previously how Marcus theory helps to predict electron transfer rates, but we have not discussed how to evaluate the driving forces. The most versatile tool to assess the viability of bimolecular electron transfer reactions is assessing redox potentials.[7] Redox potentials represent the capability to receive or donate electrons with respect to a reference electrode e.g. the standard hydrogen electrode. Furthermore, it is a common practice to use another reference redox couple as an internal reference when the solvent effect on redox potentials is of interest. Ferrocence/ferrocenium is a broadly used redox couple in non-aqueous solvents, the most common media for measuring redox potentials of transition metal complexes. There are many practical problems to measure redox potentials experimentally, e.g. problems in stability, reversibility, or limitations of the available redox window.[189] First-principles calculations can provide a reliable tool to predict redox potentials of interesting redox reactions, such as hydrogen production.

Hydrogen has recently attracted much attention as a potential replacement for fossil fuels.[28, 29, 31, 33, 34] Molecular transition metal catalysts have been introduced as crucial chemical elements to access less energy-costly hydrogen reduction. Using light as a clean energy source to trigger hydrogen reduction opens up the use of molecular photosensitizers. As mentioned in subsection 5.1, the recent discovery of efficient photosensitizers made of earth-abundant materials as an alternative to scarce metals such as Ru or Ir enables a complete green photocycle. In paper **VII**, we aim to assess the driving force of the first step of hydrogen reduction, which is the activation

of the proton reduction catalyst (PRC). A long list of proton reduction catalysts has been already investigated and proposed, based on multiple ligand designs, as well as with various earth-abundant transition metals e.g. cobalt, nickel, iron, or copper.[33] Overall, the main elements needed to initiate a catalytic reaction for hydrogen reduction are (i) a photosensitizer, (ii) a proton reduction catalyst, and (iii) an electron donor.

Box 5: Photocatalytic cycle

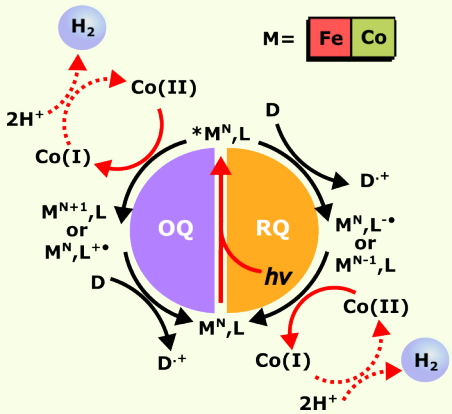

- **Oxidative quenching (OQ):** the photosensitizer can primarily be oxidized by the PRC to yield the active species of the reaction (cobalt-based PRC typically involves a Co(II/I) redox couple). In the second step of the catalytic cycle, the photosensitizer is recovered by oxidation of a sacrificial molecule.
- **Reductive quenching (RQ):** the photosensitizer can be initially quenched by a sacrificial molecule *via* reduction, whereas the photosensitizer is reverted to the natural ground state by reducing the PRC.

Harvesting light by the photosensitizer is the first step of the reaction.[138] As mentioned earlier in this chapter, the advantage of photochemistry compared to more conventional chemical reactions resides in the increasing redox capabilities of the photosensitizer.[7] Since these harvesters can be both good oxidative and reductive agents, the catalytic reaction can lead along two bifurcated paths: reductive quenching and oxidative quenching (see Box 5).[33, 190] Despite both paths being equivalent and yielding the same products, one can be preferred over the other one. The mechanism of the reaction will tightly depend on the driving forces of each element of the reaction. An evaluation of the redox potentials can help to determine an ideal combination of photosensitizer, catalyst, and electron donor molecules.

5.5.1 Finding a suitable DFT functional

A set of cobalt proton reduction catalysts with earth-abundant light harvesters to drive either reductive or oxidative quenching was evaluated by DFT in paper **VII**.

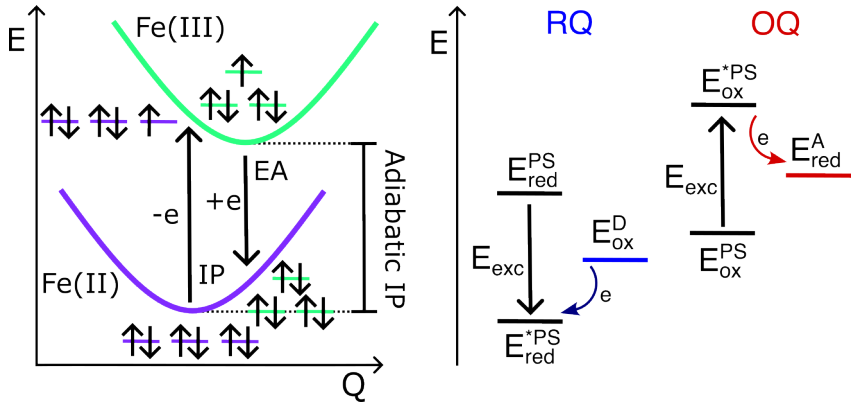

Figure 5.8: (left) Electron affinity (EA) and ionization potential (IP) in a redox transformation. (right) Reductive quenching (RQ) and oxidative quenching (OQ) between a photosensitizer (PS), an acceptor (A) and a donor (D) molecule.

We have presented a simple evaluation of reduction potentials by establishing energy correction factors from linear regression of available experimental data and calculated electronic energy difference between the natural ground state and the reduced (or oxidized) forms of the target chemical system ($\Delta_r E_{red/ox}$). This corresponds to the adiabatic ionization potential and electron affinities, respectively (Figure 5.8). The reduction potentials were calculated with respect to the ferrocenium/ferrocene redox couple ($\Delta_r E_{Fc(+1/0)}$) according to the expression:

$$E^{calc}_{red/ox} = -\Delta_r E_{red/ox} + \Delta_r E_{Fc(+1/0)} \tag{5.2}$$

Utilizing correction factors from a linear fit of $E^{calc}_{red/ox}$ potentials to the experimental data, the corrected potentials (E^{corr}_{red} and E^{corr}_{ox}) can be elucidated and the photoredox potentials were calculated according to equations 5.3 and 5.4.[7]

$$^{*}E_{red} = E^{corr}_{red} + \Delta E_{exc} \tag{5.3}$$

$$^{*}E_{ox} = E^{corr}_{ox} - \Delta E_{exc} \tag{5.4}$$

Here, ΔE_{exc} is the excitation energy i.e. the energy difference between the excited state in its equilibrium geometry and the ground state, corresponding to the zero-zero

vibration energy levels of the ground and excited state. This value is challenging to determine experimentally and computationally.

In total, cobalt proton reduction catalysts Co(II/I), photosensitizer metal PS(III/II), photosensitizer ligand L(0/-1), and electron donor D(+1/0) reduction potentials were successfully fitted (the fit of Co(II/I) potentials is shown in Figure 5.9). The quality of the fit was assessed for a selection of pure functionals (BLYP and BP86), hybrid functionals (TPSSh, B3LYP, B3LYP*, and M06), and hybrid range-separated functionals (ωB97X and CAM-B3LYP). Since the photocycle also includes the quenching of the photosensitizer excited states, the photoredox potentials were calculated from excited state energy gaps calculated for all functionals.

For an adequate evaluation of the complete photocycle, the DFT functional should accurately describe both ground and excited state properties. Despite all functionals adequately estimating ground state reduction potentials, the calculation of ΔE_{exc} became a bottleneck for the full photocycle description (Figure 5.9). Among the studied functionals, the hybrid B3LYP* and TPSSh functionals demonstrated the most promising capabilities to mimic experimental emission energies (with standard deviations often lower than 0.2 eV) regardless of the nature of the state. On the other hand, other functionals significantly underestimated and overestimated excited state energies (more than 1 V), including more advanced functionals such as ωB97X and CAM-B3LYP functionals.

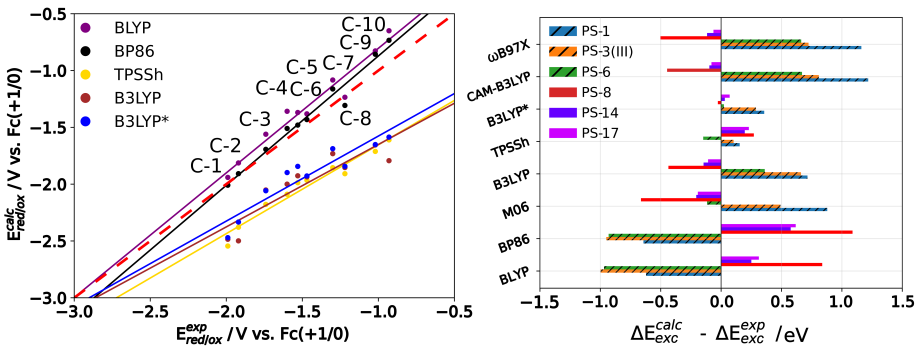

Figure 5.9: (left) Cobalt proton reduction catalyst Co(II/I)(C-n, n= 1-10) reduction potentials fit for a selection of DFT functionals. (right) Excited states energy gap errors for several photosensitizers (PS-n, n=1, 3, 6, 8, 14, 17) for a selection of DFT functionals.

Although the pure functionals deviated most in estimating ΔE_{exc} energies, these functionals reproduce ground state redox potentials with a similar or better accuracy as the other exchange-correlation functionals (less than 0.18 V). Therefore, we propose BLYP and BP86 as good quality/cost alternatives for ground state redox potentials. On the other side, hybrid range-separated functionals adequately describe photosen-

sitizer metal oxidation processes. In contrast, the predictions deviated significantly for Co(II/I) and donor D(+1/0) reduction potentials. Thus, both range-separated functionals yielded larger errors for the description of the complete photocycle.

5.6 Designing hydrogen reduction molecular catalysts

When the photosensitizer excited state is sufficiently long-lived to drive electron transfer under favorable driving forces, *via* photoreductive or photoxidation quenching, in addition to slow recombination (favoring cage escape dynamics), it maximizes the likelihood for the successful activation of a proton reductive catalyst. The activity of many catalysts often diminishes in water solution because of undesirable side reactions, challenging their application for water splitting. However, hydrogen formation from proton supply from other sources than water is possible. Investigations of hydrogen evolution from alternative proton sources facilitate the study of the water splitting reductive half-reaction because the parallel oxidation half-reaction can be neglected. The most popular electron donors e.g. amine derivatives have low solubility in water, limiting their use for water splitting.[167] A recurrent chemical choice to work with aqueous solutions is ascorbic acid. This organic acid is attractive because it can provide both electrons and protons to the overall reaction.

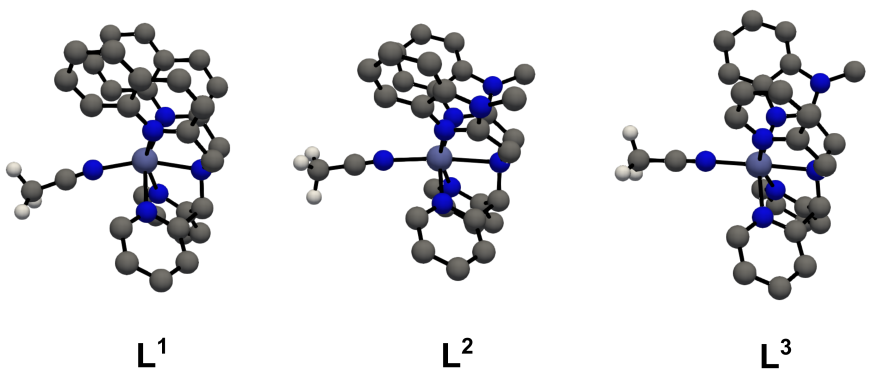

Figure 5.10: Chemical structures of Co(II) proton reduction catalysts with the ligand series L^1, L^2 and L^3.

Within the large variety of catalysts designed for hydrogen evolution, those based on cobalt are the most recurrent options among the first-row transition metals.[33, 190, 191] One of the first cobalt catalysts that showed to be hydrogen active belonged to the cobaloxime family.[192] Despite the good performance of cobaloxime complexes, these molecules are characterized by planar skeletons that often suffer from hydrolysis. Therefore, new ligand designs have tried to improve this concern, often addressed with pentadentate ligands. These cobalt catalysts can be found in different

natural oxidation states, in particular Co(II). This is the case of the aminopyridine $[Co(PY5Me_2)(H_2O)]^{2+}$ ($PY5Me_2$ = 2,6-bis(1,1-bis(2-pyridyl)ethyl)pyridinecomplex), which has featured a turnover number (TON) of 290 (the number of product molecules that a catalyst can produce during its lifetime).[193] Tuning the electronic structure of the complex e.g. by adding electron donor or acceptor chemical groups, impacts the hydrogen generation performance.[194–196] In paper **VIII**, the original $[Co(R\text{-}PY5Me_2)(H_2O)]^{2+}$ complex was used as a base for structural modifications by tuning the π conjugation of the ligand (chemical structures are shown in Figure 5.10).

5.6.1 Detailed reaction mechanism

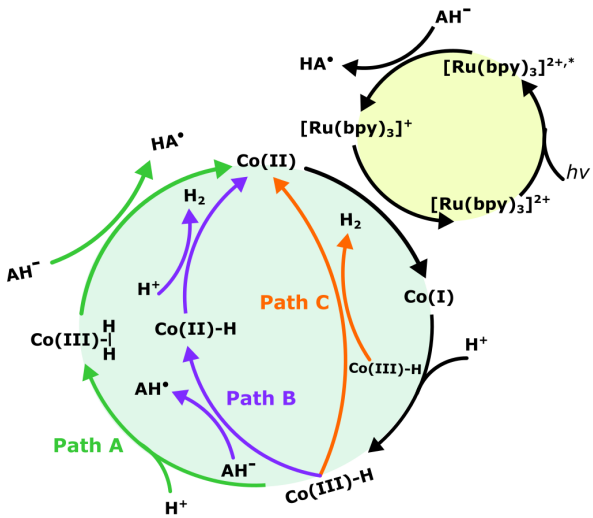

Figure 5.11: Schematic representation of the hydrogen reduction mechanism governed by a Co-catalyst (green panel) and a photosensitizer (yellow panel).

The detailed mechanisms for hydrogen reduction are often unknown, mainly due to the short-lived nature of the intermediate states. However, the Co(I) state of the complex has repetitively been pointed to as the catalytic active species triggering the reduction reaction.[195] The high energy costs to generate the reactive Co(I) oxidation state are covered by the driving forces gained in the photocatalytic cycle (yellow panel in Figure 5.11). Here, the photoactivation of the Co(II) catalyst to oxidation state Co(I) is driven by the photosentizer recovery, which was previously photoreduced by the electron donor (ascorbic acid). The high oxidation potential of the Co(I) species triggers the reduction of a proton in the media, generating the hydride Co(III)–H complex. The final hydrogen formation can proceed *via* three reaction paths (Path A, B, and C in Figure 5.11), one homolyptic and two heterolytic paths (see Box 6). DFT

is a practical tool to reveal the step-by-step energy profile of the reaction and compete with the alternative paths, which often are elusive due to experimental limitations.

Box 6: Protonation mechanisms

After catalyst activation *via* one-electron reduction, it reduces a proton to a hydride, which coordinates with the metal. For a Co(I) species, a Co(III)–H complex is formed. The final generation of hydrogen can proceed through three channels.[33]

- **Heterolytic pathway:** The Co(III)-hydride bound can interact with a second proton, releasing hydrogen (Path A). The Co(III) species can be recovered subsequently by one-electron reduction by the photosensitizer or a sacrificial electron donor. Alternatively, the Co(III)-hydride can be reduced first and protonated in a second step (Path B).
- **Homolytic pathway:** The hydride Co(III)-hydride bound can instead interact with a second Co(III)–H complex producing molecular hydrogen and two restored Co(II) catalysts (Path C).

The three reaction pathways,Path A, Path B, and Path C, were evaluated by DFT (B3LYP/6-31+G(d)/CPCM(Water)) in paper **VIII**. The two heterolytic mechanisms (Path A and Path B) differ in the order of the reaction step; protonation and one-electron reduction (Path A) or *vice versa* (Path B). The calculated reaction energies reveal that the first Co(III)–H protonation is uphill by more than 5 kcal/mol for the series of complexes (Figure 5.12). The low hydride reactivity was attributed to the weaker electrostatics caused by the smaller charge localization in the hydride H^- compared to the Co(III) metal, which is in a high oxidation state. Another remarkable observation was the tight coordination of the hydride to the metal, revealing a significant energy costs to release the hydrogen molecule ($\sim$ 1-5 kcal/mol). In contrast, the protonation of the Co(II)–H intermediate was a downhill process, and the formed H_2 molecule was observed to automatically dissociate from the catalyst. These two aspects favor Path B for the formation of hydrogen. Still, a high redox potential is required to initiate the Co(III/II) reduction. Therefore, the viability of the catalytic Path B will depend on the redox potential of the electron donor.

On the other hand, DFT calculations on two interacting Co(III)–H catalysts demonstrated a favorable energy gain for the formation of hydrogen *via* Path A ($\sim$ 10 kcal/mol). The strong steric effects, arising from the bulky pyridine groups of the ligand, require a proper orientation when the two molecules encounter in solution. Furthermore, the weak Coulomb-type interaction between the two anions is reflected by the large energy of the crossing point between the quartet and doublet state ($\sim$ 10-20 kcal/mol).

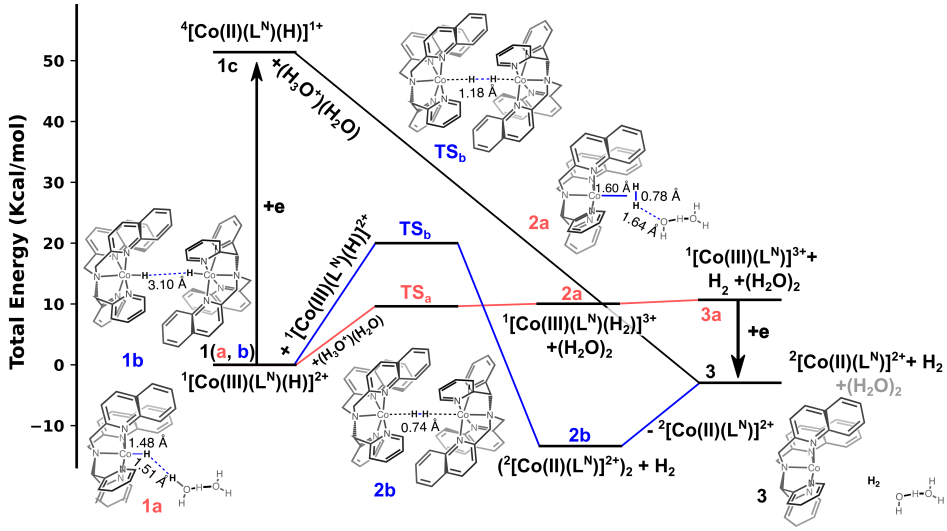

Figure 5.12: Energy diagram for the various mechanisms in hydrogen reduction reactions of the Co(II) catalyst with the ligand L^1 calculated at the (B3LYP/6-31+G(d)/CPCM(Water)) level.

Therefore, the three considered reaction paths may occur in competition, depending on the reaction conditions e.g. pH conditions, reductive agent redox potential, and catalyst concentration. The distinctive ligand designs yield different hydrogen reduction performances. $[Co(II)(L^1)]^{2+}$ catalyst achieved the highest TON numbers, although still with moderate performance compared to other cobalt catalysts.[33] The difference in reactivity was attributed to the distinct preferred reaction mechanisms, $[Co(II)(L^1)]^{2+}$ favoring path B and $[Co(II)(L^2)]^{2+}$ and $[Co(II)(L^3)]^{2+}$ path A. This mechanistic study is a milestone for the understanding of hydrogen reduction reactions and refining the molecular design to maximize the performance of homogeneous catalysis.

Chapter 6

Conclusions and Outlook

The photophysics and photochemical properties of several transition metal complexes have been extensively explored in this thesis. One of the main goals addressed in this work is the search for sustainable alternatives to the broadly used photosensitizers in dye-sensitized solar cells and photocatalysis. Fundamental challenges, extending from comprehending excited state deactivation mechanisms to elucidating reactive channels for photochemical transformations, have also been addressed using density functional theory and molecular simulations.

Hindering fast charge transfer excited state decay in Fe(II)-d^6 complexes is a major goal towards replacing rare Ru(II)-d^6 complexes. Recent advances in earth-abundant photosensitizers demonstrated that photofunctional iron complexes can be achieved with proper molecular design. Understanding the state balancing by computational modeling can aid in the improvement of the metal complex optical properties. We have evaluated in paper **II** how the excited state landscapes can be affected by replacing the Fe(II) central metal with its isoelectronic Co(III) congener. The overall charge increase minimizes the structural distortions associated with the population of ligand-field states, promoting ^{3}MC states more nested with the ground state. This yields highly energetic ^{3}MC states in the Co(III) complex. The synthesis and spectroscopic characterization of this hexa-carbene Co(III) complex, included in paper **I**, demonstrated that this complex, as observed for a parent hexa-cyanide Co(III) complex, exhibits weak luminescence and a lifetime of 1μs from a triplet excited state, which was assigned to a ^{3}MC state according to TD-DFT simulations. The most immediate drawback of this Co(III) complex is the absence of light–absorption in the visible spectra range. A Rh(III) phenanthroline complex, similar to the mentioned Co(III) complex, displays luminescence from a ^{3}MC state. However, the extended π-conjugation of the ligand provides a low-energy ^{3}LC state easily excited in the visible

spectrum. In addition, the dual emission from both ^{3}LC and ^{3}MC states is known to be temperature-dependent. In paper **III**, *ab initio* molecular dynamics on a crossover reaction between a ^{3}LC and a ^{3}MC state demonstrated that multiple distorted states are involved in the process and that the mechanism is a two-electron rearrangement involving the population of the ^{3}MC states. This crossover reaction was observed to be driven by a gain in entropy, attributed to Jahn–Teller distortions. On the other side of the periodic table, titanocenes and scandocenes adopting d^0 electronic configurations are characterized by the absence of MC states. Despite neglecting the typical undesirable effect of MC states in excited state deactivation, stretched and folded distorted states arise on the potential energy surface. This promotes both photoinduced bond cleavage and excited states energy loss by minimal bending distortions as discussed in paper **IV**. Therefore, the success of the design of photoactive transition metal complexes resides in the overall balance of excited states, for which quantum chemical calculations can provide vital insight, together with spectroscopic investigations.

Similar reduction and oxidation potentials in transition metal complexes can promote the occurrence of photoinduced charge disproportionation events after photoexcitation. This is the case for a Fe(III) complex, whose ^{2}LMCT state is quenched by the ground state of a second Fe(III) complex as is outlined in paper **V**. TD-DFT calculations in this system provided details of the electron transfer process, revealing an almost barrierless charge separation with an excited Fe(IV) state, as well as a characteristic inverted Marcus charge recombination. The same Fe(III) complex, in the presence of a donor molecule, can also promote electron transfer reactions. Initial electron-transfer reactions are key steps to generate active species, and to maximize their lifetimes, the cage-escape rates should outcompete the charge–recombination. In paper **VI**, MD simulations are used to study the solvent effect on ion-pairing of the charge-separated species and the impact on the cage escape dynamics. Once the charge-separated species are freely available in the media, these can encounter an active molecule to proceed with desirable reactions, for instance, hydrogen reduction. Since hydrogen is one of the most promising alternative solar fuels, a screening tool to evaluate the driving forces of molecular proton reduction catalysts with respect to photosensitizers and sacrificial molecules would be convenient. A DFT fitting protocol of the redox potentials of each species involved in the activation of a proton reduction catalyst is presented in paper **VII**. It is demonstrated that both TPSSh and B3LYP* provide accurate calculations of redox and excited states energies. DFT is also a practical tool to elucidate the detailed mechanism of hydrogen reduction driven by cobalt catalysts, as shown in paper **VIII**. The calculated reaction steps for a Co(II) catalyst, considering both heterolytic and homolytic hydrogen formation channels, indicate that the three considered mechanisms can all be competitive, depending on the chemical conditions and the ligands of the complex.

Despite the narrow selection of chemical systems covered by this thesis, the fundamental understanding can be extrapolated to similar systems. The contributions of this work to sustainable chemistry and spectroscopy motivate us to investigate other transition metal complexes and their applications to photochemistry. Future avenues to continue with this research include detailed modeling of the excited states dynamics from the Frank–Condon region. Another aspect to address is further comprehending the change of the photophysical properties by electronic structure tuning or modeling photosensitizers in macroscopic systems for material chemistry applications.

Bibliography

[1] European Commission and Directorate-General for Energy. *EU energy in figures – Statistical pocketbook 2023*. Publications Office of the European Union, 2023.

[2] H. B. Gray. "Powering the planet with solar fuel". *Nature Chemistry*, **1**(1), 2009, pp. 7–7.

[3] EU Commission. "A hydrogen strategy for a climate neutral europe". *https://ec. europa. eu/commission/, checked on*, **1**(5), 2020, p. 2022.

[4] N. S. Lewis. "Toward cost-effective solar energy use". *Science*, **315**(5813), 2007, pp. 798–801.

[5] F. A. Cotton, G. Wilkinson, C. A. Murillo, and M. Bochmann. *Advanced inorganic chemistry*. John Wiley & Sons, 1999.

[6] M. Stradiotto and R. J. Lundgren. *Ligand design in metal chemistry*. Wiley Online Library, 2016.

[7] V. Balzani, P. Ceroni, and A. Juris. *Photochemistry and photophysics: concepts, research, applications*. John Wiley & Sons, 2014.

[8] A. Kraft. "What a chemistry student should know about the history of Prussian blue". *ChemTexts*, **4**(4), 2018, p. 16.

[9] N. S. Hosmane. *Advanced inorganic chemistry: applications in everyday life*. Academic Press, 2017.

[10] D. Kim, V. Q. Dang, and T. S. Teets. "Improved transition metal photosensitizers to drive advances in photocatalysis". *Chemical Science*, **15**, 2024, pp. 77–94.

[11] O. S. Wenger. "Photoactive complexes with earth-abundant metals". *Journal of the American Chemical Society*, **140**(42), 2018, pp. 13522–13533.

[12] C. Förster and K. Heinze. "Photophysics and photochemistry with Earth-abundant metals – fundamentals and concepts". *Chemical Society Reviews*, **49**, 2020, pp. 1057–1070.

[13] D. R. Lide. *CRC handbook of chemistry and physics*. CRC press, 1993.

[14] C. S. J. Ponseca, P. Chábera, J. Uhlig, P. Persson, and V. Sundström. "Ultrafast electron dynamics in solar energy conversion". *Chemical Reviews*, **117**(16), 2017, pp. 10940–11024.

[15] D. Zigmantas, T. Polívka, P. Persson, and V. Sundström. "Ultrafast laser spectroscopy uncovers mechanisms of light energy conversion in photosynthesis and sustainable energy materials". *Chemical Physics Reviews*, **3**(4), 2022, p. 041303.

[16] D. Bahnemann and A. O. T. Patrocinio. *Springer handbook of inorganic photochemistry*. Springer Nature, 2022.

[17] A. Hagfeldt, G. Boschloo, L. Sun, L. Kloo, and H. Pettersson. "Dye-sensitized solar cells". *Chemical Reviews*, **110**(11), 2010, pp. 6595–6663.

[18] A. B. Muñoz-García, I. Benesperi, G. Boschloo, J. J. Concepcion, J. H. Delcamp, E. A. Gibson, G. J. Meyer, M. Pavone, H. Pettersson, A. Hagfeldt, and M. Freitag. "Dye-sensitized solar cells strike back". *Chemical Society Reviews*, **50**, 2021, pp. 12450–12550.

[19] B. Bozic-Weber, E. C. Constable, and C. E. Housecroft. "Light harvesting with Earth abundant d-block metals: Development of sensitizers in dye-sensitized solar cells (DSCs)". *Coordination Chemistry Reviews*, **257**(21), 2013, pp. 3089–3106.

[20] M. A. Green, E. D. Dunlop, J. Hohl-Ebinger, M. Yoshita, N. Kopidakis, K. Bothe, D. Hinken, M. Rauer, and X. Hao. "Solar cell efficiency tables (Version 60)". *Progress in Photovoltaics: Research and Applications*, **30**(7), 2022, pp. 687–701.

[21] B. O. Reagen and M. Gratzel. "A low-cost, high-efficiency solar cell based on dye-sensitized colloidal TiO_2 Films". *Nature*, **353**(6346), 1991, p. 737.

[22] Q. Zhang and G. Cao. "Nanostructured photoelectrodes for dye-sensitized solar cells". *Nano Today*, **6**(1), 2011, pp. 91–109.

[23] A. Listorti, B. O'Regan, and J. R. Durrant. "Electron transfer dynamics in dye-sensitized solar cells". *Chemistry of Materials*, **23**(15), 2011, pp. 3381–3399.

[24] J. W. Ondersma and T. W. Hamann. "Recombination and redox couples in dye-sensitized solar cells". *Coordination Chemistry Reviews*, **257**(9), 2013, pp. 1533–1543.

[25] Q. Wang, C. Pornrungroj, S. Linley, and E. Reisner. "Strategies to improve light utilization in solar fuel synthesis". *Nature Energy*, **7**(1), 2022, pp. 13–24.

[26] D. Gust, T. A. Moore, and A. L. Moore. "Solar fuels via artificial photosynthesis". *Accounts of Chemical Research*, **42**(12), 2009, pp. 1890–1898.

[27] A. Züttel, A. Remhof, A. Borgschulte, and O. Friedrichs. "Hydrogen: the future energy carrier". *Philosophical Transactions of the Royal Society A: Mathematical, Physical and Engineering Sciences*, **368**(1923), 2010, pp. 3329–3342.

[28] N. Armaroli and V. Balzani. "The hydrogen issue". *ChemSusChem*, **4**(1), 2011, pp. 21–36.

[29] N. Rambhujun, M. S. Salman, T. Wang, C. Pratthana, P. Sapkota, M. Costalin, Q. Lai, and K.-F. Aguey-Zinsou. "Renewable hydrogen for the chemical industry". *MRS Energy & Sustainability*, 7, 2020, E33.

[30] M. G. Walter, E. L. Warren, J. R. McKone, S. W. Boettcher, Q. Mi, E. A. Santori, and N. S. Lewis. "Solar water splitting cells". *Chemical Reviews*, **110**(11), 2010, pp. 6446–6473.

[31] A. J. Bard and M. A. Fox. "Artificial photosynthesis: solar splitting of water to hydrogen and oxygen". *Accounts of Chemical Research*, **28**(3), 1995, pp. 141–145.

[32] A. J. Esswein and D. G. Nocera. "Hydrogen production by molecular photocatalysis". *Chemical Reviews*, **107**(10), 2007, pp. 4022–4047.

[33] A. Mazzeo, S. Santalla, C. Gaviglio, F. Doctorovich, and J. Pellegrino. "Recent progress in homogeneous light-driven hydrogen evolution using first-row transition metal catalysts". *Inorganica Chimica Acta*, **517**, 2021, p. 119950.

[34] S. Fukuzumi, Y.-M. Lee, and W. Nam. "Thermal and photocatalytic production of hydrogen with earth-abundant metal complexes". *Coordination Chemistry Reviews*, **355**, 2018, pp. 54–73.

[35] Z. Wang, C. Li, and K. Domen. "Recent developments in heterogeneous photocatalysts for solar-driven overall water splitting". *Chemical Society Reviews*, **48**(7), 2019, pp. 2109–2125.

[36] F. Jensen. *Introduction to computational chemistry*. John wiley & sons, 2017.

[37] W. Koch and M. C. Holthausen. *A chemist's guide to density functional theory*. John Wiley & Sons, 2015.

[38] E. G. Lewars. *Computational chemistry. Introduction to the theory and applications of molecular and quantum mechanics*. Springer, 2011.

[39] P. Politzer and J. M. Seminario. *Modern density functional theory: a tool for chemistry*. Elsevier, 1995.

[40] D. R. Hartree. "The wave mechanics of an atom with a non-Coulomb central field. Part I. Theory and methods". In: vol. 24. 1. Cambridge university press. 1928, pp. 89–110.

[41] V. Fock. "Näherungsmethode zur Lösung des quantenmechanischen Mehrkörperproblems". *Zeitschrift für Physik*, **61**, 1930, pp. 126–148.

[42] J. C. Slater. "Atomic shielding constants". *Physical Review*, **36**(1), 1930, p. 57.

[43] S. F. Boys. "Electronic wave functions-I. A general method of calculation for the stationary states of any molecular system". *Proceedings of the Royal Society of London. Series A. Mathematical and Physical Sciences*, **200**(1063), 1950, pp. 542–554.

[44] W. J. Hehre, R. F. Stewart, and J. A. Pople. "Self-consistent molecular-orbital methods. I. Use of Gaussian expansions of Slater-type atomic orbitals". *The Journal of Chemical Physics*, **51**(6), 1969, pp. 2657–2664.

[45] F. Weigend and R. Ahlrichs. "Balanced basis sets of split valence, triple zeta valence and quadruple zeta valence quality for H to Rn: design and assessment of accuracy". *Physical Chemistry Chemical Physics*, 7(18), 2005, pp. 3297–3305.

[46] T. H. Dunning Jr. "Gaussian basis sets for use in correlated molecular calculations. I. The atoms boron through neon and hydrogen". *The Journal of Chemical Physics*, **90**(2), 1989, pp. 1007–1023.

[47] C. C. J. Roothaan. "New developments in molecular orbital theory". *Reviews of Modern Physics*, **23**(2), 1951, p. 69.

[48] P. Hohenberg and W. Kohn. "Inhomogeneous electron gas". *Physical Review*, **136**(3B), 1964, B864.

[49] P. A. Dirac. "Note on exchange phenomena in the Thomas atom". In: *Mathematical proceedings of the Cambridge philosophical society*. Vol. 26. 3. Cambridge University Press. 1930, pp. 376–385.

[50] W. Kohn and L. J. Sham. "Self-consistent equations including exchange and correlation effects". *Physical Review*, **140**(4A), 1965, A1133.

[51] A. D. Becke. "Density-functional exchange-energy approximation with correct asymptotic behavior". *Physical Review A*, **38**, 1988, pp. 3098–3100.

[52] C. Lee, W. Yang, and R. G. Parr. "Development of the Colle-Salvetti correlation-energy formula into a functional of the electron density". *Physical Review B*, **37**, 1988, pp. 785–789.

[53] J. P. Perdew. "Density-functional approximation for the correlation energy of the inhomogeneous electron gas". *Physical Review B*, **33**, 1986, pp. 8822–8824.

[54] J. P. Perdew, K. Burke, and M. Ernzerhof. "Generalized dradient approximation made simple". *Physical Review Letters*, 77, 1996, pp. 3865–3868.

[55] Y. Zhao and D. G. Truhlar. "A new local density functional for main-group thermochemistry, transition metal bonding, thermochemical kinetics, and noncovalent interactions". *The Journal of Chemical Physics*, **125**(19), 2006, p. 194101.

[56] J. Tao, J. P. Perdew, V. N. Staroverov, and G. E. Scuseria. "Climbing the density functional ladder: nonempirical meta–generalized gradient approximation designed for molecules and solids". *Physical Review Letters*, **91**, 2003, p. 146401.

[57] A. D. Becke. "Density-functional thermochemistry. III. The role of exact exchange". *The Journal of Chemical Physics*, **98**(7), 1993, pp. 5648–5652.

[58] M. Reiher, O. Salomon, and B. Artur Hess. "Reparameterization of hybrid functionals based on energy differences of states of different multiplicity". *Theoretical Chemistry Accounts*, **107**, 2001, pp. 48–55.

[59] J. P. Perdew, M. Ernzerhof, and K. Burke. "Rationale for mixing exact exchange with density functional approximations". *The Journal of Chemical Physics*, **105**(22), 1996, pp. 9982–9985.

[60] V. N. Staroverov, G. E. Scuseria, J. Tao, and J. P. Perdew. "Comparative assessment of a new nonempirical density functional: molecules and hydrogen-bonded complexes". *The Journal of Chemical Physics*, **119**(23), 2003, pp. 12129–12137.

[61] Y. Zhao and D. G. Truhlar. "The M06 suite of density functionals for main group thermochemistry, thermochemical kinetics, noncovalent interactions, excited states, and transition elements: two new functionals and systematic testing of four M06-class functionals and 12 other functionals". *Theoretical Chemistry Accounts*, **120**, 2008, pp. 215–241.

[62] J. D. Chai and M. Head-Gordon. "Systematic optimization of long-range corrected hybrid density functionals". *The Journal of Chemical Physics*, **128**(8), 2008, p. 084106.

[63] T. Yanai, D. P. Tew, and N. C. Handy. "A new hybrid exchange–correlation functional using the Coulomb-attenuating method (CAM-B3LYP)". *Chemical Physics Letters*, **393**(1), 2004, pp. 51–57.

[64] J. Wang, R. M. Wolf, J. W. Caldwell, P. A. Kollman, and D. A. Case. "Development and testing of a general amber force field". *Journal of Computational Chemistry*, **25**(9), 2004, pp. 1157–1174.

[65] D. A. Case, H. M. Aktulga, K. Belfon, I. Ben-Shalom, S. R. Brozell, D. S. Cerutti, T. E. Cheatham III, V. W. D. Cruzeiro, T. A. Darden, R. E. Duke, et al. *Amber 2021*. University of California, San Francisco, 2021.

[66] J.-P. Ryckaert, G. Ciccotti, and H. J. Berendsen. "Numerical integration of the cartesian equations of motion of a system with constraints: molecular dynamics of n-alkanes". *Journal of Computational Physics*, **23**(3), 1977, pp. 327–341.

[67] T. Darden, D. York, and L. Pedersen. "Particle mesh Ewald: An N.log(N) method for Ewald sums in large systems". *The Journal of Chemical Physics*, **98**(12), 1993, pp. 10089–10092.

[68] X. Wu and B. R. Brooks. "Self-guided Langevin dynamics simulation method". *Chemical Physics Letters*, **381**(3), 2003, pp. 512–518.

[69] H. J. C. Berendsen, J. P. M. Postma, W. F. van Gunsteren, A. DiNola, and J. R. Haak. "Molecular dynamics with coupling to an external bath". *The Journal of Chemical Physics*, **81**(8), 1984, pp. 3684–3690.

[70] D. Marx and J. Hutter. *Ab initio molecular dynamics: basic theory and advanced methods*. Cambridge University Press, 2009.

[71] M. E. Tuckerman. "Ab initio molecular dynamics: basic concepts, current trends and novel applications". *Journal of Physics: Condensed Matter*, **14**(50), 2002, R1297.

[72] T. Helgaker, E. Uggerud, and H. J. A. Jensen. "Integration of the classical equations of motion on ab initio molecular potential energy surfaces using gradients and Hessians: application to translational energy release upon fragmentation". *Chemical Physics Letters*, **173**(2-3), 1990, pp. 145–150.

[73] R. Car and M. Parrinello. "Unified approach for molecular dynamics and density-functional theory". *Physical Review Letters*, **55**(22), 1985, p. 2471.

[74] J. Tomasi, B. Mennucci, and R. Cammi. "Quantum mechanical continuum solvation models". *Chemical Reviews*, **105**(8), 2005, pp. 2999–3094.

[75] B. Mennucci. "Polarizable continuum model". *Wiley Interdisciplinary Reviews: Computational Molecular Science*, **2**(3), 2012, pp. 386–404.

[76] S. Miertuš, E. Scrocco, and J. Tomasi. "Electrostatic interaction of a solute with a continuum. A direct utilizaion of ab initio molecular potentials for the prevision of solvent effects". *Chemical Physics*, **55**(1), 1981, pp. 117–129.

[77] A. Warshel and M. Levitt. "Theoretical studies of enzymic reactions: dielectric, electrostatic and steric stabilization of the carbonium ion in the reaction of lysozyme". *Journal of Molecular Biology*, **103**(2), 1976, pp. 227–249.

[78] M. J. Field, P. A. Bash, and M. Karplus. "A combined quantum mechanical and molecular mechanical potential for molecular dynamics simulations". *Journal of Computational Chemistry*, **11**(6), 1990, pp. 700–733.

[79] G. Henkelman, B. P. Uberuaga, and H. Jónsson. "A climbing image nudged elastic band method for finding saddle points and minimum energy paths". *The Journal of Chemical Physics*, **113**(22), 2000, pp. 9901–9904.

[80] G. M. Torrie and J. P. Valleau. "Nonphysical sampling distributions in Monte Carlo free-energy estimation: Umbrella sampling". *Journal of Computational Physics*, **23**(2), 1977, pp. 187–199.

[81] A. Grossfield. *WHAM: the weighted histogram analysis method*. Version 2.0.10.

[82] B. Wardle. *Principles and applications of photochemistry*. John Wiley & Sons, 2009.

[83] A. Vogler and H. Kunkely. "Luminescent metal complexes: diversity of excited states". In: *Transition metal and rare earth compounds: excited states, transitions, interactions I*. Ed. by H. Yersin. Berlin, Heidelberg: Springer Berlin Heidelberg, 2001, pp. 143–182.

[84] P. W. Atkins, M. S. Child, and C. S. G. Phillips. *Tables for group theory*. 2. Oxford University Press Oxford, 1970.

[85] E. Dodsworth, M. Hasegawa, M. Bridge, and W. Linert. "2.27 - Solvatochromism". In: *Comprehensive coordination chemistry II*. Ed. by J. A. McCleverty and T. J. Meyer. Oxford: Pergamon, 2003, pp. 351–365.

[86] A. M. Brown, C. E. McCusker, and J. K. McCusker. "Spectroelectrochemical identification of charge-transfer excited states in transition metal-based polypyridyl complexes". *Dalton Transactions*, **43**, 2014, pp. 17635–17646.

[87] M. Kasha. "Characterization of electronic transitions in complex molecules". *Discussions of the Faraday society*, **9**, 1950, pp. 14–19.

[88] P. W. Atkins and R. S. Friedman. *Molecular quantum mechanics*. Oxford university press, 2011.

[89] Y. Tanabe and S. Sugano. "On the absorption spectra of complex ions II". *Journal of the Physical Society of Japan*, **9**(5), 1954, pp. 766–779.

[90] M. Nihei, T. Shiga, Y. Maeda, and H. Oshio. "Spin crossover iron(III) complexes". *Coordination Chemistry Reviews*, **251**(21), 2007, pp. 2606–2621.

[91] D. N. Bowman and E. Jakubikova. "Low-spin versus high-spin ground state in pseudo-octahedral iron complexes". *Inorganic Chemistry*, **51**(11), 2012, pp. 6011–6019.

[92] T. K. Ekanayaka, K. P. Maity, B. Doudin, and P. A. Dowben. "Dynamics of spin crossover molecular complexes". *Nanomaterials*, **12**(10), 2022, pp. 2079–4991.

[93] H. Köppel, D. R. Yarkony, and H. Barentzen. *The Jahn–Teller effect: fundamentals and implications for physics and chemistry*. Springer Science & Business Media, 2009.

[94] J. Conradie. "Jahn–Teller effect in high spin d^4 and d^9 octahedral metal-complexes". *Inorganica Chimica Acta*, **486**, 2019, pp. 193–199.

[95] M. A. Halcrow. "Jahn–Teller distortions in transition metal compounds, and their importance in functional molecular and inorganic materials". *Chemical Society Reviews*, **42**, 2013, pp. 1784–1795.

[96] A. Agresti, J. H. Ammeter, and M. Bacci. "Jahn–Teller effect in tetrahedral d^1 metal complexes". *The Journal of Chemical Physics*, **81**(4), 1984, pp. 1861–1871.

[97] M. Atanasov, B. Delley, and D. Reinen. "A DFT study of the energetical and structural landscape of the tetrahedral to square-planar conversion of tetrahalide complexes of copper(II)". *Zeitschrift für anorganische und allgemeine Chemie*, **636**(9-10), 2010, pp. 1740–1750.

[98] M. C. M. O'Brien. "The dynamic Jahn–Teller effect in octahedrally coordinated d^9 Ions". *Proceedings of the Royal Society of London. Series A, Mathematical and Physical Sciences*, **281**(1386), 1964, pp. 323–339.

[99] R. Ameis, S. Kremer, and D. Reinen. "Jahn–Teller effect of titanium (3+) in octahedral coordination: a spectroscopic study of hexachlorotitanate ($TiCl_6^{3-}$) complexes". *Inorganic Chemistry*, **24**(18), 1985, pp. 2751–2754.

[100] A. Soupart, F. Alary, J.-L. Heully, P. I. Elliott, and I. M. Dixon. "Recent progress in ligand photorelease reaction mechanisms: theoretical insights focusing on Ru(II) ^{3}MC states". *Coordination Chemistry Reviews*, **408**, 2020, p. 213184.

[101] A. Soupart, F. Alary, J.-L. Heully, P. I. P. Elliott, and I. M. Dixon. "Exploration of uncharted ^{3}PES territory for $[Ru(bpy)_3]^{2+}$: a new ^{3}MC minimum prone to ligand loss photochemistry". *Inorganic Chemistry*, **57**(6), 2018, pp. 3192–3196.

[102] A. Soupart, F. Alary, J.-L. Heully, P. I. P. Elliott, and I. M. Dixon. "Theoretical study of the full photosolvolysis mechanism of $[Ru(bpy)_3]^{2+}$: providing a general mechanistic roadmap for the photochemistry of $[Ru(N\wedge N)_3]^{2+}$-Type complexes toward both cis and trans photoproducts". *Inorganic Chemistry*, **59**(20), 2020, pp. 14679–14695.

[103] T. J. Meyer. "Photochemistry of metal coordination complexes: metal to ligand charge transfer excited states". *Pure and Applied Chemistry*, **58**(9), 1986, pp. 1193–1206.

[104] A. Juris, V. Balzani, F. Barigelletti, S. Campagna, P. Belser, and A. von Zelewsky. "Ru(II) polypyridine complexes: photophysics, photochemistry, eletrochemistry, and chemiluminescence". *Coordination Chemistry Reviews*, **84**, 1988, pp. 85–277.

[105] D. M. Arias-Rotondo. "The fruit fly of photophysics". *Nature Chemistry*, **14**(6), 2022, pp. 716–716.

[106] A. W. Adamson and J. N. Demas. "New photosensitizer. Tris (2,2'-bipyridine) ruthenium (II) chloride". *Journal of the American Chemical Society*, **93**(7), 1971, pp. 1800–1801.

[107] A. Yoshimura, M. Z. Hoffman, and H. Sun. "An evaluation of the excited state absorption spectrum of $Ru(bpy)_3{}^{2+}$ in aqueous and acetonitrile solutions". *Journal of Photochemistry and Photobiology A: Chemistry*, **70**(1), 1993, pp. 29–33.

[108] D. W. Thompson, A. Ito, and T. J. Meyer. "$[Ru\ (bpy)_3]^{2+*}$ and other remarkable metal-to-ligand charge transfer (MLCT) excited states". *Pure and Applied Chemistry*, **85**(7), 2013, pp. 1257–1305.

[109] N. H. Damrauer, G. Cerullo, A. Yeh, T. R. Boussie, C. V. Shank, and J. K. McCusker. "Femtosecond dynamics of excited-state evolution in $[Ru(bpy)_3]^{2+}$". *Science*, **275**(5296), 1997, pp. 54–57.

[110] P. S. Wagenknecht and P. C. Ford. "Metal centered ligand field excited states: their roles in the design and performance of transition metal based photochemical molecular devices". *Coordination Chemistry Reviews*, **255**(5-6), 2011, pp. 591–616.

[111] E. A. Juban, A. L. Smeigh, J. E. Monat, and J. K. McCusker. "Ultrafast dynamics of ligand-field excited states". *Coordination Chemistry Reviews*, **250**(13), 2006, pp. 1783–1791.

[112] M. Chergui. "Ultrafast photophysics of transition metal complexes". *Accounts of Chemical Research*, **48**(3), 2015, pp. 801–808.

[113] S. Campagna, F. Puntoriero, F. Nastasi, G. Bergamini, and V. Balzani. "Photochemistry and photophysics of coordination compounds: ruthenium". *Photochemistry and Photophysics of Coordination Compounds I*, 2007, pp. 117–214.

[114] C. Daniel. "Photochemistry and photophysics of transition metal complexes: Quantum chemistry". *Coordination Chemistry Reviews*, **282-283**, 2015, pp. 19–32.

[115] J. K. McCusker. "Electronic structure in the transition metal block and its implications for light harvesting". *Science*, **363**(6426), 2019, pp. 484–488.

[116] C. Sousa, C. de Graaf, A. Rudavskyi, R. Broer, J. Tatchen, M. Etinski, and C. M. Marian. "Ultrafast deactivation mechanism of the excited singlet in the light-induced spin crossover of $[Fe(2,2'\text{-bipyridine})_3]^{2+}$". *Chemistry – A European Journal*, **19**(51), 2013, pp. 17541–17551.

[117] W. Zhang, R. Alonso-Mori, U. Bergmann, C. Bressler, M. Chollet, A. Galler, W. Gawelda, R. G. Hadt, R. W. Hartsock, T. Kroll, K. S. Kjær, K. Kubiček, H. T. Lemke, H. W. Liang, D. A. Meyer, M. M. Nielsen, C. Purser, J. S. Robinson, E. I. Solomon, Z. Sun, D. Sokaras, T. B. van Driel, G. Vankó, T.-C. Weng, D. Zhu, and K. J. Gaffney. "Tracking excited-state charge and spin dynamics in iron coordination complexes". *Nature*, **509**(7500), 2014, pp. 345–348.

[118] W. Gawelda, A. Cannizzo, V.-T. Pham, F. van Mourik, C. Bressler, and M. Chergui. "Ultrafast nonadiabatic dynamics of $[Fe^{II}(bpy)_3]^{2+}$ in solution". *Journal of the American Chemical Society*, **129**(26), 2007, pp. 8199–8206.

[119] J. K. McCusker, K. N. Walda, R. C. Dunn, J. D. Simon, D. Magde, and D. N. Hendrickson. "Subpicosecond ^{1}MLCT $\rightarrow$ $^5T_2$ intersystem crossing of low-spin polypyridyl ferrous complexes". *Journal of the American Chemical Society*, **115**, 1993, pp. 298–307.

[120] C. Wegeberg and O. S. Wenger. "Luminescent first-row transition metal complexes". *JACS Au*, **1**(11), 2021, pp. 1860–1876.

[121] N. Sinha and O. S. Wenger. "Photoactive metal-to-ligand charge transfer excited states in $3d^6$ complexes with Cr^0, Mn^I, Fe^{II}, and Co^{III}". *Journal of the American Chemical Society*, **145**(9), 2023, pp. 4903–4920.

[122] J. E. Monat and J. K. McCusker. "Femtosecond excited-state dynamics of an iron(II) polypyridyl solar cell sensitizer model". *Journal of the American Chemical Society*, **122**(17), 2000, pp. 4092–4097.

[123] S. Kaufhold and K. Wärnmark. "Design and synthesis of photoactive iron N-heterocyclic carbene complexes". *Catalysts*, **10**(1), 2020, pp. 2073–4344.

[124] D. N. Bowman, A. Bondarev, S. Mukherjee, and E. Jakubikova. "Tuning the electronic structure of Fe(II) polypyridines via donor atom and ligand scaffold modifications: a computational study". *Inorganic Chemistry*, **54**(17), 2015, pp. 8786–8793.

[125] Y. Vukadinovic, L. Burkhardt, A. Päpcke, A. Miletic, L. Fritsch, B. Altenburger, R. Schoch, A. Neuba, S. Lochbrunner, and M. Bauer. "When donors turn into acceptors: ground and excited state properties of Fe^{II} complexes with amine-substituted tridentate bis-imidazole-2-ylidene pyridine ligands". *Inorganic Chemistry*, **59**(13), 2020, pp. 8762–8774.

[126] I. M. Dixon, F. Alary, M. Boggio-Pasqua, and J.-L. Heully. "Reversing the relative ^{3}MLCT–^{3}MC order in Fe (II) complexes using cyclometallating ligands: a computational study aiming at luminescent Fe (II) complexes". *Dalton Transactions*, **44**(30), 2015, pp. 13498–13503.

[127] L. Lindh, P. Chábera, N. W. Rosemann, J. Uhlig, K. Wärnmark, A. Yartsev, V. Sundström, and P. Persson. "Photophysics and photochemistry of iron carbene complexes for solar energy conversion and photocatalysis". *Catalysts*, **10**(3), 2020, pp. 2073–4344.

[128] O. S. Wenger. "Is iron the new ruthenium?" *Chemistry – A European Journal*, **25**(24), 2019, pp. 6043–6052.

[129] P. Dierks, Y. Vukadinovic, and M. Bauer. "Photoactive iron complexes: more sustainable, but still a challenge". *Inorganic Chemistry Frontiers*, **9**, 2022, pp. 206–220.

[130] P. Gütlich, Y. Garcia, and H. A. Goodwin. "Spin crossover phenomena in Fe (II) complexes." *Chemical Society Reviews*, **29**(6), 2000, pp. 419–427.

[131] Y. Liu, P. Persson, V. Sundström, and K. Wärnmark. "Fe N-heterocyclic carbene complexes as promising photosensitizers". *Accounts of Chemical Research*, **49**(8), 2016, pp. 1477–1485.

[132] P. Chábera, K. S. Kjaer, O. Prakash, A. Honarfar, Y. Liu, L. A. Fredin, T. C. B. Harlang, S. Lidin, J. Uhlig, V. Sundström, R. Lomoth, P. Persson, and K. Wärnmark. "Fe^{II} hexa N-heterocyclic carbene complex with a 528 ps metal-to-ligand charge-transfer excited-state lifetime". *The Journal of Physical Chemistry Letters*, **9**(3), 2018, pp. 459–463.

[133] P. Chábera, L. Lindh, N. W. Rosemann, O. Prakash, J. Uhlig, A. Yartsev, K. Wärnmark, V. Sundström, and P. Persson. "Photofunctionality of iron(III) N-heterocyclic carbenes and related d^5 transition metal complexes". *Coordination Chemistry Reviews*, **426**, 2021, p. 213517.

[134] L. A. Fredin, M. Pápai, E. Rozsályi, G. Vankó, K. Wärnmark, V. Sundström, and P. Persson. "Exceptional excited-state lifetime of an iron(II)–N-heterocyclic carbene complex explained". *The Journal of Physical Chemistry Letters*, **5**(12), 2014, pp. 2066–2071.

[135] Y. Liu, T. Harlang, S. E. Canton, P. Chábera, K. Suárez-Alcántara, A. Fleckhaus, D. A. Vithanage, E. Göransson, A. Corani, R. Lomoth, V. Sundström, and K. Wärnmark. "Towards longer-lived metal-to-ligand charge transfer states of iron(II) complexes: an N-heterocyclic carbene approach". *Chemical Communications*, **49**, 2013, pp. 6412–6414.

[136] P. Chábera, Y. Liu, O. Prakash, E. Thyrhaug, A. E. Nahhas, A. Honarfar, S. Essén, L. A. Fredin, T. C. Harlang, K. S. Kjær, et al. "A low-spin Fe (III) complex with 100-ps ligand-to-metal charge transfer photoluminescence". *Nature*, **543**(7647), 2017, pp. 695–699.

[137] K. S. Kjær, N. Kaul, O. Prakash, P. Chábera, N. W. Rosemann, A. Honarfar, O. Gordivska, L. A. Fredin, K.-E. Bergquist, L. Häggström, T. Ericsson, L. Lindh, A. Yartsev, S. Styring, P. Huang, J. Uhlig, J. Bendix, D. Strand, V. Sundström, P. Persson, R. Lomoth, and K. Wärnmark. "Luminescence and reactivity of a charge-transfer excited iron complex with nanosecond lifetime". *Science*, **363**(6424), 2019, pp. 249–253.

[138] J. C. Scaiano. "A beginners guide to understanding the mechanisms of photochemical reactions: things you should know if light is one of your reagents". *Chemical Society Reviews*, **52**, 2023, pp. 6330–6343.

[139] C. E. Johnson, J. Schwarz, M. Deegbey, O. Prakash, K. Sharma, P. Huang, T. Ericsson, L. Häggström, J. Bendix, A. K. Gupta, et al. "Ferrous and ferric complexes with cyclometalating N-heterocyclic carbene ligands: a case of dual emission revisited". *Chemical Science*, **14**(37), 2023, pp. 10129–10139.

[140] J. Steube, A. Kruse, O. S. Bokareva, T. Reuter, S. Demeshko, R. Schoch, M. A. Argüello Cordero, A. Krishna, S. Hohloch, F. Meyer, et al. "Janus-type emission from a cyclometalated iron (III) complex". *Nature Chemistry*, **15**(4), 2023, pp. 468–474.

[141] Y. Ye, P. Garrido-Barros, J. Wellauer, C. M. Cruz, R. Lescouëzec, O. S. Wenger, J. M. Herrera, and J.-R. Jiménez. "Luminescence and excited-state reactivity in a heteroleptic tricyanido Fe(III) complex". *Journal of the American Chemical Society*, **146**(1), 2024, pp. 954–960.

[142] J. V. Caspar and T. J. Meyer. "Application of the energy gap law to nonradiative, excited-state decay". *The Journal of Physical Chemistry*, **87**(6), 1983, pp. 952–957.

[143] E. M. Kober, J. V. Caspar, R. S. Lumpkin, and T. J. Meyer. "Application of the energy gap law to excited-state decay of osmium (II)-polypyridine complexes: calculation of relative nonradiative decay rates from emission spectral profiles". *The Journal of Physical Chemistry*, **90**(16), 1986, pp. 3722–3734.

[144] S. Paulson, B. P. Sullivan, and J. V. Caspar. "Luminescent ligand-to-metal charge-transfer excited states based on pentamethylcyclopentadienyl complexes of tantalum". *Journal of the American Chemical Society*, **114**(17), 1992, pp. 6905–6906.

[145] C. Conti, F. Castelli, and L. S. Forster. "Photophysics of hexakis(cyano)chromate(3-) and hexakis(cyano)cobaltate(3-) in polyalcohol-water solutions at room temperature". *The Journal of Physical Chemistry*, **83**(18), 1979, pp. 2371–2376.

[146] M. M. Alowakennu, A. Ghosh, and J. K. McCusker. "Direct evidence for excited ligand field state-based oxidative photoredox chemistry of a cobalt(III) polypyridyl photosensitizer". *Journal of the American Chemical Society*, **145**(38), 2023, pp. 20786–20791.

[147] A. Y. Chan, A. Ghosh, J. T. Yarranton, J. Twilton, J. Jin, D. M. Arias-Rotondo, H. A. Sakai, J. K. McCusker, and D. W. C. MacMillan. "Exploiting the Marcus inverted region for first-row transition metal–based photoredox catalysis". *Science*, **382**(6667), 2023, pp. 191–197.

[148] M. T. Indelli, C. Chiorboli, and F. Scandola. "Photochemistry and photophysics of coordination compounds: Rhodium". *Photochemistry and Photophysics of Coordination Compounds I*, 2007, pp. 215–255.

[149] F. Bolletta, A. Rossi, F. Barigelletti, S. Dellonte, and V. Balzani. "Phosphorescence emission from ligand-centered and metal-centered excited states in the tris-phenanthroline rhodium (III) complex". *Gazzetta Chimica Italiana*, **111**(5-6), 1981, pp. 155–158.

[150] M. T. Indelli, A. Carioli, and F. Scandola. "Excited-state absorption of tris (phenanthroline) rhodium (III). A handle on the excited-state behavior of a powerful photochemical oxidant". *The Journal of Physical Chemistry*, **88**(13), 1984, pp. 2685–2686.

[151] M. T. Indelli and F. Scandola. "Crossover from metal-centered to ligand-centered emission in rhodium (III) polypyridine complexes: Rh $(phen)_2(NH_3)Cl^{2+}$, $Rh(phen)_2(NH_3)_2{}^{3+}$, Rh $(phen)_2(CN)^{2+}$". *Inorganic Chemistry*, **29**(16), 1990, pp. 3056–3058.

[152] A. Soupart, I. M. Dixon, F. Alary, and J.-L. Heully. "DFT rationalization of the room-temperature luminescence properties of $Ru(bpy)_3{}^{2+}$ and $Ru(tpy)_2^{2+}$: ^{3}MLCT–^{3}MC minimum energy path from NEB calculations and emission spectra from VRES calculations". *Theoretical Chemistry Accounts*, **137**, 2018, pp. 1–11.

[153] O. A. Borg, S. S. M. C. Godinho, M. J. Lundqvist, S. Lunell, and P. Persson. "Computational study of the lowest triplet state of ruthenium polypyridyl complexes used in artificial photosynthesis". *The Journal of Physical Chemistry A*, **112**(19), 2008, pp. 4470–4476.

[154] H. C. London, T. J. Whittemore, A. G. Gale, C. D. McMillen, D. Y. Pritchett, A. R. Myers, H. D. Thomas, G. C. Shields, and P. S. Wagenknecht. "Ligand-to-metal charge-transfer photophysics and photochemistry of emissive d^0 titanocenes: a spectroscopic and computational investigation". *Inorganic Chemistry*, **60**(18), 2021, pp. 14399–14409.

[155] H. C. London, D. Y. Pritchett, J. A. Pienkos, C. D. McMillen, T. J. Whittemore, C. J. Bready, A. R. Myers, N. C. Vieira, S. Harold, G. C. Shields, and P. S. Wagenknecht. "Photochemistry and photophysics of charge-transfer excited states in emissive d^{10}/d^0 heterobimetallic titanocene tweezer complexes". *Inorganic Chemistry*, **61**(28), 2022, pp. 10986–10998.

[156] M. Barker, T. J. Whittemore, H. C. London, J. M. Sledesky, E. A. Harris, T. M. Smith Pellizzeri, C. D. McMillen, and P. S. Wagenknecht. "Design strategies for luminescent titanocenes: improving the photoluminescence and photostability of arylethynyltitanocenes". *Inorganic Chemistry*, **62**(43), 2023, pp. 17870–17882.

[157] Y. Zhang, J. L. Petersen, and C. Milsmann. "A Luminescent zirconium(IV) complex as a molecular photosensitizer for visible light photoredox catalysis". *Journal of the American Chemical Society*, **138**(40), 2016, pp. 13115–13118.

[158] C. C. Quadri and E. Le Roux. "Copolymerization of cyclohexene oxide with CO_2 catalyzed by tridentate N-heterocyclic carbene titanium(IV) complexes". *Dalton Transactions*, **43**(11), 2014, pp. 4242–4246.

[159] B. W. Pfennig, M. E. Thompson, and A. B. Bocarsly. "A new class of room temperature luminescent organometallic complexes: luminescence and photophysical properties of permethylscandocene chloride in fluid solution". *Journal of the American Chemical Society*, **111**(24), 1989, pp. 8947–8948.

[160] M. R. M. Bruce, A. Sclafani, and D. R. Tyler. "Photochemical consequences of the manipulation of the lowest energy excited states by substitution of the Cp (Cp = η5-cyclopentadienyl) ligands in titanium Cp_2TiX_2 (X = Br, I) complexes". *Inorganic Chemistry*, **25**(15), 1986, pp. 2546–2549.

[161] "Photochemistry of titanocene(IV) derivatives". *Journal of Organometallic Chemistry*, **81**(1), 1974, pp. 79–85.

[162] Z.-T. Tsai and C. H. Brubaker. "Photolysis of titanocene dichloride". *Journal of Organometallic Chemistry*, **166**(2), 1979, pp. 199–210.

[163] J. W. I. Kenney, D. R. Boone, D. R. Striplin, Y. H. Chen, and K. B. Hamar. "Electronic luminescence spectra of charge transfer states of titanium(IV) metallocenes". *Organometallics*, **12**(9), 1993, pp. 3671–3676.

[164] M. R. Bruce and D. R. Tyler. "Electronic structure and photochemistry of the $(\eta^5\text{-}C_5H_5)_2TiI_2$ complex". *Organometallics*, **4**(3), 1985, pp. 528–533.

[165] F. Juliá. "Ligand-to-metal charge transfer (LMCT) photochemistry at 3d-metal complexes: an emerging tool for sustainable organic synthesis". *ChemCatChem*, **14**(19), 2022, e202200916.

[166] F. Glaser, A. Aydogan, B. Elias, and L. Troian-Gautier. "The great strides of iron photosensitizers for contemporary organic photoredox catalysis: On our way to the holy grail?" *Coordination Chemistry Reviews*, **500**, 2024, p. 215522.

[167] Y. Pellegrin and F. Odobel. "Sacrificial electron donor reagents for solar fuel production". *Comptes Rendus Chimie*, **20**(3), 2017, pp. 283–295.

[168] M. D. Woodhouse and J. K. McCusker. "Mechanistic origin of photoredox catalysis involving iron(II) polypyridyl chromophores". *Journal of the American Chemical Society*, **142**(38), 2020, pp. 16229–16233.

[169] A. Gualandi, M. Marchini, L. Mengozzi, M. Natali, M. Lucarini, P. Ceroni, and P. G. Cozzi. "Organocatalytic enantioselective alkylation of aldehydes with $[Fe(bpy)_3]Br_2$ Catalyst and Visible Light". *ACS Catalysis*, **5**(10), 2015, pp. 5927–5931.

[170] S. Otto, A. M. Nauth, E. Ermilov, N. Scholz, A. Friedrich, U. Resch-Genger, S. Lochbrunner, T. Opatz, and K. Heinze. "Photo-chromium: sensitizer for visible-light-induced oxidative C–H bond functionalization—electron or energy transfer?" *ChemPhotoChem*, **1**(8), 2017, pp. 344–349.

[171] L. A. Büldt, X. Guo, A. Prescimone, and O. S. Wenger. "A Molybdenum(0) isocyanide analogue of Ru(2,2'-bipyridine)$_3{}^{2+}$: a strong reductant for photoredox catalysis". *Angewandte Chemie International Edition*, **55**(37), 2016, pp. 11247–11250.

[172] O. Prakash, L. Lindh, N. Kaul, N. W. Rosemann, I. B. Losada, C. Johnson, P. Chábera, A. Ilic, J. Schwarz, A. K. Gupta, et al. "Photophysical integrity of the iron (III) scorpionate framework in iron (III)–NHC complexes with long-lived ^{2}LMCT excited states". *Inorganic Chemistry*, **61**(44), 2022, pp. 17515–17526.

[173] N. W. Rosemann, P. Chábera, O. Prakash, S. Kaufhold, K. Wärnmark, A. Yartsev, and P. Persson. "Tracing the full bimolecular photocycle of iron(III)–carbene light harvesters in electron-donating solvents". *Journal of the American Chemical Society*, **142**(19), 2020, pp. 8565–8569.

[174] A. Aydogan, R. E. Bangle, A. Cadranel, M. D. Turlington, D. T. Conroy, E. Cauët, M. L. Singleton, G. J. Meyer, R. N. Sampaio, B. Elias, and L. Troian-Gautier. "Accessing photoredox transformations with an iron(III) photosensitizer and green light". *Journal of the American Chemical Society*, **143**(38), 2021, pp. 15661–15673.

[175] A. Aydogan, R. E. Bangle, S. De Kreijger, J. C. Dickenson, M. L. Singleton, E. Cauët, A. Cadranel, G. J. Meyer, B. Elias, R. N. Sampaio, and L. Troian-Gautier. "Mechanistic investigation of a visible light mediated dehalo-

genation/cyclisation reaction using iron (III), iridium (III) and ruthenium (II) photosensitizers". *Catalysis Science & Technology*, **11**(24), 2021, pp. 8037–8051.

[176] J. Schwarz, A. Ilic, C. Johnson, R. Lomoth, and K. Wärnmark. "High turnover photocatalytic hydrogen formation with an Fe(III) N-heterocyclic carbene photosensitiser". *Chemical Communications*, **58**, 2022, pp. 5351–5354.

[177] A. Ilic, J. Schwarz, C. Johnson, L. H. M. de Groot, S. Kaufhold, R. Lomoth, and K. Wärnmark. "Photoredox catalysis via consecutive ^{2}LMCT- and ^{3}MLCT-excitation of an Fe(III/II)–N-heterocyclic carbene complex". *Chemical Science*, **13**, 2022, pp. 9165–9175.

[178] A. K. Pal, C. Li, G. S. Hanan, and E. Zysman-Colman. "Blue-emissive cobalt (III) complexes and their use in the photocatalytic trifluoromethylation of polycyclic aromatic hydrocarbons". *Angewandte Chemie*, **130**(27), 2018, pp. 8159–8163.

[179] E. J. Piechota and G. J. Meyer. "Introduction to electron transfer: theoretical foundations and pedagogical examples". *Journal of Chemical Education*, **96**(11), 2019, pp. 2450–2466.

[180] E. Vauthey. "Elucidating the mechanism of bimolecular photoinduced electron transfer reactions". *The Journal of Physical Chemistry B*, **126**(4), 2022, pp. 778–788.

[181] D. Rehm and A. Weller. "Kinetics of fluorescence quenching by electron and H-atom transfer". *Israel Journal of Chemistry*, **8**(2), 1970, pp. 259–271.

[182] V. O. Saik, A. A. Goun, and M. D. Fayer. "Photoinduced electron transfer and geminate recombination for photoexcited acceptors in a pure donor solvent". *The Journal of Chemical Physics*, **120**(20), 2004, pp. 9601–9611.

[183] G. L. Closs and J. R. Miller. "Intramolecular long-distance electron transfer in organic molecules". *Science*, **240**(4851), 1988, pp. 440–447.

[184] N. Kaul and R. Lomoth. "The carbene cannibal: photoinduced symmetry-breaking charge separation in an Fe(III) N-heterocyclic carbene". *Journal of the American Chemical Society*, **143**(29), 2021, pp. 10816–10821.

[185] B. J. Shields, B. Kudisch, G. D. Scholes, and A. G. Doyle. "Long-lived charge-transfer states of nickel(II) aryl halide complexes facilitate bimolecular photoinduced electron transfer". *Journal of the American Chemical Society*, **140**(8), 2018, pp. 3035–3039.

[186] J. Olmsted and T. J. Meyer. "Factors affecting cage escape yields following electron-transfer quenching". *Journal of Physical Chemistry*, **91**(6), 1987, pp. 1649–1655.

[187] C. D. Clark and M. Z. Hoffman. "Ion-pairing control of excited-state electron-transfer reactions effect of cations on cationic reactants". *Journal of Photochemistry and Photobiology A: Chemistry*, **111**(1), 1997, pp. 9–13.

[188] A. Bard, A. Ledwith, and H. Shine. "Formation, properties and reactions of cation radicals in solution". In: ed. by V. Gold and D. Bethell. Vol. 13. Advances in Physical Organic Chemistry. Academic Press, 1976, pp. 155–278.

[189] N. Elgrishi, K. J. Rountree, B. D. McCarthy, E. S. Rountree, T. T. Eisenhart, and J. L. Dempsey. "A practical beginner's guide to cyclic voltammetry". *Journal of Chemical Education*, **95**(2), 2018, pp. 197–206.

[190] V. Artero, M. Chavarot-Kerlidou, and M. Fontecave. "Splitting water with cobalt". *Angewandte Chemie International Edition*, **50**(32), 2011, pp. 7238–7266.

[191] P. Du and R. Eisenberg. "Catalysts made of earth-abundant elements (Co, Ni, Fe) for water splitting: recent progress and future challenges". *Energy & Environmental Science*, **5**(3), 2012, pp. 6012–6021.

[192] J. Hawecker, J. Lehn, and R. Ziessel. "Efficient homogeneous photochemical hydrogen generation and water reduction mediated by cobaloxime or macrocyclic cobalt complexes". *New Journal of Chemistry*, 7(5), 1983.

[193] M. Nippe, R. S. Khnayzer, J. A. Panetier, D. Z. Zee, B. S. Olaiya, M. Head-Gordon, C. J. Chang, F. N. Castellano, and J. R. Long. "Catalytic proton reduction with transition metal complexes of the redox-active ligand bpy2PYMe". *Chemical Science*, **4**, 2013, pp. 3934–3945.

[194] J. Xie, Q. Zhou, C. Li, W. Wang, Y. Hou, B. Zhang, and X. Wang. "An unexpected role of the monodentate ligand in photocatalytic hydrogen production of the pentadentate ligand-based cobalt complexes". *Chemical Communications*, **50**(49), 2014, pp. 6520–6522.

[195] W. K. Lo, C. E. Castillo, R. Gueret, J. Fortage, M. Rebarz, M. Sliwa, F. Thomas, C. J. McAdam, G. B. Jameson, D. A. McMorran, et al. "Synthesis, characterization, and photocatalytic H_2-evolving activity of a family of [Co(N4Py)(X)]$^{n+}$ complexes in aqueous solution". *Inorganic Chemistry*, **55**(9), 2016, pp. 4564–4581.

[196] A. Call, F. Franco, N. Kandoth, S. Fernández, M. González-Béjar, J. Pérez-Prieto, J. M. Luis, and J. Lloret-Fillol. "Understanding light-driven H_2 evolution through the electronic tuning of aminopyridine cobalt complexes". *Chemical Science*, **9**(9), 2018, pp. 2609–2619.

Scientific publications

Author contributions

Paper I: Microsecond Photoluminescence and Photoreactivity of a Metal-Centered Excited State in a Hexacarbene–Co(III) Complex

I performed all the calculations and the corresponding analysis of the data.

Paper II: Excited State Rebalancing of Hexa-Carbene d^6 Complexes – Comparative Calculations for Fe^{II}, Ru^{II}, Co^{III}, and Rh^{III}

I was responsible for performing the calculations, analysing the data, and writing the paper.

Paper III: Ligand-Centered to Metal-Centered Activation of a Rh(III) Photosensitizer Revealed by Ab Initio Molecular Dynamics Simulations

I was responsible for performing the calculations, analysing the data, and writing the paper.

Paper IV: Modeling the Competition Between Luminescence and Photoinduced Homolysis in Titanocenes and Scandocenes

I was responsible for designing the study, performing the calculations, analysing the data, and writing the paper.

Paper V: Competing Dynamics of Intramolecular Deactivation and Bimolecular Charge Transfer Processes in Luminescent Fe (III) N-Heterocyclic Carbene Complexes

I was responsible for performing the calculations, analysing this data, and contributed to the writing of the computational results.

Paper VI: Understanding Anomalous Cage-Escape Dynamics in Photoredox Processes Driven by Fe(III) N-Heterocyclic Carbene Complexes

I was responsible for designing the study, performing the calculations, analysing the data, and writing the paper.

Paper VII: Photoredox Matching of Earth-Abundant Photosensitizers with Hydrogen Evolving Catalysts by First Principles Predictions

I was responsible for performing the calculations, analysing the data, and writing the paper.

Paper VIII: Photoinduced Hydrogen Evolution Catalyzed by New Co(II) Complexes of N5-Donor Ligands

I performed all the calculations and the corresponding analysis in the manuscript.